Process Development for Forging Lightweight Multi-Material Gears

A Thesis Submitted for the

Degree of Doctor of Philosophy

of Imperial College London

and

Diploma of Imperial College

By

Denis Politis

MEng (1st Class Honours), ACGI, AMIMechE

Mechanics of Materials Division

Department of Mechanical Engineering

Imperial College London

2013

CERTIFICATE OF AUTHORSHIP

I certify that this thesis has not already been submitted for any degree and is not being submitted as part of candidature for any other degree.

I also certify that the thesis has been written by me and that any assistance that I have received in preparing this thesis and all sources used have been acknowledged in this thesis.

Signature of Candidate

Denis Politis

The copyright of this thesis rests with the author and is made available under a Creative Commons Attribution Non-Commercial No Derivatives licence. Researchers are free to copy, distribute or transmit the thesis on the condition that they attribute it, that they do not use it for commercial purposes and that they do not alter, transform or build upon it. For any reuse or redistribution, researchers must make clear to others the licence terms of this work.

Acknowledgements

The performance of research and completion of a thesis provides the challenge for any researcher to investigate new themes and the opportunity to work with a large number of people with a wide range of expertise.

I would first like to thank Dr. Daniel Balint and Prof. Jianguo Lin for their advice, guidance, time and invaluable contribution through the duration of the project. Their assistance has indeed driven the research to its completion. I would also like to thank Prof. Trevor Dean for sharing his extensive knowledge and experience of forging.

I am also grateful to the Department of Mechanical Engineering, Imperial College London for providing me the opportunity and facilities to conduct this work. Furthermore, I am sincerely thankful to the Engineering and Physical Sciences Research Council (EPSRC) for providing the DTA scholarship, enabling this project, which would have otherwise not been possible. I hope EPSRC would continue to support researchers in the future to ascertain and elicit ground-breaking technologies for mankind and society.

A special note of thanks go to my friends and colleagues Qian Bai, Thomas Dunnett, Omar al Fakir, Erofili Kardoulaki, Morad Karimpour, Nan Li, Ali Mehmanparast and many others for their approachability and emotional support during difficult times.

Last but not least, a special note of thanks goes to my parents and brother who have shown their support and patience throughout the duration of the project.

December, 2013

London, United Kingdom

Denis Politis

Abstract

The work presented in this thesis discusses the development of an innovative method for manufacturing tailored gears, specifically bi-metallic lightweight gears through the use of the forging process. Utilising this method, gears can be constructed from multiple metals, where high strength, high density materials are located in regions of high stress concentration, such as the tooth flank, tooth root and regions in contact with shaft attachment mechanisms. On the other hand, lower strength, lower density materials can be located at less critical regions, such as the central region of the gear, hence reducing weight. A patent has been filed for the production process of forging multi-material lightweight gears.

To investigate this process, bi-metallic gear construction was studied, where a high strength outer ring; and low strength cylindrical or annular core placed within the confines of the ring, allowed for the production of high strength teeth. Experimental and simulation work was conducted to better understand the material flow which occurs during the forging process, and hence its implications on the structural integrity of the gear. To allow for experimental trials, a tool set was designed and manufactured, and used in conjunction with a forming press to forge gears of a spur gear profile. Gears were produced under both cold and hot forging conditions using model materials (lead and copper) and engineering alloys (aluminium and mild steel) respectively. This construction was evaluated for a range of ring thicknesses.

A simplified Finite Element (FE) model was established to analyse the material flow and ring thickness distribution during the cold forging operation. Data for the materials commercially pure lead, copper (C101), aluminium alloy (Al 6082), mild steel (230M07) and gear steel (16MnCr5) were obtained through compressive experiments undertaken on Instron and Gleeble testing machines. Constitutive equations were calibrated to a unified constitutive equation model incorporating the physical parameters of stress, plastic strain rate, isotropic hardening, and dislocation density to model the behaviour of aluminium alloy, mild steel and gear steel allowing for the creation of a FE model representing the hot forging process.

Furthermore, three locking mechanisms between the two materials were examined: macro-mechanical locking, micro-mechanical locking and diffusion bonding; which when coupled together may prevent disengaging during operation. In addition, the root and contact stresses experienced by bi-metallic gears were also compared to a single material steel gear through

an FE model to identify performance differences. Finally, recommendations and future research directions are presented.

Keywords: Bi-metallic gears, cold and hot forging process, constitutive equations, diffusion bonding, experimentation, lightweight gears, macro-mechanical locking, material modelling, micro-mechanical locking, simulation.

Nomenclature

A	Temperature dependent constant for dislocation density
A'	Power law constant
A''	Exponential law constant
A'''	Hyperbolic sine law constant
A_o	Temperature independent constant for dislocation density
b	Facewidth in British Standards equations
B	Temperature dependent constant for isotropic hardening
B_o	Temperature independent constant for isotropic hardening
C	Temperature dependent constant for dislocation density
C_o	Temperature independent constant for dislocation density
d	Pitch diameter for AGMA and Buckingham equations
d_1	Pitch diameter in British Standards equations
E	Elastic modulus
E_n	Elastic modulus of driven gear
E_o	Temperature independent constant for elastic modulus
E_r	Elastic modulus of driver gear
F	Facewidth in AGMA equations
F_n	Normal contact force
F_t	Tangential load in Lewis and British Standards equations
k	Temperature dependent yield stress
k_o	Temperature independent yield stress constant
K	Temperature dependent stress constant
K_A	Application factor
K_B	Rim thickness factor
K_H	Load distribution factor
$K_{H\alpha}$	Transverse load factor
$K_{H\beta}$	Face load factor

K_m Material factor

K_o Temperature independent stress constant

K_{OF} Overload factor

K_s Size factor

K_t Stress concentration factor

K_V Dynamic factor for British Standards equations

$K_V^{'}$ Dynamic factor for AGMA equations

m Module

$m^{'}$ Strain rate hardening exponent

n Plastic strain rate exponent

n' Power law exponent

$n^{''}$ Hyperbolic sine law exponent

N Strain hardening exponent constant

N_n Number of teeth of driven gear

N_r Number of teeth of driver gear

N_t Number of gear teeth

p Pitch diameter in Lewis equation

Q Activation energy

Q_{aa} Activation energy for isotropic hardening term

Q_A Activation energy for stress constant term

Q_B Activation energy for isotropic hardening equation

Q_C Activation energy for isotropic hardening equation

Q_E Activation energy for elastic modulus term

Q_g Gear ratio factor

Q_p Activation energy for yield stress term

r_b Radius of base circle

R Isotropic hardening

R_g Gas constant

s Compressive displacement

s_f Final compressive displacement

t Measured ring thickness

t_o Initial ring thickness

T Temperature

T_m Melting temperature

T_q Torque

u Gear ratio

W_t Tangential load in AGMA equations

x_i Coordinate of involute profile

y_i Coordinate of involute profile

Y Lewis form factor

Y_J Geometry factor for bending strength

Z Zener-Hollomon parameter

Z_β Helix angle factor

Z_B Single pair tooth contact factor

Z_e Elastic coefficient

Z_E Elasticity factor

Z_ε Contact ratio factor

Z_H Zone factor

Z_I Geometry factor

Z_R Surface condition factor

Greek Letters:

α Hyperbolic sine law constant

β Exponential law constant

δ Exponent in dislocation density

$\dot{\varepsilon}$ Strain rate

ε_p Plastic strain

$\dot{\varepsilon}_p$ Plastic strain rate

ε_T Total strain

θ Angle of rotation

μ Friction coefficient

υ Poisson's ratio

ρ Current dislocation density

$\bar{\rho}$ Normalised dislocation density

ρ_i Initial dislocation density

σ Flow stress

σ_B Hertz contact stress

σ_{BE} AGMA bending stress

σ_c AGMA contact stress

σ_y Yield stress

$\sigma_{H1,2}$ British Standard tooth contact stress

σ_{HO} British Standard nominal contact stress at pitch point

σ_L Lewis bending stress

φ Pressure angle

List of Figures

Figure 1.1: Various transmission devices: (a) Belt drive (Wired, 2008), (b) Chain drive (Suzuki Motorcycles, 2008), and (c) Gearing (Car and Driver Magazine, 2013)…… 22

Figure 1.2: Aircraft accessory gearbox (Rolls Royce Plc, 1996).……... 24

Figure 1.3: Gear types: (a) Spur gears, (b) Bevel gears, (c) Helical gears, and (d) Worm gears (Childs, 2003).…….. 24

Figure 1.4: Abaqus CAE simulation of contact stresses of gears……..... 26

Figure 2.1: Nomenclature of a spur gear tooth (Shigley and Mischke, 2001).……..... 28

Figure 2.2: Gear manufacturing processes: (a) Gear machining (Premier Machine & Gear Ltd, 2004), (b) Sintered powder gear (Precision Powdered Metal Parts Inc, 2013), (c) Gear rolling (Van Dyck, 2011), and (d) Gear forging (Brooks, 2013).....……..... 30

Figure 2.3: Grain orientation in: (a) Forged vs machined bevel gear tooth and (b) Forged crankshaft (Forging Industry Association, 2007).……..... 35

Figure 2.4: Various stages of spur gear forging and corresponding location on a load-displacement curve.....……..... 36

Figure 2.5: Tool setup for gear forging (Tuncer and Dean, 1988; Tuncer and Dean, 1985).……..... 37

Figure 2.6: Tool design involving: (i) Non-penetrating punch, (ii) Moving die/container and (iii) Ejecting counterpunch/anvil (1-NME) (Tuncer and Dean, 1985).……..... 39

Figure 2.7: Tool design involving: (i) Ejecting punch, (ii) Fixed die/container and (iii) Penetrating counterpunch/anvil (2-EFP) (Tuncer and Dean, 1985).…..... 39

Figure 2.8: Tool design for: (a) 1A-MMNS with (i) Moving die/container, (ii) Moving mandrel and (iii) Non-penetrating punch and (b) 1B-MMNS with (i) Moving die/container, (ii) Moving mandrel and (iii) Non-penetrating counterpunch/anvil (1B-MMNS) (Tuner and Dean, 1987).……..... 41

Figure 2.9: Multi-metal products: (a) Bi-metal bearing (Jiashan PVB Sliding Bearing Co., 2012a), (b) Bi-metal bush (Jiashan PVB Sliding Bearing Co., 2012b), (c) Bi-metal engine valve (Friction Welding Technologies Pvt., 2013), and (d) Bi-metal pipe (Penticton Foundry, 2007).…..……..... 43

Figure 2.10: Laminated gear structure (Streander, 1973).……...……..... 45
Figure 2.11: Friction welded gear (Wadleigh, 1993).……...……..... 45
Figure 2.12: EDM cross-section of bi-metallic gear: locking between two metals shown through gear……...……..... 45
Figure 2.13: Multi-metal gears: (a) Bi-metallic gear and (b) Tri-metallic gear..... 47
Figure 2.14: Schematic of bi-metal hot forging process…..... 47
Figure 3.1: Gear forging tool design cross-sectional view..... 50
Figure 3.2: Toolset: (a) Mounted on press and (b) Ring and core assembly in die..... 51
Figure 3.3: Experimental setup for hot forging.....……..... 52
Figure 3.4: Components: (ai) Lead core, (aii) Copper ring, (aiii) Lead-copper assembly and (bi) Aluminium core, (bii) Steel ring, (biii) Aluminium-steel assembly……...……..... 53
Figure 3.5: Cold forging of lead-copper gears with ring thicknesses: (a) 2mm, (b) 4mm, and (c) 6mm…..... 55
Figure 3.6: Vertical cross section of lead-copper gears for: (a) 2mm, (b) 4mm and (c) 6mm gears..... 56
Figure 3.7: Hot forging of aluminium-mild steel gears with ring thicknesses: (a) 2mm, (b) 4mm, and (c) 6mm..... 58
Figure 3.8: Vertical cross section for: (a) 2mm, (b) 4mm and (c) 6mm gears..... 59
Figure 3.9: Asymmetric separation..... 60
Figure 3.10: Interface boundary sample: (a) Extracted through EDM from tooth and (b) Mounted in bakelite..... 62
Figure 3.11: SEM photo of interface between steel and aluminium at: (a) low and (b) high magnification..... 62
Figure 3.12: EDX analysis of interface region: (a) Line scan of joining zone, (b) Enhanced version of line scan, and (c) Elemental composition chart..... 63
Figure 3.13: SEM photo of protrusion of steel in aluminium in tooth root..... 64
Figure 4.1: Gleeble compression tests: (a) Experimental set-up and (b) Sample before and after compression..... 70
Figure 4.2: Thermal cycle during Gleeble testing for 230M07 mild steel..... 71
Figure 4.3: Al 6082-O Gleeble test results for: (a) Strain rate of $1s^{-1}$ and (b) Temperature of $550^{o}C$..... 72

Figure 4.4: 230M07 Gleeble test results for: (a) Strain rate of $1s^{-1}$, (b) Temperature of 900°C and (c) 1100°C…..... 73
Figure 4.5: 16MnCr5 Gleeble test results for: (a) Strain rate of $1s^{-1}$ and (b) Temperature of 950°C..... 74
Figure 4.6: Al 6082-O experimental data (crosses) and constitutive equation set results (coloured lines) at 550°C..... 76
Figure 4.7: Al 6082-O results for different temperatures at $1s^{-1}$ strain rate comparing experimental data (crosses) with constitutive equations (coloured lines)..... 77
Figure 4.8: 230M07 experimental data (crosses) and constitutive equation set results (coloured lines) at 900°C..... 78
Figure 4.9: 230M07 results for different temperatures at $1s^{-1}$ strain rate comparing experimental data (crosses) with constitutive equations (coloured lines)..... 78
Figure 4.10: 16MnCr5 experimental data (crosses) and constitutive equation set results (coloured lines) at 950°C..... 79
Figure 4.11: 16MnCr5 results for different temperatures at $1s^{-1}$ strain rate comparing experimental data (crosses) with constitutive equations (coloured lines)..... 79
Figure 5.1: FE Model of bi-metal gear forging: (a) Die and work-piece segment and (b) Strain for 2mm ring gear..... 81
Figure 5.2: True stress versus true strain data for the ring (copper) and core (lead) materials compared to mild steel..... 82
Figure 5.3: Predicted die filling for 2mm ring from: (a) Vertical and (b) Horizontal directions, where μ=0.1 on the punch and counterpunch and s_f=14 mm..... 83
Figure 5.4: Comparison of tooth filling: (a) Experimental and (b) Predicted for different ring thicknesses, where μ=0.1 on the punch and counterpunch..... 84
Figure 5.5: Comparison of computed (solid curves) and experimental (symbols) ring thicknesses in the vertical direction for different ring thickness, where μ=0.1 on punch and counterpunch..... 85
Figure 5.6: Comparison of computed (solid curves) and experimental (symbols) die filling in the vertical direction for different ring thickness (normalised thicknesses)..... 87
Figure 5.7: Comparison of thickness variations on the cross-section of: (a) Experimental and (b) Simulation for different ring thickness, where μ=0.1 on the punch and counterpunch..... 88

Figure 5.8: Comparison of computed (solid lines) and experimental (symbols) thickness variation for the formed tooth for different ring thicknesses. Cross-sections were taken at the mid-height of each gear. μ=0.1 on punch and counterpunch for simulations..... 89
Figure 5.9: Comparison of computed (solid lines) and experimental (symbols) thickness variation for the formed tooth for different ring thicknesses shown as normalised thickness..... 90
Figure 5.10: Effect of friction on the thickness variations in the vertical direction for the ring thickness of 4mm..... 91
Figure 5.11: Effect of friction on the thickness variations in the horizontal direction for the ring thickness of 4mm..... 92
Figure 5.12: Effects of material interfacial friction on thickness variations in the vertical direction for μ=0 and μ=0.577 for an initially 4 mm thick ring. Computations are carried out using tool/work-piece interfacial friction coefficient of 0.2..... 93
Figure 5.13: Effects of material interfacial friction on thickness variations in the horizontal direction for μ=0 and μ=0.577 for an initially 4 mm thick ring..... 94
Figure 5.14: Effect of material property difference on ring thickness variations in the vertical direction. Computations are carried using ring thickness of 4mm... 95
Figure 5.15: Effect of material property difference on ring thickness variations in the horizontal direction. Computations are carried using ring thickness of 4mm..... 96
Figure 6.1: Discretised regions for meshing..... 104
Figure 6.2: Steel stress distribution: (a) Principal stress and (b) von Mises stress..... 105
Figure 6.3: 1mm ring stress distribution..... 107
Figure 6.4: 2mm ring stress distribution..... 107
Figure 6.5: 4mm ring stress distribution..... 109
Figure 6.6: 6mm ring stress distribution..... 109
Figure 6.7: Stress perpendicular to contact point (first contact) for uniform ring gears. 110
Figure 6.8: Compressive surface root stress comparison for uniform ring thickness..... 111
Figure 6.9: Tensile surface root stress comparison for uniform ring thickness..... 112

Figure 6.10: Gear meshing stress distribution for thinned ring profiles for: (a) 2mm, (b) 4mm and (c) 6mm rings..... 113
Figure 6.11: Stress perpendicular to contact point (first contact) for thinned rings..... 114
Figure 6.12: Compressive surface root stress comparison for thinned rings..... 115
Figure 6.13: Tensile surface root stress comparison for thinned rings..... 115
Figure A1: Toolset fully open..... 140
Figure A2: Toolset fully closed..... 140
Figure A3: Toolset rendering..... 140
Figure C1: Convergence test showing contact stress vs no. nodes per tooth..... 161

List of Tables

Table 2.1: Possible design alternatives for three working part tool design (Tuncer and Dean, 1985)..... 38

Table 2.2: Possible design alternatives for four working part tool design (Tuncer and Dean, 1987)..... 40

Table 3.1: Al 6082 chemical composition (Aalco Metals Ltd., 2013)..... 52

Table 3.2: 230M07 chemical composition (Chandler, 1995)..... 52

Table 3.3: Lead-copper dimensions..... 54

Table 3.4: Aluminium-steel dimensions..... 54

Table 4.1: Compression test matrix..... 71

Table 4.2: Constants for Al 6082-O..... 76

Table 4.3: Constants for 230M07..... 77

Table 4.4: Constants for 16MnCr5..... 78

Table 6.1: Summary of stresses through different regions of gear tooth (uniform ring profiles)..... 108

Table 6.2: Stresses through regions of gear tooth (thinned ring profiles)..... 113

Table B1: Determination of Lewis Form Factor (Mitchener and Mabie, 1982)..... 159

Table of Contents

Acknowledgements 4
Abstract 5
Nomenclature 7
List of Figures 11
List of Tables 16
Table of Contents 17
Chapter 1 Gear Technologies 20
1.1 Introduction to Market 20
1.2 Power Transmission Applications 21
1.3 Market Requirements and Challenges 25
1.4 Aims and Objectives of the Research 26
1.5 Structure of Thesis 27
Chapter 2 Gear Production and Lightweight Technologies 28
2.1 Gear Terminology 28
2.2 Manufacturing Methods for Gear Production 29
2.3 Gear Forging 33
2.4 Multi-Material Gears 42
2.5 Development of Multi-Metal Gear Forging Process 46
Chapter 3 Forging of Multi-Metal Gears 49
3.1 Equipment and Forging Tool 49
3.2 Experimental Programme 51
3.3 Test Materials and Billet Dimensions 52
3.4 Cold Forging Multi-Metal Gears from Model Materials 54
3.5 Hot Forging Multi-Metal Gears from Engineering Alloys 56
3.6 Material Locking Mechanisms 60
3.6.1 Macro-Mechanical Locking 61
3.6.2 Diffusion Bond Interface 61
3.6.3 Micro-Mechanical Locking 64
Chapter 4 Development of Unified Visco-Plastic Constitutive Equations 65
4.1 General Constitutive Equations 65

4.2 Unified Visco-Plastic Constitutive Equations 67
4.3 Gleeble Compression Tests 69
4.3.1 Al 6082-O Aluminium Alloy Compression Test Results 71
4.3.2 230M07 Mild Steel Compression Test Results 72
4.3.3 16MnCr5 Gear Steel Compression Test Results 74
4.4 Calibration of Unified Visco-Plastic Constitutive Equations 75
4.4.1 Al 6082-O Constitutive Equation Calibration 76
4.4.2 230M07 Constitutive Equation Calibration 77
4.4.3 16MnCr5 Constitutive Equation Calibration 78
Chapter 5 Finite Element Simulation of Forging Bi-Metallic Gears 80
5.1 Numerical Procedures for Cold Forging 80
5.2 Instron Tests to Determine Material Properties 82
5.3 Results 82
5.3.1 Vertical Cross Section 84
5.3.2 Horizontal Cross Section 87
5.3.3 Punch and Counterpunch Frictional Effects 90
5.3.4 Material Interfacial Friction 92
5.3.5 Alternative Material Combinations 94
5.4 Numerical Procedures for Hot Forging 96
5.4.1 Implementation of Constitutive Equations Using VUMAT 97
Chapter 6 Finite Element Simulation of Contact Performance of Multi-Metal Gears 98
6.1 Analytical/Empirical Estimation of Tooth Stresses 98
6.1.1 Contact Stress Calculations 100
6.1.2 Root Stress Calculations 102
6.2 Numerical Procedures 102
6.3 Stress Distribution in a Gear Tooth 105
6.3.1 Steel Tooth Stress Distribution 105
6.3.2 Uniform Ring Thickness Stress Distribution 106
6.3.3 Forged Ring Profile Stress Distribution 112
Chapter 7 Conclusions and Suggestions for Future Research 117
7.1 Conclusions 117
7.2 Recommendations of Future Research 120
References 123

Appendix A Tool-Set Engineering Drawings 140
Appendix B Analytical/Empirical Stress Calculations 156
B.1 AGMA Tooth Contact Stress 156
B.2 British Standard Tooth Contact Stress 157
B.3 Lewis Bending Stress 159
B.4 AGMA Bending Stress 160
Appendix C FE Model Convergence Test 161
C.1 Node Convergence Test per Tooth 161

Chapter 1 Gear Technologies

This chapter presents a background to the research project, including the global gear market, and power transmission applications. The aims and objectives of the research are presented, along with the overall structure of the thesis.

1.1 Introduction to Market

Modern society is heavily dependent on the transportation sector and on the oil which, at a fundamental level, powers it. The use of vehicles, aircraft and shipping, has revolutionised the way that goods are exchanged globally. Although many benefits have been achieved through transportation, the transport sector utilises a large percentage of the world's energy consumption. For example, road transport accounts for 26.5% of the total EU energy consumption (Commission of the European Communities, 2007). Therefore, governments have recently shown a particular interest in reducing fuel consumption to increase their energy security and reduce dependability. Furthermore, there has been increased concern by governments over environmental implications of emissions and greenhouse gases, which has been highlighted by targets set in the Kyoto Protocol, and more recently, in the Copenhagen climate conference held in 2009 (UN Chronicle, 2009). Two large industry sectors where governments have recently begun enforcing tougher legislation to reduce emissions are automobile and aircraft. In addition to legislative pressure, rapidly fluctuating oil fuel prices particularly affecting the air travel sector has resulted in airlines demanding lower fuel consumption for their aircraft (Fein, 2009). Legislative pressure has led both aircraft and automobile manufacturers to re-examine the designs of all components and develop more efficient alternatives.

In an attempt to increase fuel efficiency, automotive companies have been using complex power train systems, including hybrid technology, on vehicles. There has also been great attention focused on completely eliminating the use of fossil fuel for vehicles and using either hydrogen fuel cells or batteries with electric motors. These new propulsion technologies have required substantial investment to develop and may take time to gain acceptance from customers. The common method to reduce fuel consumption, particularly in the aerospace and increasingly in the automotive industry, has been the reduction in weight of components. The reduction of weight to improve fuel efficiency has been the priority topic of much research due to the substantial savings that can be made. For example, 'lowering car weight

by 100 kg makes it possible to save 0.5 litres of petrol per 100 km' (Dobrzanski *et al.*, 2007). In relation to aircraft, a general rule of thumb is that for every '1% weight reduction', there is a corresponding '0.75% to 1% reduction in fuel consumption' (Ohrn, 2007).

Typically, manufacturers have focused on non-structural components to achieve these weight reductions by substituting lightweight materials such as aluminium alloys, magnesium alloys and polymer composites as replacements for steel. However, to achieve additional fuel savings, the weight of structural and mechanical components must be reduced as well. This has been evident with the development and production of the Airbus A-380, whereby the structure is constructed with '61% aluminum alloys, 22% composites, 10% titanium and steel and 3% fibre metal laminate' (Key to Metals AG, 2009). This is a substantial improvement on the airbus A340, in which only 12% composite is utilized, compared to the 22% of the more recent A380 (Key to Metals AG, 2009). However, as argued by Ostrovsky and Henn (2007), the use of non-metallic materials 'is not possible in some areas' due to 'low performance at high or low temperatures, no electrical conductivity, and low impact resistance and damage tolerance'.

Weight reduction of components in power transmission systems of mass produced vehicles has, as yet, received little attention. In addition to less dead weight, reduction in weight of high speed rotating components also provides the added benefit of reduced inertial forces and thus the stresses experienced during operation.

1.2 Power Transmission Applications

Selection of a system for transmitting power from prime movers such as gas turbines, internal combustion engines, and electric motors to the driven mechanism typically involves design considerations such as the torque and speed of the components as well as size and cost. Typical methods used include 'belts, pulleys, chains, hydraulic and electrical systems, and gears' (Childs, 2003), three of which are shown in Figure 1.1.

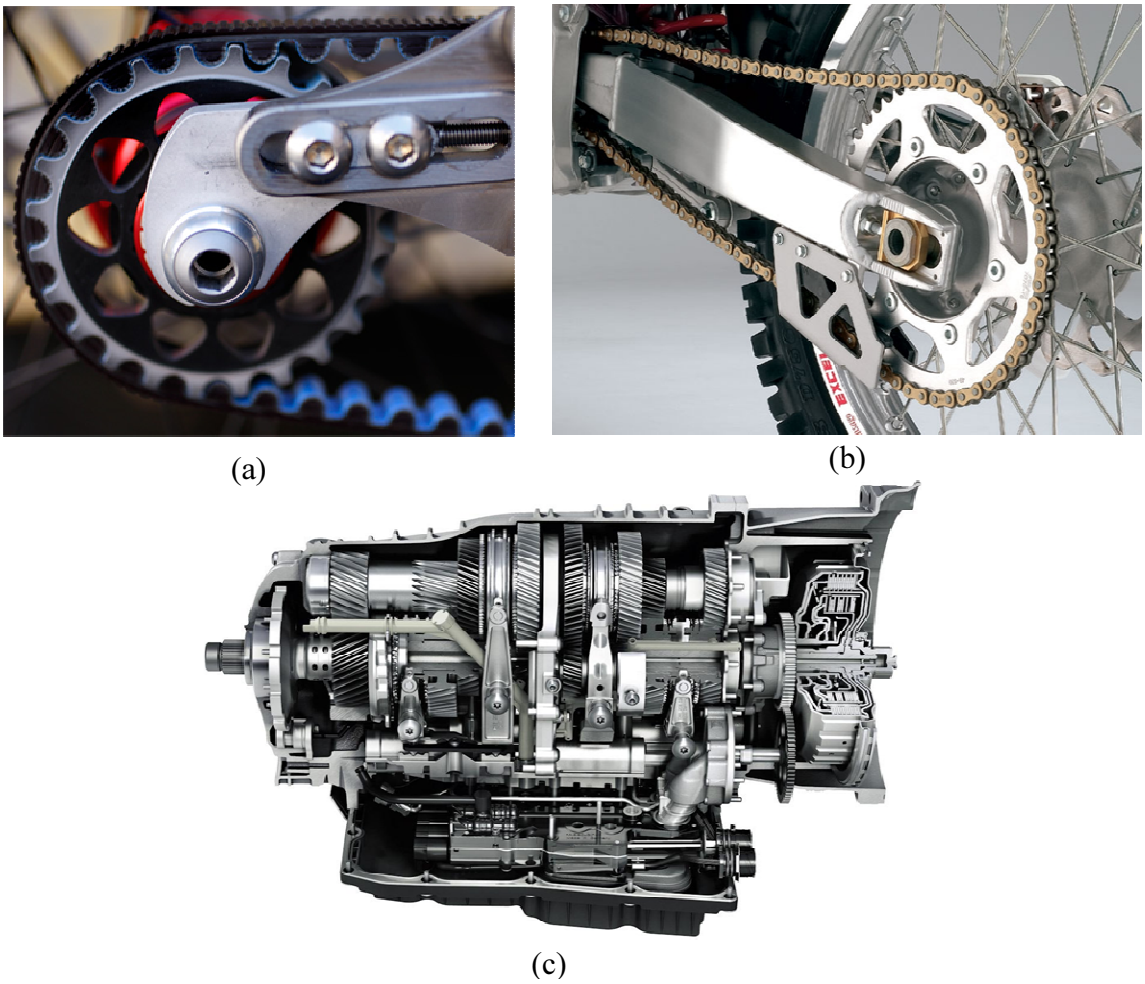


Figure 1.1: Various transmission devices: (a) Belt drive (Wired, 2008), (b) Chain drive (Suzuki Motorcycles, 2008), and (c) Gearing (Car and Driver Magazine, 2013)

Each system presents its own unique capabilities which allow them to be utilised in different applications. For example, belt drives have the advantage of being easy to install, require relatively little maintenance, and are used for drives spanning large distances. However, the primary limitation of belt drives is their limited power transmission due to belt slippage and tensile strength of the belt, although toothed belts obviate slippage (Koyama and Marshek, 1988). Chain drives, with the most common consisting of roller chains and sprockets, are used for higher performance applications than are belts, such as 'motorcycle transmissions, automotive camshaft drives, and machine tools' (Childs, 2003) as the interlocking chain with sprocket are constructed from higher performance materials than belt drives and 'can therefore support higher tension and transmit greater power' (Childs, 2003). However, the main disadvantages associated with chain drives are: lower speed and torque limits for a

given size compared to gears; lubrication issues as they are used primarily in exposed drivetrains for large transmission distances; progressive loosening due to wear; cost increases, and noise (Conwell and Johnson, 1996). Gears achieve power transmission through the repeated rolling and contact of the gear teeth (Chacon *et al.*, 2010), with the main advantages being: generally quieter operation; ease of mass production and resistance to corrosion (Imrek, 2009), and the ability to assemble into compact drives. However, they require accurately aligned shafts and effective lubrication to prevent overheating and micro-pitting of the gear surface.

Early forms of gears date back to antiquity where they were constructed from wooden wheels with cylindrical wooden cogs typically powered by water wheels in order to perform required functions such as grinding grain. One of the earliest examples of a complex mechanical system comprised of metallic gears is the Antikythera mechanism, a form of analogue computer constructed from 32 bronze gears encased in a wooden box (Pastore, 2010) to predict astronomical positions of the sun, moon and various planets. Gear technology progressed substantially during the industrialisation period of the 16^{th} - 18^{th} century with applications in machine tools for the textile industry, clocks, and geared steam locomotives. Various mathematical theories were also implemented to improve the performance of gears with the use of involute profiles as proposed by Euler (1754-55), and the estimation of tooth bending (Lewis, 1892) and contact stresses (Hertz, 1881).

In recent times they have become the primary method used for power transmission in the automotive and aerospace industry (Figure 1.2) as well as for marine, agricultural, power station reduction gearboxes, mining equipment, and wind turbines. The largest application for gears in the automotive industry is found in the gearbox, whereas for aircraft, gears are utilised in the Accessory Gearbox, in the Auxiliary Power Unit (APU) and for Geared Turbofan engines (Riegler and Bichlmaier, 2007), such as the Pratt & Whitney PW1000G engine.

A wide range of gear types are commercially available which generally fall in the categories of straight spur, bevel, helical, worm and worm wheel, and sprockets (Daryani, 2002), some of which are shown in Figure 1.3.

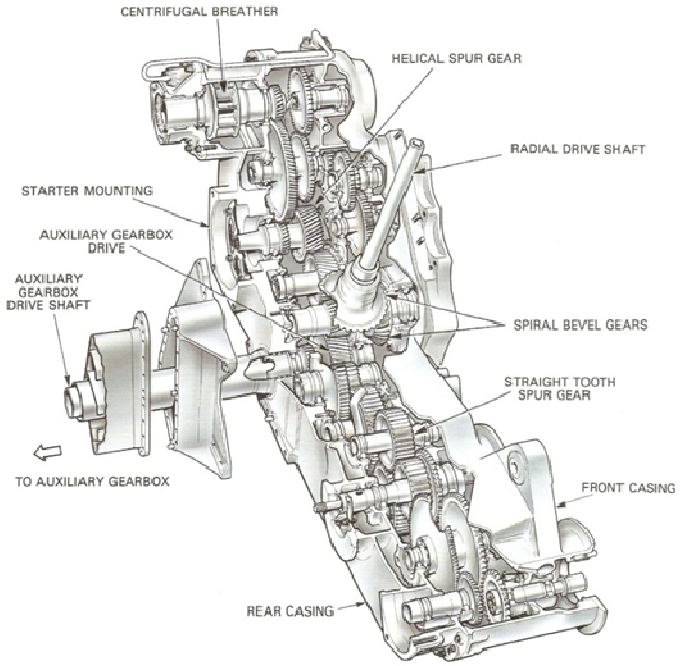
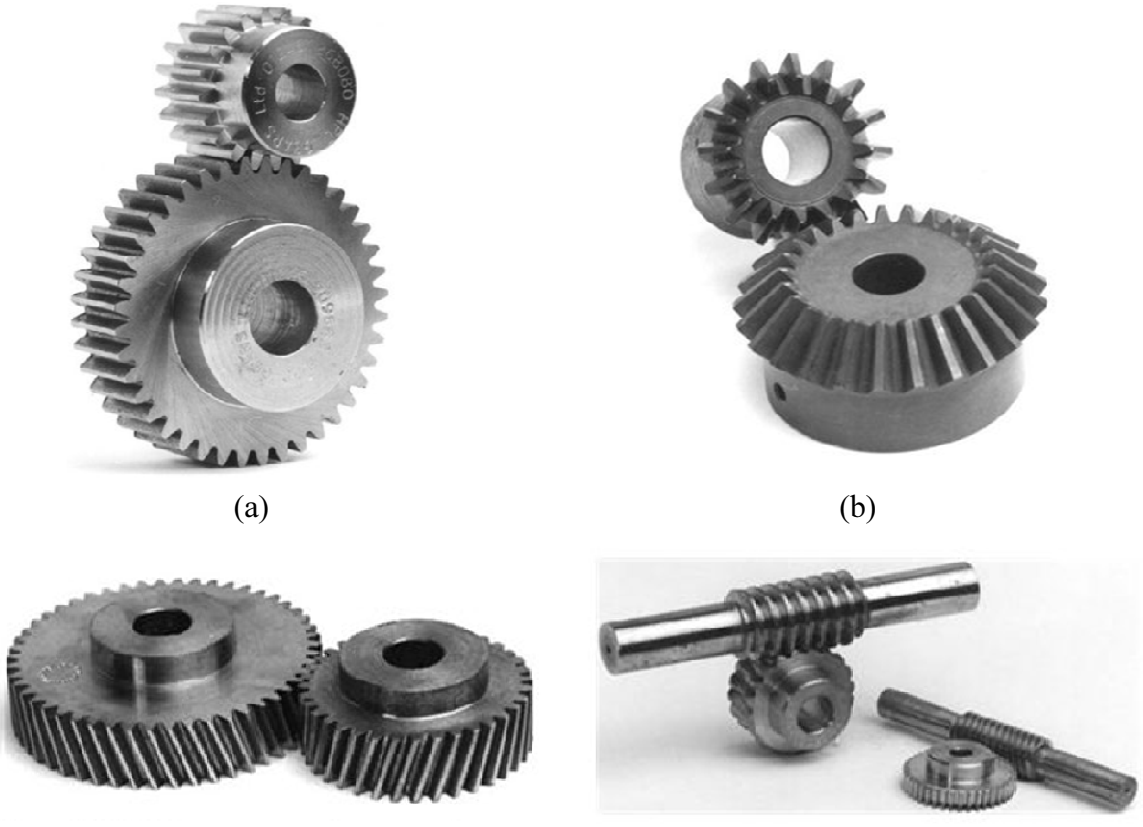


Figure 1.2: Aircraft accessory gearbox (Rolls Royce Plc, 1996)



(a) (b)

(c) (d)

Figure 1.3: Gear types: (a) Spur gears, (b) Bevel gears, (c) Helical gears, and (d) Worm gears (Childs, 2003)

1.3 Market Requirements and Challenges

The wide range of applications and gear types described in Section 1.2 has resulted in an industry with an estimated market value of $169.5 billion by 2013 (Freedonia, 2010). The automotive sector in particular is the largest market where 'seven-tenths of all product sales were automotive related, with motor vehicle transmissions alone accounting for 45% of the entire gear market' (McGuinn, 2011). The gear industry has seen a rapid growth rate at an estimated 4.7% annually until 2013, primarily driven by the industrialisation of many developing countries, and the rising demand of automobiles and machinery. For example, a review of the literature (Freedonia, 2010) revealed that 'China is expected to account for one-third of all additional gear demand through 2013 and will surpass Japan to become the second largest national market behind the USA. By 2018, the total gear sales in China will exceed product demand in the USA'. This market demand as well as competition for market share between manufacturers of gears, has led to the expectation of gears with improved mechanical performance, reduced overall weight and little or no increase in cost.

The significance of weight reduction of the transmission system for economical operation of aircraft has been demonstrated during studies performed for the Future Air Attack Vehicle (FAAV) tilt-rotor helicopter as part of the Boeing Advanced Rotorcraft Transmission (ART) program. It has been estimated that a drive-train weight reduction of 24.6% has the capability of reducing overall aircraft gross takeoff weight by 5.5% (Krantz, 1993). According to Krantz (1993), a saving of $116 million in operating costs throughout the aircraft operating life can be achieved for a fleet of 400 aircraft expected in the USA. As weight savings of transmission systems have already been achieved through the use of aluminium and magnesium alloys for non-critical components such as casings, further weight reductions can only be achieved through reduction of the power transmitting components, primarily the gears themselves. The weight reduction of gears has traditionally involved the use of narrow webs, or the drilling of holes in low stress regions. However, further weight reductions have been proved difficult without negatively affecting the reliability and performance of the gear.

It is essential that any weight reduction of gears maintains the mechanical performance of the teeth, as the stress is greatest at the contact point and 'decreases in the normal direction to the surface' (Vijayarangan and Ganesan, 1994), as can be seen in the simulation of Figure 1.4. According to the literature (Vijayarangan and Ganesan, 1994), the stress at a depth of 0.5 mm perpendicular to the contact surface reduces to approximately a half of the contact stress

value for the module 10mm gear whose dimensions are outlined in the literature. Vijayarangan and Ganesan (1994) suggested that this value gives the 'designer an idea as to the depth of hardness required at the contacting surface'. Moreover, studies performed by Pederson (2010), Orthwein (1975) and Okubo *et al.* (1968) have shown that although contact and root stresses are a common cause of failure for teeth, the presence of shaft attachment mechanisms such as splines, 'parallel keys, tapered keys or Woodruff keys' (Pederson, 2010), which present regions of stress concentration, require a material located in these regions which has the capability of coping with high stress and fatigue requirements. Hence, the foremost challenge is to reduce the weight of a gear, whilst maintaining or exceeding the current mechanical performance, at an acceptable cost.

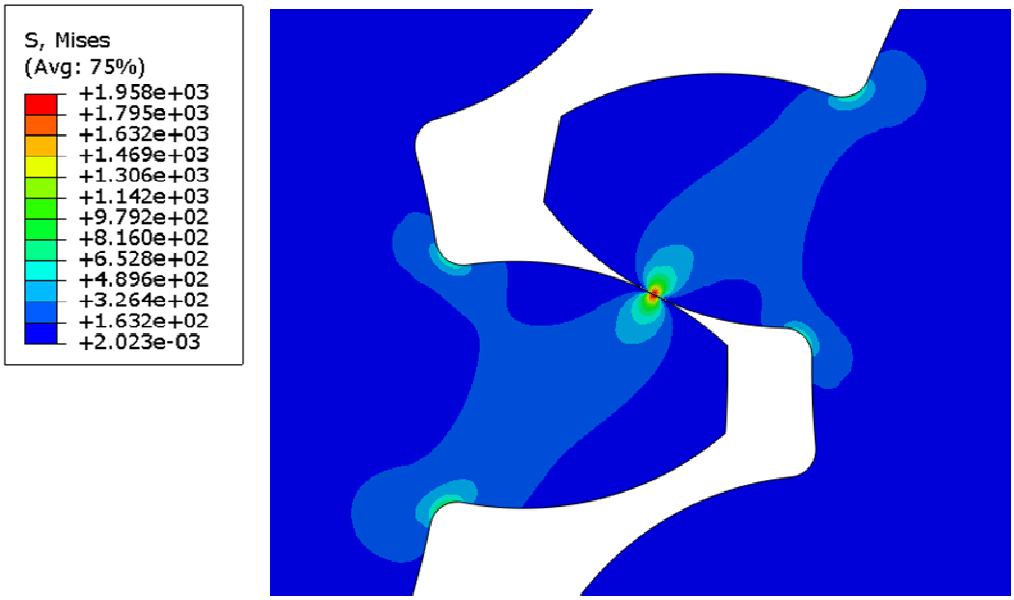


Figure 1.4: Abaqus CAE simulation of contact stresses of gears

Therefore, ideally the market requirements of performance, weight and cost can be met by a gear with tailored properties allowing for high strength, high density materials to be used in the high stress regions, and lower strength, density and low cost materials in less critical regions.

1.4 Aims and Objectives of the Research

The aim of the research was to develop an innovative method of manufacturing tailored gears, specifically lightweight gears through the use of the forging process. Through this technique, a gear was constructed of multiple metals, whereby high strength, high density materials are located in regions of high stress concentration, such as the gear teeth, whereas

lower strength, lower density materials are located at less critical regions, such as the central region of the gear. A patent has been filed for the production process of forging multi-metallic lightweight gears.

1.5 Structure of Thesis

In the chapters that follow, experimental and numerical work performed for the development of the bi-metallic gear forging process is outlined. Chapter 2 reviews existing gear production technologies and the various techniques currently employed to minimise the mass of a gear. Furthermore, existing methods for the production of bi-metallic gears is discussed and the proposed multi-metal forging process is presented. Chapter 3 discusses the equipment and forging tool which were designed and manufactured to facilitate forging trials. The results of bi-metallic cold forging from model materials, as well as hot forging from engineering alloys, is presented. Locking mechanisms providing structural integrity between the two forged metals are also identified and discussed.

Chapter 4 describes the compressive tests performed to determine the mechanical behaviour of the metals during forging. Furthermore, a unified-constitutive model, including the variables, stress, plastic strain rate, isotropic hardening and dislocation density are outlined and the calibration of the constitutive equations is shown. Chapter 5 presents the finite element model, utilising the Abaqus FEA software, which was created in order to model the forging of multi-metal gears. The use of the unified constitutive equations through the Variable User MATerial (VUMAT) subroutine is discussed.

The mechanical performance of these forged multi-metal gears is simulated and presented in Chapter 6, where tooth root and the contact stresses are investigated. Finally, a discussion and conclusions derived from this research are presented in Chapter 7, together with, recommendations to further develop the multi-metal gear forging process.

Chapter 2 Gear Production and Lightweight Technologies

The following chapter discusses the methods typically used for the production of gears. An overview of these methods is presented along with post-production processes to complete a gear. The benefits of forging over these processes, as well as tool designs to achieve effective precision forging of gears are discussed. The benefits of the use of multiple materials over a single material, such as increased strength, reduced weight, and lower material consumption for several commonly used components are presented as well as the potential benefits of this arrangement for the construction of a gear. Finally, a proposed process for the forging of multi-metal gears benefitting from both the advantages offered by the forging process and multi-metal construction is presented.

2.1 Gear Terminology

As stated in Chapter 1, a gear transmits power through the repeated rolling and contact of the gear teeth (Chacon *et al.*, 2010). The terminology of the various regions of gear teeth are shown in Figure 2.1. The pitch circle diameter, is defined as the diameter through the pitch point, which is the point of intersection 'between the axes of the line of centres and the line of action' of gears (Buckingham, 1935). This diameter is used as the basis for other tooth dimensions.

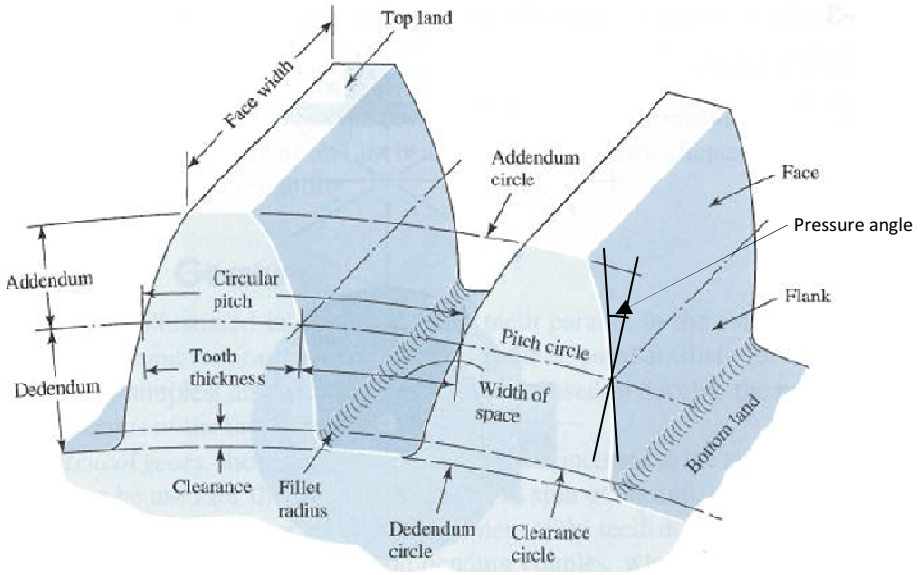


Figure 2.1: Nomenclature of a spur gear tooth (Shigley and Mischke, 2001)

The addendum and dedendum are defined as the radial distances from this pitch circle to the top land and bottom land respectively (Shigley and Mischke, 2001). The pressure angle is 'the angle between a tangent to the tooth profile, and a line perpendicular to the pitch surface' (Buckingham, 1935). Finally, the module is the 'ratio of the pitch diameter to the number of teeth' (Shigley and Mischke, 2001).

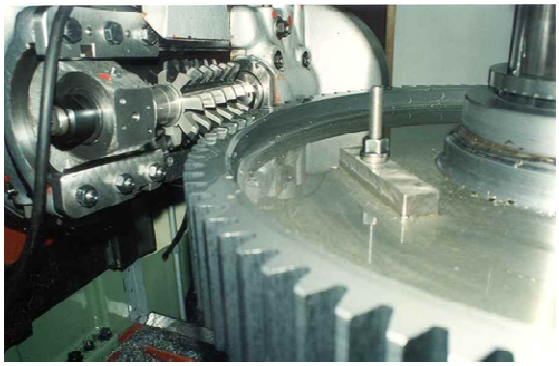
2.2 Manufacturing Methods for Gear Production

In order to produce gear teeth from billet material, various manufacturing processes are available. The method chosen to manufacture a gear depends on the application and the material used. Gears are typically manufactured from two materials: metals or polymers. Polymers, such as nylon, acetal, polyester (PBT) (DuPont, 2007) and polyphenylene sulphide (PPS) are typically used for applications requiring corrosion resistance and minimal lubrication, such as electronics, printers, food processing machinery and robotics. Steel and nickel based super-alloys, such as 16MnCr5, AISI 4320, AISI 9310, Maraging 350 and HP 9-4-30 (Rakhit, 2000) are typically used for higher performance applications whereby the high Young's modulus, yield strength and fatigue strength as well as high wear resistance, are utilised in automotive, marine, aerospace and industrial machinery where 'over 90% of the gears…are made from alloy steels' (Rakhit, 2000).

Typical methods described by Davis (2005) for the production of gears include: (i) machining, such as milling, shaping and hobbing, (ii) casting, such as 'sand casting, shell moulding, investment casting, permanent mould casting, die casting, and centrifugal casting' (Shigley and Mischke, 2001), (iii) stamping, (iv) extrusion, (v) powder metallurgy, (vi) gear rolling and (vii) forging. Some of these processes and product are shown in Figure 2.2.

Hobbing is 'the most common method of cutting gear teeth' (Daryani, 2002). The method of hobbing involves generating the gear teeth on the work-piece by a rotating cutting tool called a hob through progressive cuts. Through a two spindle arrangement, the work-piece is held in one spindle and the hob in the other. The number of gear teeth cut into the work-piece can be adjusted by varying speed ratio of the two spindles. Milling of a gear involves cutting the teeth 'using form cutters rather than by a generating process' (Daryani, 2002). A gear can also be machined through the shaping process, where 'a cutter conjugating to the desired gear form is reciprocated parallel to the work-piece and fed in as the tool and gear blank are rotated in opposite directions' (Daryani, 2002). Machining methods are common for gear manufacturing as they produce accurate gear profiles whilst providing the manufacturer with

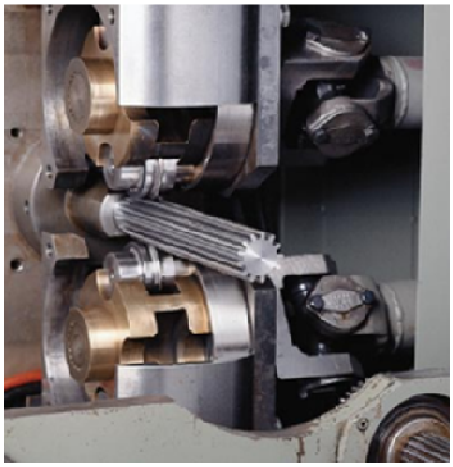
the flexibility to repurpose equipment for other components. However, a disadvantage is that production is slow. In light of this, machining is still used only as a common finishing process for mass produced gears.



(a)



(b)



(c)



(d)

Figure 2.2: Gear manufacturing processes: (a) Gear machining (Premier Machine & Gear Ltd, 2004), (b) Sintered powder gear (Precision Powdered Metal Parts Inc, 2013), (c) Gear rolling (Van Dyck, 2011), and (d) Gear forging (Brooks, 2013)

Casting is commonly used to produce pre-forms for subsequent machining processes for gears. It is also used to produce completed gears (with teeth that require finishing operations) in applications requiring low volume, complicated shapes, large diameters [3 metres or greater (Uherek, 2012)] or large mass which are difficult to produce with other means. For example, girth gears can be produced up to 14 metres in diameter, and weighing up to 105,000kg (David Brown Engineering, 2013). The main disadvantage with casting is that the process may introduce voids and impurities in the completed gear resulting in potentially reduced mechanical properties such as brittleness and poor surface quality (Cáceres and Selling, 1996).

The stamping method is generally used to produce thin flat gears from sheet material from a thickness range of 0.25 to 3mm thick (Townsend, 1992). According to Davis (2005), this process is primarily used for 'toys, clock and timer mechanisms, watches,...mixers and blenders'. Although a simple and low cost production method, it is only suitable for 'no-load' to medium duty applications (Davis, 2005).

Extrusion is primarily used for the production of spur gears, although the production of helical gears using this method has been described in the literature (Choi *et al.*, 1994; Samanta, 1976). Essentially, a bar of material is extruded through a die containing the toothed profile in order to achieve the final tooth form. It is described as being the 'least tool expenditure for mass production of spur gears' (Davis, 2005). A drawback with this method is the difficulty in obtaining close tolerances on fine pitch gears.

Powder metallurgy can be used for the production of 'spur, helical, bevel, face, spur-helical, and helical-helical gears' (Shturtz, 1998). It involves the application of pressure to form a green compact and temperature to sinter the powdered material into the desired shape. It is particularly beneficial in 'processing materials normally regarded as immiscible' (Whittaker, 1991), such as cemented carbides, or processing materials of high melting point like 'tungsten, molybdenum or tantalum, ceramic materials' (Whittaker, 1991). The main disadvantages are that this process is not economical in low quantity production, and is not suitable for the worm and helical gears 'with helix angle exceeding 35^{o}' (Davis, 2005).

Gear rolling is primarily performed for worm gears, although it is also applied to spur and helical gears under certain restrictions. The process involves positioning bar stock between two round rollers containing the tooth profile, which rotate in the same direction and progressively form the gear teeth. The rolling process is a fast production process, with an estimated turnover '50 times as fast as gear cutting' (Davis, 2005). Moreover, the strength of the teeth is increased compared to cutting, as the teeth are formed to a high surface quality and there is no material loss (Neugebauer *et al.*, 2012). The main limitations with gear rolling are the types of gears which can be produced. According to Davis (2005), spur gears can be rolled provided that the gear has at least 18 teeth, and it is 'impractical to roll teeth with pressure angle less than 20^{o}'. Furthermore, similar problems are present in the rolling of helical gears, with the added restriction of the helix angle, where fewer than 18 teeth can be rolled provided the helix angle is large.

The gear forging process involves the use of equipment such as mechanical, hydraulic or screw presses (Altan *et al.*, 2005) to plastically deform a work-piece into a closed die cavity of the required gear geometry. Gears are generally produced from near-net shape forgings, which forge the work-piece to the approximate gear dimensions and require additional post-processing such as machining or grinding to achieve the required tolerances (Altan *et al.*, 2005). Precision forgings, which require little or no subsequent machining is also used as the gear is formed to the required design tolerances (Dieter *et al.*, 2003) and without flash (Altan *et al.*, 2005). Forging is used to produce a wide range of gear types including helical, spur, and bevel gears.

Post-production treatments such as shot-peening or surface treatment of the gear teeth are commonly performed in order to delay failure; including bending and contact (pitting) fatigue, and wear of gear teeth (Rakhit, 2000). Heat treatment is necessary after warm or hot forging as the microstructures produced 'from hot working operations alone are not optimized for most applications, so the microstructure of forging must be tailored by heat treatment to result in the optimum grain size, grain-boundary morphology, phases, and phase distributions' (Altan *et al.*, 2005). Heat treatment is used to obtain a high hardness for wear resistance and fine grain size for fatigue resistance. According to the literature (Rakhit, 2000) the most common heat treatment processes used for alloy steel gears are 'through hardening, case carburizing and hardening, nitriding, carbonitriding, and induction hardening' with materials such as AISI 1045, 4130 and 8640 for through hardened steels and AISI 1018, 4320, 5120 for carburising (Herring and Lindell, 2007). For automotive, aerospace and industrial applications, case carburizing and hardening is used as it is cost effective and 'the torque capacity can be three to four times higher than that of a through-hardened' material gear set (Rakhit, 2000), and hence over '60% of industrial and aerospace gears are made by this process' (Rakhit, 2000).

Gear finishing processes are also performed after the production of a gear to: 'improve surface finish, to remove nicks and burrs and to change or correct the tooth geometry' (Wright and Schriefer, 1997), from distortion encountered during heat treating (Hazelton, 2003). Gear finishing processes include shaving, grinding, honing, lapping and skiving (Daryani, 2002).

Gear shaving involves the removal of small amounts of metal from the gear teeth using a serrated cutting tool (Wright and Schriefer, 1997) in order 'to correct errors in index

(displacement of theoretical to actual tooth position), helix angle, tooth profile and eccentricity' (Dugas, 1997) as well as improve tooth surface finish. According to the literature, 'gear shaving can remove 65-80% of the errors in a hobbed or shaped gear' (Dugas, 1997), resulting in improvements such as gear noise reduction, increased tooth load capacity and service life (Dugas, 1997). Shaving can be classified under four headings: axial, diagonal, tangential and plunge. The difference between these is 'the direction of reciprocation (traverse) of the work through and under the tool' (Kosal, 1998). For example, in axial shaving, 'the traverse path is along the axis of the work gear' (Kosal, 1998), whereas plunge shaving is where 'the work gear is fed into the shaving cutter with no table reciprocation' (Kosal, 1998). The choice of method is dependent on the requirements of the manufacturer. Axial shaving 'is the most economical method for shaving wide face width gears' whereas plunge shaving has a 'very short cycle time' and is used for high production operations (Kosal, 1998).

Grinding is performed using a rotating abrasive wheel to improve the surface of gear teeth, leading to less backlash, higher power transmission and increased lifespan during operation (Hazelton, 2003). Honing is 'a hard finishing process that removes stock by means of high pressure, sliding action and an abrasive honing stone' (Wright and Schriefer, 1997). The work-piece is oscillated 'along its axis ...and honing oil applied with high pressure to clean the stone' (Wright and Schriefer, 1997). Lapping is where loose abrasive slurry is applied between 'a work material and a closely fitting surface, called a lapping plate' (Davis, 2005). According to the literature, lapping can be performed 'by running a set of gears in mesh or by running one gear with a gear shaped master lapping tool' (Davis, 2005). Skiving is primarily used for spur and helical gears and involves the micro-cutting of thin slices of material on the hardened tooth surface (Cowley, 2013). Recent developments in skiving include the Klingelnberg cutting tool system which can be used on bevel gear milling machines with the stated benefits of having '10 times faster processing times compared to shaping' and '20% shorter processing times compared to hobbing' (Klingelnberg GmbH, 2013).

2.3 Gear Forging

Most spur and helical gears used in automotive gearboxes are machined from forged blanks but the forging of gear forms can be traced back to Germany in the 1950's where the lack of equipment for machining gears resulted in the development of the forging process to produce bevel gears with near finish formed teeth (Dean, 2000). Hot and cold forging bevel gears has

since become a widespread gear manufacturing method as a result of the many advantages offered over other production processes presented above, which include: high production rate, improved strength, improved surface finish, lower raw material consumption and cost and energy savings (Alves *et al.*, 2001; Choi and Choi, 1999; Choi and Choi, 1998; Doege and Nagele, 1994). Most automotive gearbox gears are machined from forged blanks, although any in-situ synchro-teeth are often finish forged cold. Net-shape forged automotive gear forms have been forged to net-shape in the laboratory using a combined warm/cold process (Zhao *et al.*, 2010), but the process is not yet industrially wide-spread.

A high production rate has been achieved by the development of new automated systems, such as the ultrafast hotformer Hotmatic series developed by Hatebur (Hatebur Umformmaschinen AG, 2013) which have the ability to produce forgings at a rate of 170 forgings per minute. According Dieter *et al.* (2003), the speed of a forging operation is dependent on the manufacturers choice of equipment used, with high speeds being achieved through hammers, intermediate speeds through mechanical and screw presses, and low speeds through the use of hydraulic presses.

Compared with cut teeth forged gear teeth have higher dynamic strengths, as the material grains align in a favourable orientation around the tooth profile (Shan *et al.*, 2004; Dean, 2000; Doege and Nagele, 1994). This is shown in a cross section of a bevel gear tooth in Figure 2.3a. Complex material alignment during forging can also be seen in other forged components such as a forged crankshaft of Figure 2.3b. This improvement in strength is discussed by the authors Abdel-Rahman and Dean (1981) who state that fully forged gear teeth exhibit a 30% greater impact strength compared to machined teeth. Moreover, it has been stated in the literature that forged gears exhibit a fatigue life double that of machined gears (Abdel-Rahman and Dean, 1981; Miller, 1967). Furthermore, figures in the range of 30% - 44% increase in operational life and strength are reported (Forging Industry Association, 2007; Kobyskovsky *et al.*, 1967).

The use of precision forging also 'allows the manufacture of gear parts without flash' (Alves *et al.*, 2001), which reduces the requirement for subsequent machining operations. Material savings have been demonstrated by Mathas (2005) who states that there is a 30% reduction in material consumption for near net-forged gears compared to cutting. The benefits of near/net shape forming have also been demonstrated by Moriguchi (1992), who states that the net shape forming of components 'can eliminate more than half of the total machining necessary

to produce any particular part'. An example of the stages of deformation occurring for a cylindrical billet forged to a spur gear profile is shown in Figure 2.4 (see page 36). Specifically: (a) illustrates the initial billet and corresponding load required to contact the die tooth root, (b) shows the flow of material into the tooth profile, (c) indicates the material flow beyond the pitch diameter of the tooth, (d) portrays the billet contact with the die tooth tip and (e) depicts the completed and finish machined gear.

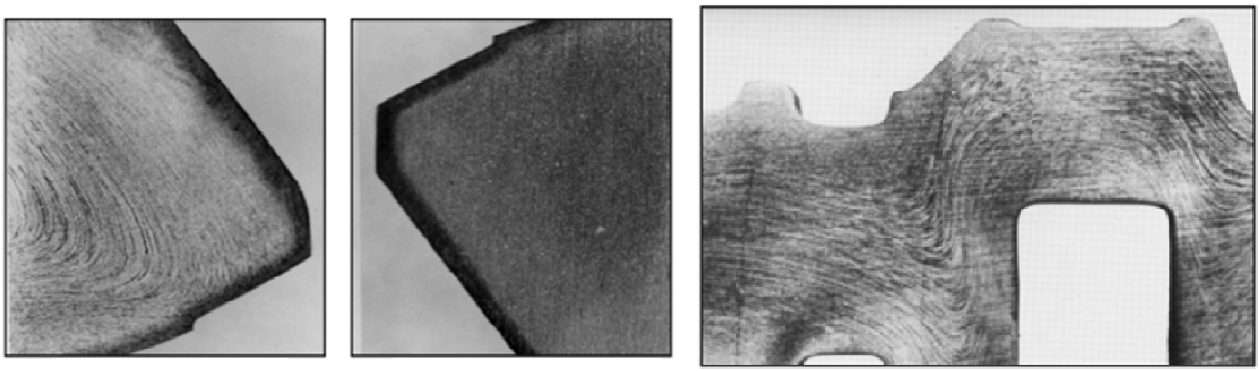


Figure 2.3: Grain orientation in: (a) Forged vs machined bevel gear tooth and (b) Forged crankshaft (Forging Industry Association, 2007)

As stated earlier, forging can be performed under cold, warm or hot conditions. Cold forging is the forging of a work-piece below recrystallisation temperature; and for common engineering alloys is performed at room temperature. It has the advantage of producing gears with 'good dimensional and form error tolerances, and good surface finish' (Dieter *et al.*, 2003). The warm [below recrystallisation temperature (Altan *et al.*, 2005)] or hot forging (above recrystallisation temperature) process, tends to be used when the cold forging process is unsuitable due to the high flow stress of the material at room temperature and load and stress limitations of the forging equipment. However, the main disadvantages with warm and specifically hot forging are: (i) the lower dimensional accuracy of the completed gear due to contraction of the work-piece during cooling; and (ii) the formation of an oxide layer pre and post forging which reduces the surface quality, wear and fatigue strength (Abdel-Rahman and Dean, 1981).

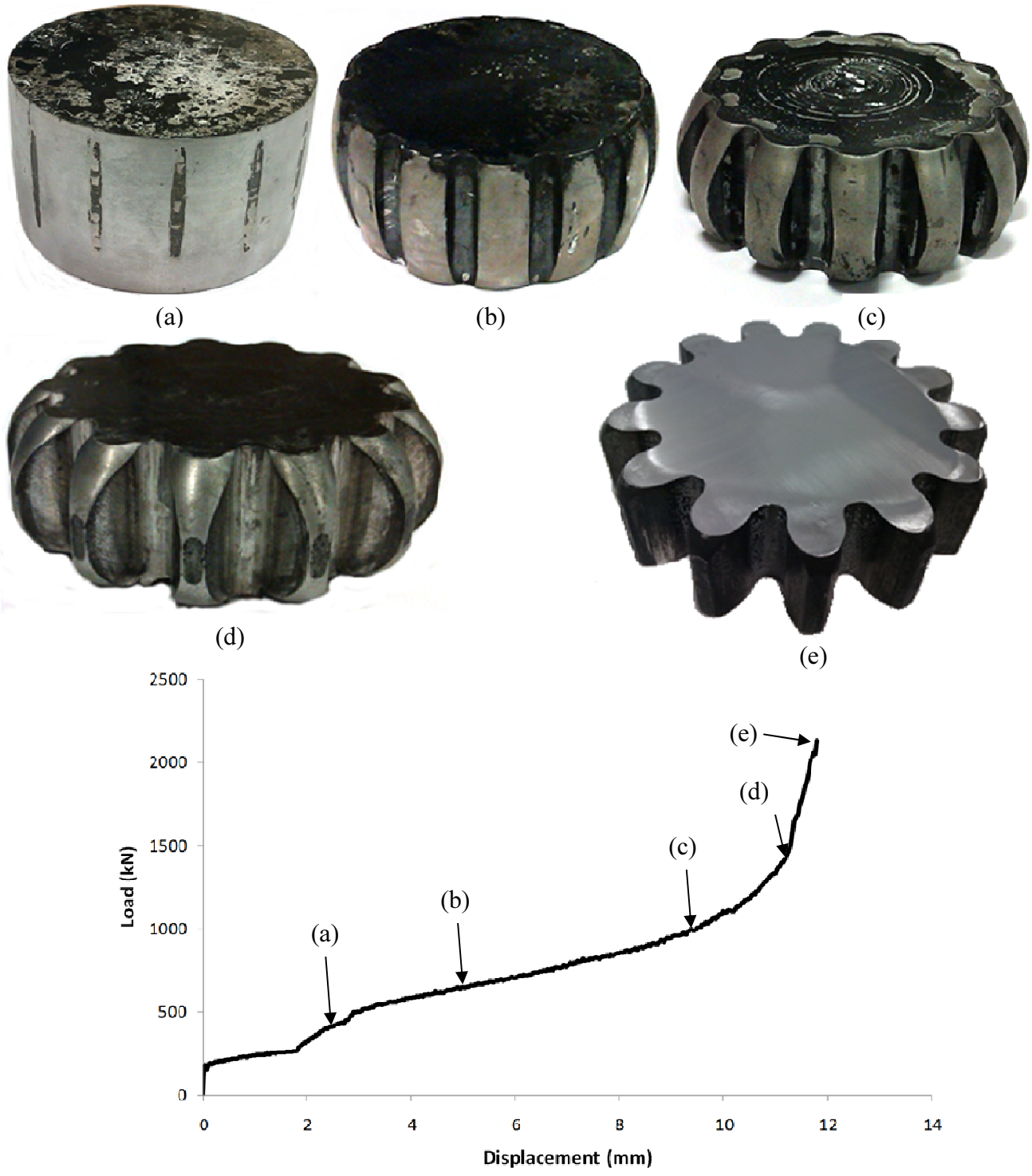


Figure 2.4: Various stages of spur gear forging and corresponding location on a load-displacement curve

A tool-set required to near net-shape forge solid gears without flash, typically consists of three working parts: a die (container), counterpunch (anvil) and a punch. In its basic form, the die is fixed to the machine bed and the tooth shaped counterpunch is positioned within the die located above an ejector. The punch is toothed shaped and penetrated the die. This tool configuration is shown in Figure 2.5 below.

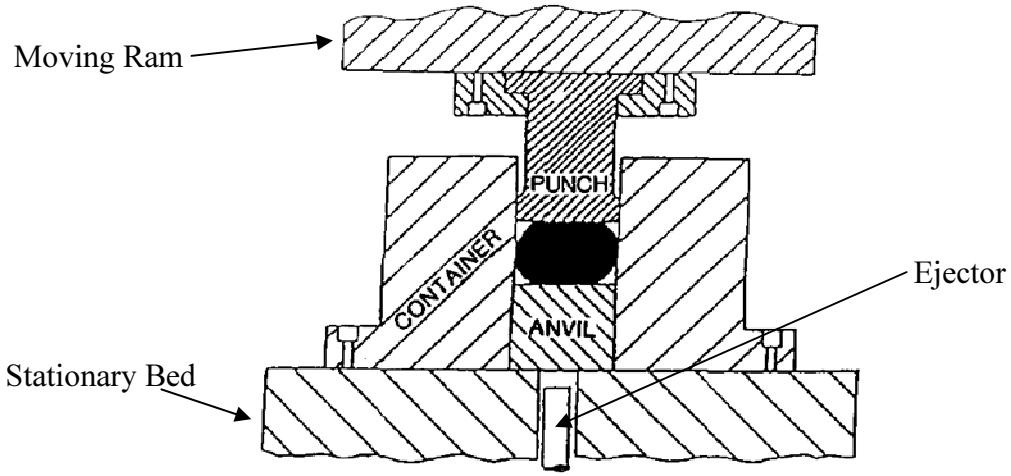


Figure 2.5: Tool setup for gear forging (Tuncer and Dean, 1988; Tuncer and Dean, 1985)

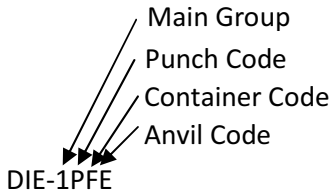
According to Tuncer and Dean (1985) there are 'sixteen different kinematic combinations' in which a three working part tool can be used, where the first eight combinations involve attaching the die to the stationary bed with the other eight attaching the die to the moving ram. Various combinations within these two groups include allowing the die to move vertically (floating die), fixing the die into position or using a penetrating or non-penetrating punch and counterpunch. However, according to the literature, due to impractical combinations such as a 'fixed container and non penetrating punch or anvil' (Tuncer and Dean, 1985) and 'ejection difficulties, only 6 of these designs are practical' (Tuncer and Dean, 1988). The above combinations of possible designs are presented in Table 2.1.

Table 2.1: Possible design alternatives for three working part tool design (Tuncer and Dean, 1985)

Main Group	Die Code	Form of Die Element		
		Punch	Container	Anvil
1	1PFE	P	F	E
	1PME	P	M	E
	1NME	N	M	E
	1NFE	N	F	E
	1PFN	P	F	N
	1NFN	N	F	N
	1PMN	P	M	N
	1NMN	N	M	N
2	2EFP	E	F	P
	2EMP	E	M	P
	2EMN	E	M	N
	2EFN	E	F	N
	2NFP	N	F	P
	2NFN	N	F	N
	2NMP	N	M	P
	2NMN	N	M	N

Note: For the Coding System The Characters Have Following Meaning

(1) Container attached to machine bed
(2) Container attached to ram of machine
(F) Fixed container
(M) Moveable container
(P) Penetrating form
(N) Non-penetrating form
(E) Ejector form



Group 1 and Group 2 designs of Table 2.1 represent the attachment of the die to machine bed and machine ram respectively. A visual representation of a design from each of these groups is shown in Figures 2.6 and 2.7 below.

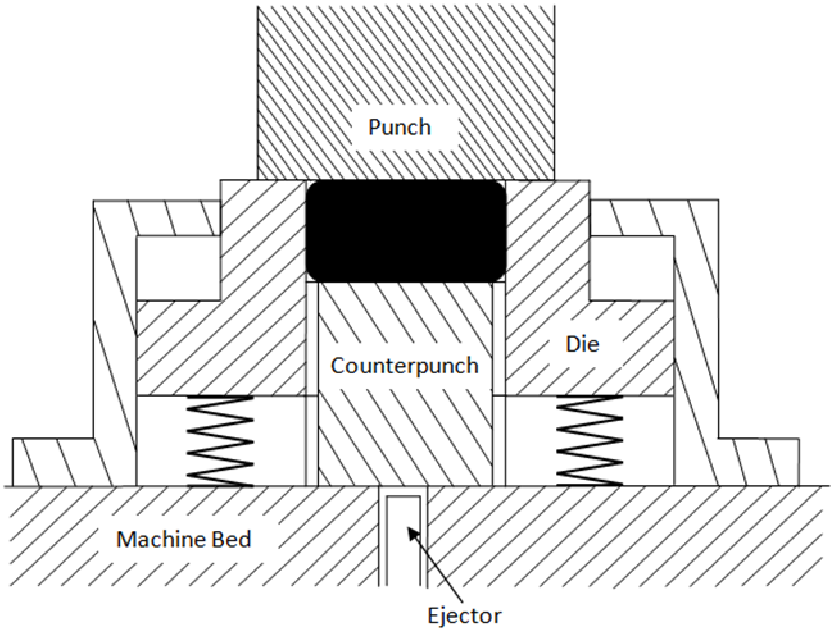


Figure 2.6: Tool design involving: (i) Non-penetrating punch, (ii) Moving die/ container and (iii) Ejecting counterpunch/anvil (1-NME) (Tuncer and Dean, 1985)

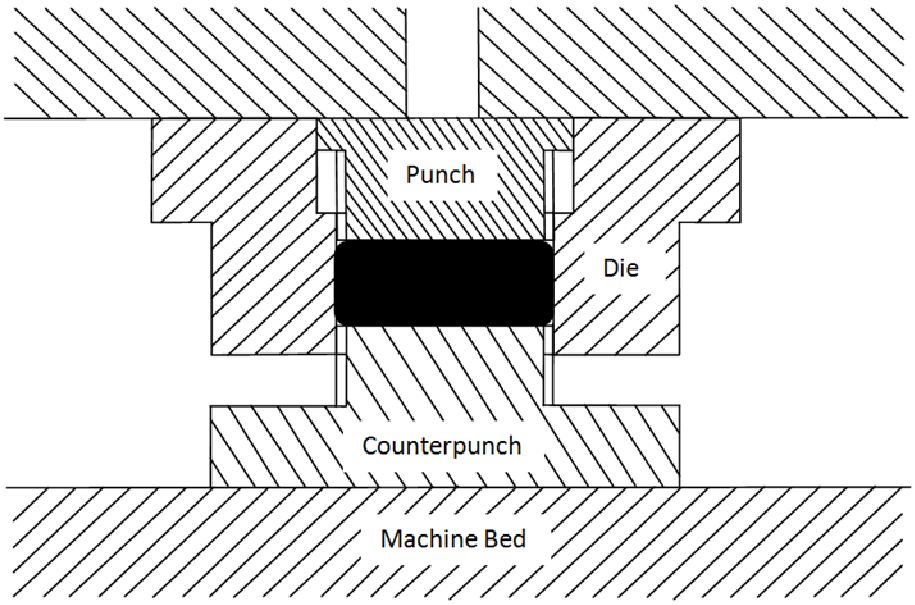


Figure 2.7: Tool design involving: (i) Ejecting punch, (ii) Fixed die/container and (iii) Penetrating counterpunch/anvil (2-EFP) (Tuncer and Dean, 1985)

An improvement to the above three working part designs has been proposed by Tuncer and Dean (1988) and Tuncer and Dean (1987), where an alternative to the use of solid cylindrical billets is the use of billets with a central hole preformed/machined before the gear forging

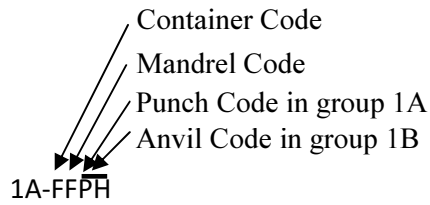
process takes place. According to the literature (Tuncer and Dean, 1988; Tuncer and Dean, 1987), substantial benefits for this hollow forging technique include: (i) the accurate forging of central bores, which can be used to attach the gear on shafts, (ii) reduction in forging load, and (iii) faster heating rates of billets compared to solid billets as heating takes place both in the inner and outer surfaces. In order to prevent material flow from closing the central hole region, a mandrel is used. Therefore, in the hollow billet gear forging, there are four main components present in the tool, namely: the die, counterpunch, punch and mandrel. According to Tuncer and Dean (1987), this brings about 18 different combinations for arranging the components: (a) 4 possibilities of punch including hollow, solid, penetrating, non-penetrating, (b) 4 possibilities of die including attached to the ram, machine bed, and have these fixed or movable, (c) 4 combinations of mandrel including being attached to the counterpunch or punch as either rigid or movable components, (d) 4 combinations of counterpunch which is either fixed or movable and either solid or hollow depending on mandrel arrangement, and (e) 2 combinations of die and mandrel positioning where they are attached either to the moving ram or the stationary machine bed. These combinations are shown in Table 2.2.

Table 2.2: Possible design alternatives for four working part tool design (Tuncer and Dean, 1987)

Group	Die Code	Situation of Die Members			
		Container	Mandrel	Punch	Anvil
1A	1A-FFPH	F	F	PH	-
	1A-FMPH	F	M	PH	-
	1A-FMPS	F	M	PS	-
	1A-MMNH	M	M	NH	-
	1A-MFNH	M	F	NH	-
	1A-MMPH	M	M	PH	-
	1A-MFPH	M	F	PH	-
	1A-MMNS	M	M	NS	-
	1A-MMPS	M	M	PS	-
1B	1B-FFPH	F	F	-	PH
	1B-FMPH	F	M	-	PH
	1B-FMPS	F	M	-	PS
	1B-MMNH	M	M	-	NH
	1B-MFNH	M	F	-	NH
	1B-MMPH	M	M	-	PH
	1B-MFPH	M	F	-	PH
	1B-MMNS	M	M	-	NS
	1B-MMPS	M	M	-	PS

Note: For the Coding System the Characters Have Following Meaning

(H) Hollow punch or counterpunch
(S) Solid punch or counterpunch
(P) Penetrating punch or counterpunch
(N) Non-penetrating punch or counterpunch
(F) Fixed
(M) Movable



From the above Table, Group 1A represents the tooling arrangement where the die (container) and mandrel are attached to the machine bed. Group 1B consists of the die (container) and mandrel being attached to the ram of the forging machine. An example of a 1A-MMNS and 1B-MMNS design presented by Tuncer and Dean (1987) is shown in Figure 2.8. As can be seen, the toolset contains a moving die (container), moving mandrel, and non-penetrating punch or counterpunch.

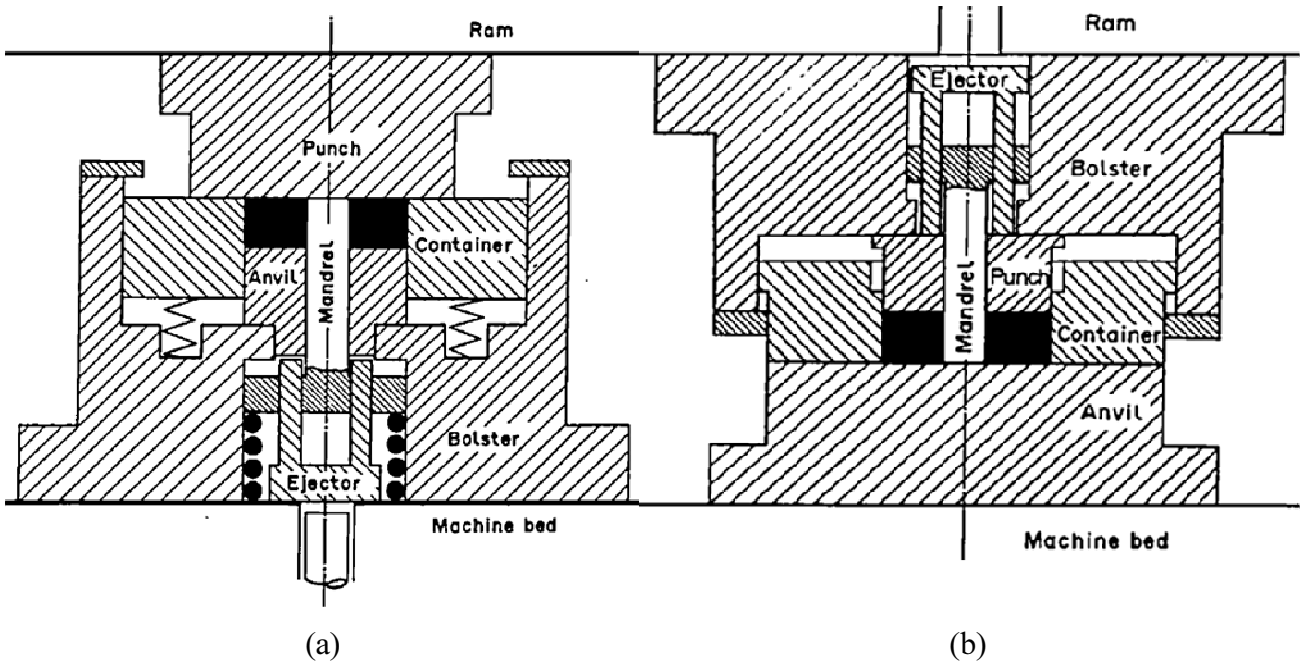


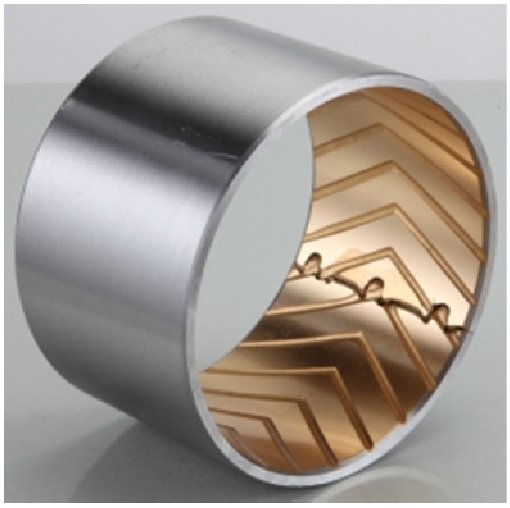
Figure 2.8: Tool design for: (a) 1A-MMNS with (i) Moving die/container, (ii) Moving mandrel and (iii) Non-penetrating punch and (b) 1B-MMNS with (i) Moving die/container, (ii) Moving mandrel and (iii) Non-penetrating counterpunch/anvil (1B-MMNS) (Tuner and Dean, 1987)

According to the literature (Tuncer and Dean, 1987) the optimum kinematic design depends on the shape of the gear to be forged. Furthermore, the literature suggests that the kinetics of the tool, and hence, the direction of the frictional forces between the tool and the work-piece, can influence the sequence of tooth corner filling (top or bottom corner).

2.4 Multi-Material Gears

The general trend for manufactured components is continuous improvement through increased strength, reduced weight, and lower material consumption whilst producing a part of these specifications at an acceptable cost. Traditional production methods such as forging have focused on the use of a single material or alloy for the work-piece, with weight reduction being achieved through machining holes or designing thinner sections in non-critical regions or using lighter alloys such as aluminium instead of steel. However, this can be costly and restricts a component to applications suitable for the material in use as every material has its own distinct properties.

Multi-metallic components are increasingly being manufactured to take advantage of the unique properties of different metals and combining them in various ways to address the difficulty of achieving lightweight, low cost and high performance through a single alloy. Some multi-metallic applications are well known. For example, bi-metallic strips produced by the rolling process (Manesh and Taheri, 2005) are used for thermostat coils to measure temperature. In this application, the most important property is the thermal expansion of the two metals which allow the component to function. Bi-metal engine components such as bi-metal bearings, valves and bushes have also shown benefits over single metal predecessors. Valves for example, experience lower temperatures at the valve stem compared to the valve head. Hence, bi-metal valves produced by friction welding (Domblesky *et al.*, 2006), allowing the use of a less expensive alloy with lower strength and wear resistant properties to be used for stems, results in reduced cost. Bi-metallic journal bearings have been produced through sintering a lead-tin-bronze layer onto steel with the possibility of subsequently applying a layer of PTFE (Tait, 1954) to benefit from the anti-friction properties of the polymer whilst maintaining the structural integrity of metals. Moreover, bi-metal bushes have been made by sintering a copper-lead bronze layer onto a steel backing (Nishan Group, 2010) in order to reduce friction and wear. Furthermore, the use of bi-metal pipes for oil and gas pipelines is discussed by Reformatskaya *et al.* (2000) to reduce the effect of pitting by oil with high water content. Some of these bi-metallic components are shown in Figure 2.9.



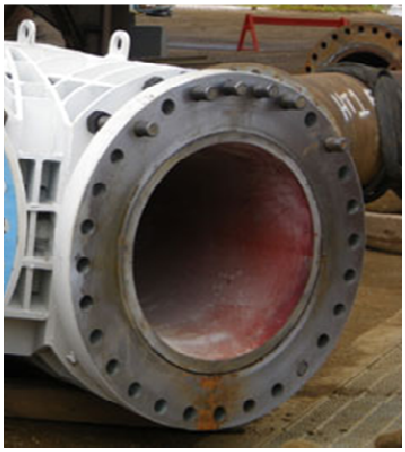
(a)



(b)



(c)



(d)

Figure 2.9: Multi-metal products: (a) Bi-metal bearing (Jiashan PVB Sliding Bearing Co., 2012a), (b) Bi-metal bush (Jiashan PVB Sliding Bearing Co., 2012b), (c) Bi-metal engine valve (Friction Welding Technologies Pvt. Ltd., 2013), and (d) Bi-metal pipe (Penticton Foundry, 2007)

As with the components above, gears also have regions where the material experiences more severe operating conditions compared with others. Examples include the contacting line between two meshing gears; the root of the tooth; and at features such as keyways or splines used to attach a gear to a shaft all of which experience greater stresses than the remaining material of the inner/core region of the gear. This presents the opportunity of using metals with higher performance for such critical surface regions, with lower performance materials in the centre. Therefore, the combination of materials can be optimised depending on application, to produce gears which can be lightweight, low cost and temperature resistant.

The use of multiple materials for a combined metallic-thermoplastic gear has been proposed by Santi (1998), where a metallic plate having gear teeth is first produced and two layers of thermoplastic material are subsequently disposed on either side and flow through apertures in the metallic centre to hold the assembly together. The intention of this is to produce a gear benefitting from the noise reduction of polymer gears whilst maintaining the torque loading of metal gears.

The production of gears with a laminated structure has been described by Everts and Rickard (1994) where a series of thin gear profiles are queued and frictionally combined to produce a completed gear. An alternative to this, where a series of discs of varying materials are secured by fasteners (Figure 2.10) thus allowing the gear teeth to be cut using conventional means is described by Streander (1973).

The use of multiple metals for the production of bi-metal gears is described by Wadleigh (1993) who has used friction welding of an inner aluminium core to an outer steel gear toothed profile (Figure 2.11) through a conical shaped interface. Wolfe and Trebnik (1971) proposed producing a gear from a bronze annulus containing the gear teeth and a steel central hub, which are joined by solder.

Bi-metal casting of gear blanks has been developed by Miller to achieve similar benefits (Miller, 1974). Moreover, lightweight gears have also been produced by combining a machined aluminium core to steel gear profile (Integy, 2013), where the two metals lock axially (although limited rotational locking) through a series of grooves possibly through heat shrinking (Figure 2.12). However, research has shown that little work has been performed in the forging of bi-metal gears in a single process through two separate components. Hence, the current research has emerged to investigate the forging methods for the production of multi-metal gears aiming at reducing the overall mass of a gear while maintaining operational performance properties (e.g. produce lightweight, high performance gears).

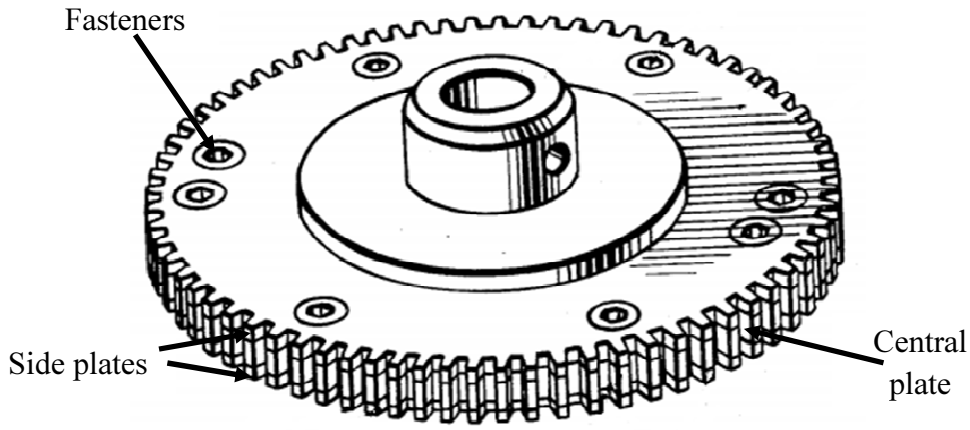


Figure 2.10: Laminated gear structure (Streander, 1973)

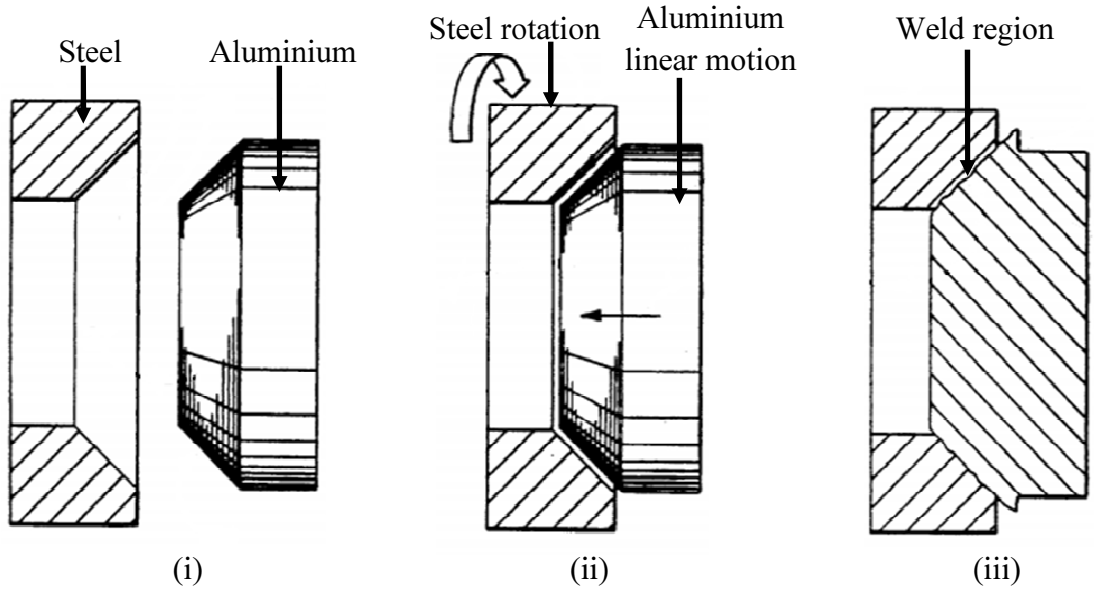


Figure 2.11: Friction welded gear (Wadleigh, 1993)



Figure 2.12: EDM cross-section of bi-metallic gear: locking between two metals shown through gear

2.5 Development of Multi-Metal Gear Forging Process

To combine the performance benefits offered from multi-metal components (lightweight, high performance etc.), as well as the benefits of forging (high production rate, improved strength, low material consumption etc.), a multi-metal gear forging process is proposed. Through this process, gears can be produced by either cold or hot forging in a single forging operation, where, the material flow between the metals locks/binds them together to form the completed gear.

The construction of a lightweight bi-metallic gear using this process consists of two components: (i) a lower strength lightweight centre (core) and (ii) high strength outer material (ring). Before forging, the outer ring is an annulus of rectangular cross-section and the inner core can be either a solid cylinder or pre-bored as a wide annulus. If the materials are ductile at room temperature, the cold forging process would involve: (i) first placing the outermost (outer ring) material into the die. This allows the material to be located concentrically into the die through contacting the tooth root profile of the die; (ii) positioning the inner (core) material pre-form within the annular shaped outer ring, thus creating a gear assembly and inherently aligning the core concentrically within the die; and (iii) forging the material assembly in a single forging step. Through this process it is expected that the two metals are mechanically locked through the flow of the material. An example of a bi-metallic gear is shown in Figure 2.13a.

Gears can be forged usefully from more than two initial components. For example, the use of three pre-forms is possible, where a high strength outer ring, lower strength and density central annulus, and high strength inner core are assembled. The high performance inner core allows for a high performance material to act as the interface to a driving shaft through keyways or splines. An example of a tri-metallic gear is shown in Figure 2.13b.

Pre-forms requiring elevated temperatures to improve material ductility may be heated before forging. In a gear combining materials of similar melting temperatures, pre-forms may be heated in a single furnace. However, for materials exhibiting substantially different forming and melting temperatures, such as aluminium and steel, two heating sources are required. The process of forging bi-metallic gears of such a material combination would be: (i) heating the core material to a temperature at which it can be formed in one furnace; (ii) heating the ring material in a second furnace at its recommended forming temperature; (iii) removing the ring material from the second furnace and positioning within the die; (iv) removing the core

material from the first furnace and positioning in the die concentrically within the ring; and (v) forming the two pre-forms together in a single step into the shape of the gear. Through this process, it is expected that in addition to mechanical locking of the two materials, the elevated temperature at the interface of the two metals may produce diffusion bonding, thus improving the structural integrity of the gear. A scheme of this hot forging process is shown in Figure 2.14.

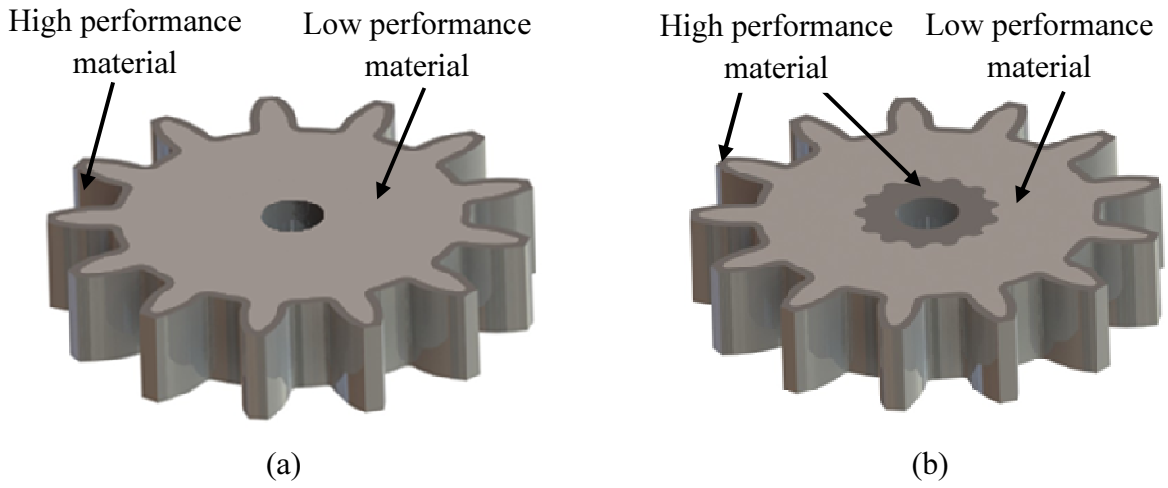


Figure 2.13: Multi-metal gears: (a) Bi-metallic gear and (b) Tri-metallic gear

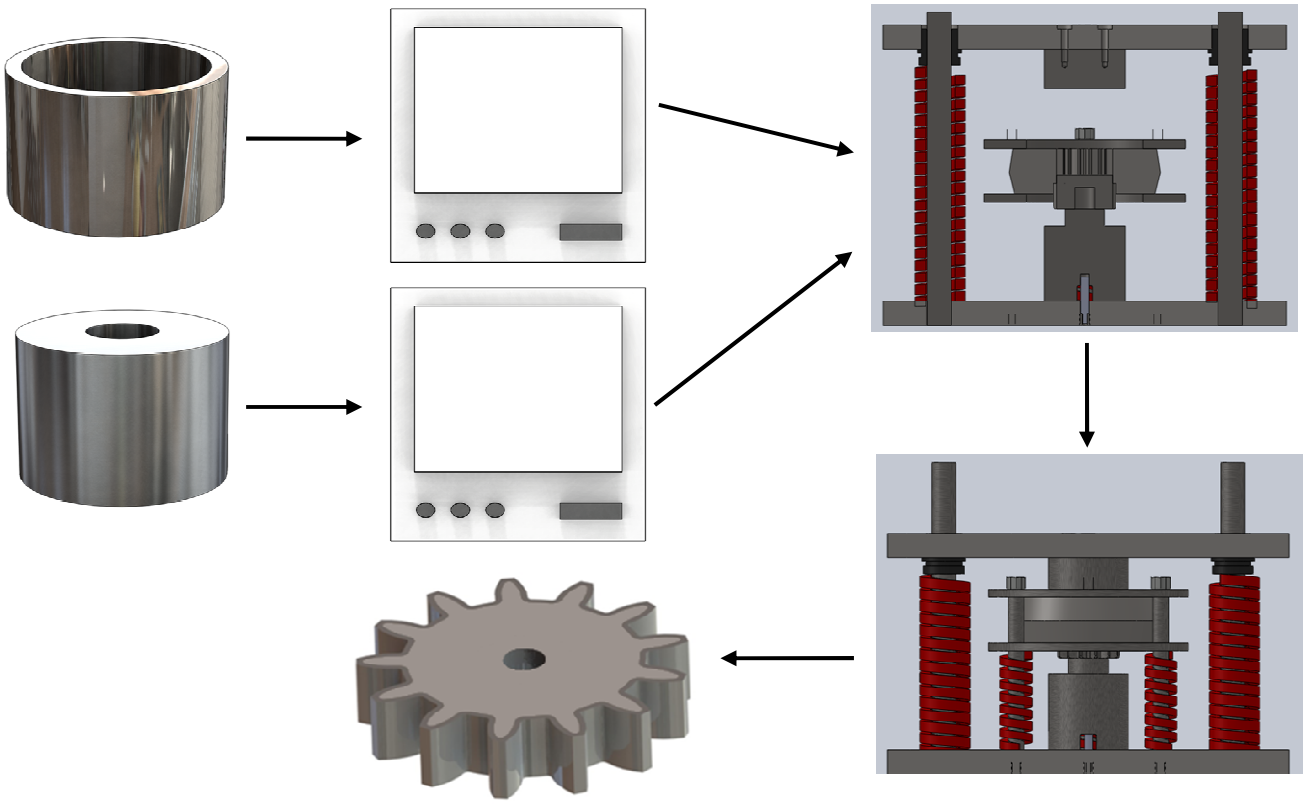


Figure 2.14: Schematic of bi-metal hot forging process

Because of the potential attractiveness of forged bi-metallic gears to industry and the dearth of scientific information relating to them, the work described in this thesis is designed to examine the feasibility of the process and obtain scientific information concerning forging characteristics and forged properties.

Chapter 3 Forging of Multi-Metal Gears

This chapter presents the tool-set which was designed and manufactured, as well as the laboratory equipment used to forge multi-metal gears. Furthermore, the dimensions and materials, allowing for both cold and hot forging using model and engineering materials are discussed. Finally, several mechanisms which were determined experimentally to lock together the two materials and prevent dismantling of the gear during operation are presented.

3.1 Equipment and Forging Tool

In order to perform gear forging in the laboratory under cold and hot forging conditions, a forging tool was designed using the Solidworks CAD program and subsequently manufactured. The tool was designed for forging spur gears as the spur gear profile is the simplest to machine through the electrical discharge machining (EDM) process, and avoids the need for complex ejection systems as used for example in helical gear forging (Sato, 1998; Sadeghi and Dean, 1992).

In relation to the design of the tool, the literature from Chapter 2 found that the Group 1B designs (4 working part toolset) offered a number of benefits. However, the fact that the majority of components, such as the mandrel and container, were attached to the ram would result in a tool set with a high centre of gravity as well as present difficulties in assembling it. As the tool set was required to be relocated frequently to free test equipment, Group 1B designs were deemed less safe than attaching the majority of components to a base plate. Therefore, Group 1A designs were considered for the tool used in this work.

With regards to the use of a penetrating punch, practical difficulties in applying to the toolset led to the use of a non-penetrating punch. For example, the costly and accurate machining as well as alignment to the ram to avoid interference with the die favoured the use of a non-penetrating punch. Furthermore, according to Tuncer and Dean (1987) the use of a moving container with a non-penetrating punch has the advantage of flash forming between the punch and the die, instead of 'extruding down the sides of the anvil and cause it to bind', thereby aiding ejection. Hence, a moving die rather than a fixed die was selected. Therefore, although the literature (Tuncer and Dean, 1987) suggests that the optimum design involves a moving die, moving mandrel, and penetrating and hollow punch, these constraints left three practical designs from Group 1A, namely: 1A-MMNH, 1A-MFNH and 1A-MMNS. In order to

simplify the design and facilitate the forging of solid gears and hollow gears for future tests, the final design chosen for the test rig was to allow the use of an interchangeable solid punch and punch with mandrel.

The final toolset assembled in a pillar tool-set arrangement is shown in Figure 3.1. As can be seen, the die is of the floating die concept positioned over a toothed counterpunch. The die is supported by springs which were compressed by the non-penetrating cylindrical punch when it descended. The mandrel is attached to the punch, and positioned beneath a spring, both of which lie on the cavity axis. During forging, this spring is compressed when the mandrel comes into contact with the counterpunch, hence avoiding damage to the mandrel. The engineering drawings of the tool set can be found in Appendix A.

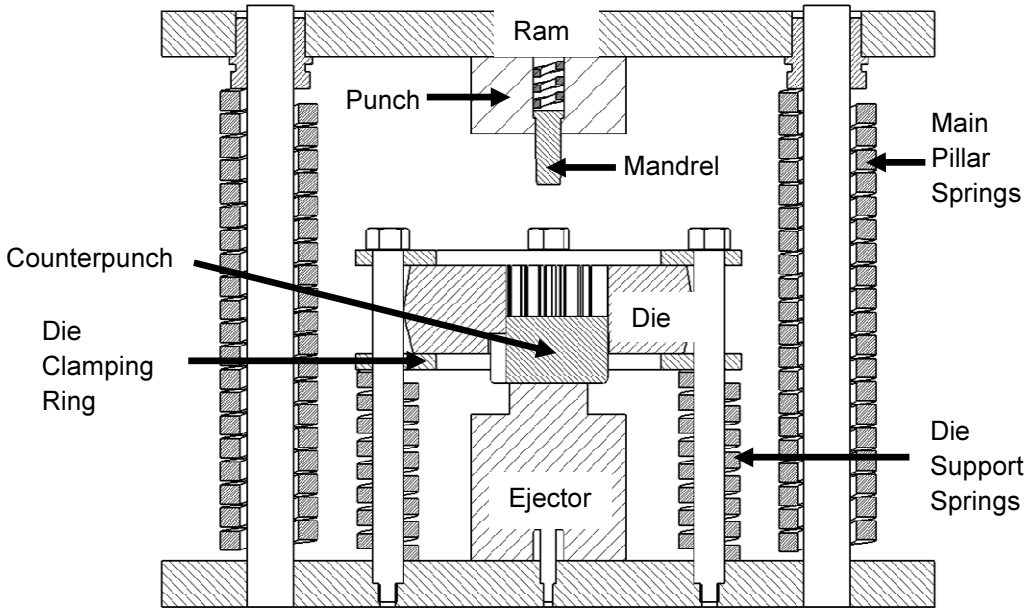


Figure 3.1: Gear forging tool design cross-sectional view

Upper and lower plates, main pillars, die guide pillars and die clamping rings were machined by DANLY UK with the remaining components machined in house. The springs, also supplied by DANLY UK were as follows: (i) 2x main pillar springs with code number 9-4048-110, (ii) 3x die support springs with code number 9-2420-110, (iii) 1x mandrel spring with code number 9-1207-110 and (iii) 2x bearing bushes with code number 6-3045-33. The dimensions of the die cavity machined through the EDM process were: (i) Addendum circle diameter = 75mm, (ii) Root circle diameter = 55mm, (iii) Pressure angle = 20^{o}, (iv) Module = 5mm and (v) 13 gear teeth. A 13 toothed gear was chosen in accordance to the literature; 13 teeth is the minimum required to avoid interference during gear meshing (Shigley and

Mischke, 2001), and as such is a practical, manufacturable component. The working tool components were machined from H13 tool steel in order to benefit from excellent strength and temperature resistance of this material. Furthermore, the die was required to be pre-stressed as according to Altan *et al.* (2005) this can lead to a 'two to tenfold improvement in the die life'.

3.2 Experimental Programme

To facilitate forging, the toolset was placed within the Instron 2.5 MN press as it was the largest load capacity press available in the laboratories (Figure 3.2a). In order to perform bi-metallic forging, the outer (ring) material was first positioned in the die followed by the central (core) material in order to ensure concentricity of the materials into the die during assembly. An example of the ring-core assembly into the die is shown in Figure 3.2b.

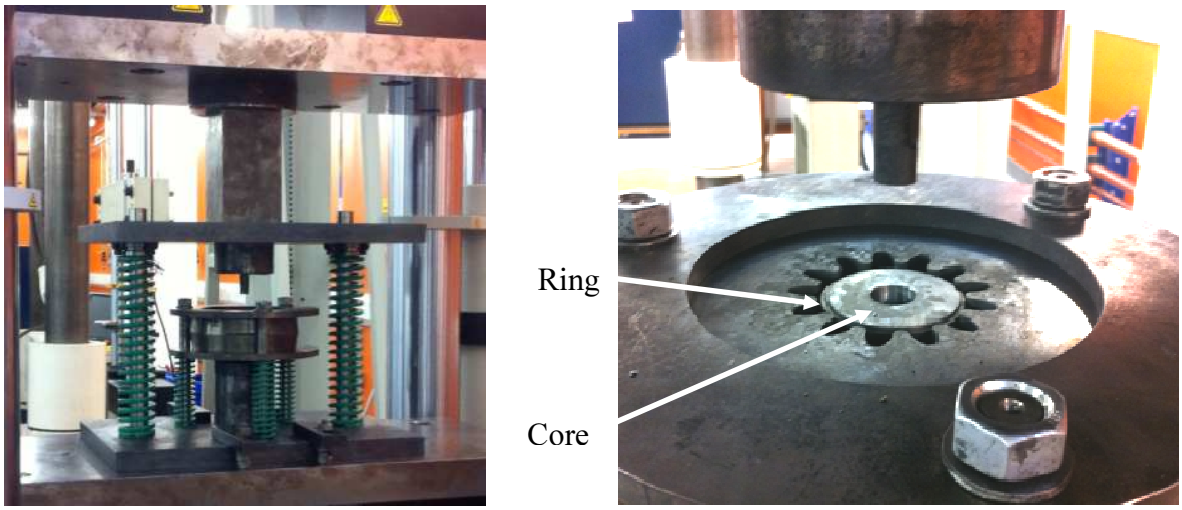


Figure 3.2: Toolset: (a) Mounted on press and (b) Ring and core assembly in die

To allow the hot-forging of multi-metal gears, specifically bi-metallic gears from engineering alloys, a Lenton AWF 13/5 and a Lenton chamber furnace of an unknown model were used for preheating ring and core to their respective recommended forming temperatures. A propane gas torch was used in the instance of hot forging, to pre-heat the toolset in order to minimise heat loss from the work-piece during forging. This experimental setup is shown in Figure 3.3.

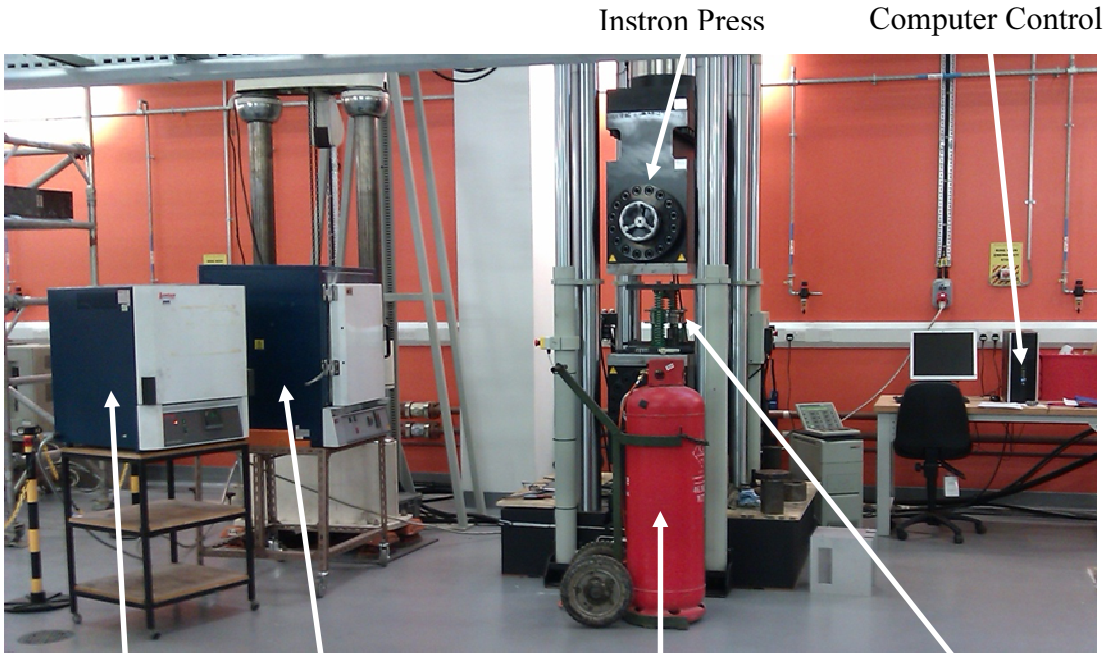


Figure 3.3: Experimental setup for hot forging

3.3 Test Materials and Billet Dimensions

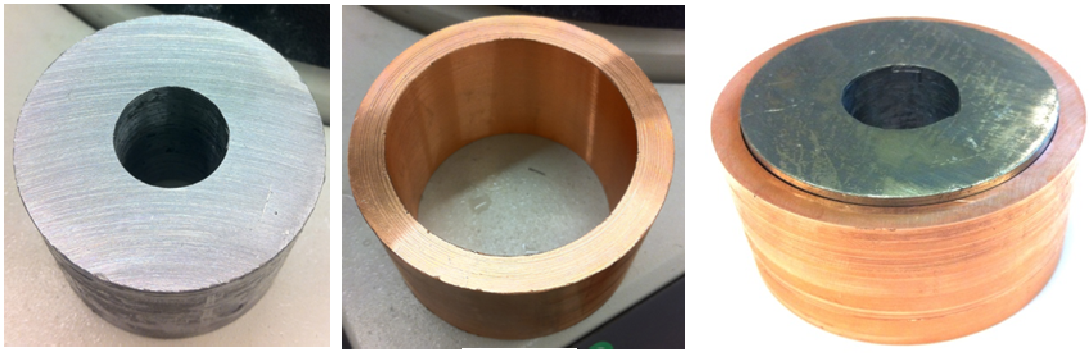
To forge bi-metallic gears, tests were performed under cold forging and hot forging conditions. Cold forging tests were performed using the model materials; copper C101 (tooth ring material) and commercially pure lead (core material). They are highly ductile at room temperature and so can be used to eliminate thermal effects from the forging process. Hot forging tests were performed using engineering alloys to forge lightweight gears. Aluminium (Al 6082-O) was used as the core material with steel (230M07) being used as the high strength ring material whose chemical composition is shown in Tables 3.1 and 3.2. The hot forging of these materials was necessary to reduce the overall forging load which was limited to 2.5MN by the press. Examples of these two pairings are shown in Figure 3.4.

Table 3.1: Al 6082 chemical composition (Aalco Metals Ltd., 2013)

Mn (%)	Fe (%)	Mg (%)	Si (%)	Cu (%)	Zn (%)	Ti (%)	Cr (%)	Others (Total)	Al (%)
0.40-1.00	0.0-0.50	0.60-1.20	0.70-1.30	0.0-0.10	0.0-0.20	0.0-0.10	0.0-0.25	0.0-0.15	Bal

Table 3.2: 230M07 chemical composition (Chandler, 1995)

C (%)	Mn (%)	P (%)	S (%)	Fe (%)
0-0.13	0.7-1.00	0.07-0.12	0.24-0.33	Bal



(ai) (aii) (aiii)



(bi) (bii) (biii)

Figure 3.4: Components: (ai) Lead core, (aii) Copper ring, (aiii) Lead-copper assembly and (bi) Aluminium core, (bii) Steel ring, (biii) Aluminium-steel assembly

The dimensions of the billet were constrained by the root diameter of the teeth in the die cavity and the volume of the forged gear. The outer diameter of the rings were approximately 54mm to allow them to be located concentrically, by the teeth roots, within the die. In order to evaluate the effect of ring thickness on the quality of a forged gear, ring thicknesses of 2mm, 4mm and 6mm were used. Furthermore, due to the differing thermal expansion of the two metals under hot forging conditions, the cold outer diameter of the aluminium core was calculated to ensure that it will expand to a value 0.2mm less than the inner diameter of the ring material, a gap which would allow the core to be located easily within the ring during assembly of the work-piece to be forged. In the hot forging experiments preliminary trials showed that the heating of the toolset resulted in core material flowing beneath the mandrel due to reduced mandrel spring stiffness, and hence a solid punch was used instead. In the cold forging experiments, lead billets were cast in three dies to each of the approximate dimensions required in order to minimise machining. A hole within the centre of the core was machined to 16.5mm to provide a small clearance with the 16mm mandrel of the toolset. Finally, the height of the core material (34mm) was greater than the height of the ring material (32mm) so that during forging, the core is compressed first, thus closing the space

between the core and ring, and between the core and mandrel before the ring is compressed. The dimensions of the cold and hot forged billets are shown in Tables 3.3 and 3.4, respectively. Finally, before forging, the surfaces of all ring and core components were polished with 1200 abrasive paper in order to reduce friction between them and the tools.

Table 3.3: Lead-copper dimensions

	Lead Core			Copper Ring		
Ring Thickness (mm)	**Height (mm)**	**Inner Diameter (mm)**	**Outer Diameter (mm)**	**Height (mm)**	**Inner Diameter (mm)**	**Outer Diameter (mm)**
2	34	16.5	49.6	32	49.8	53.8
4	34	16.5	45.6	32	45.8	53.8
6	34	16.5	41.6	32	41.8	53.8

Table 3.4: Aluminium-steel dimensions

	Aluminium Core		Steel Ring		
Ring Thickness (mm)	**Height (mm)**	**Outer Diameter (mm)**	**Height (mm)**	**Inner Diameter (mm)**	**Outer Diameter (mm)**
2	34	48.4	32	49.8	53.8
4	34	44.5	32	45.8	53.8
6	34	40.9	32	41.8	53.8

3.4 Cold Forging Multi-Metal Gears from Model Materials

The forging of bi-metallic gears under cold forging conditions involved the use of lead as the low strength core material and copper (C101) as the high strength outer ring material as they are highly ductile at room temperature and their relative flow stresses are similar to those of steel and magnesium or aluminium alloy, the metals that probably would be used in industrial processes. To minimise friction, graphite lubricant was applied to all tool surfaces that would come into contact with the work-piece. Fluorinated ethylene propylene (FEP) film and Mobil Grease 28 was also used on the punch and counterpunch to further reduce friction on these surfaces. In order to perform the forgings, the Bluehill 2 software was used with the Instron 2.5MN press at a low speed of 2.8mm/s throughout the stroke in order to minimise heat generated through deformation and to avoid a rapid overshoot in the load at the end of the forging which might have damaged the load cell.

Gears with ring thicknesses of 2mm, 4mm and 6mm were forged as discussed earlier. In order to analyse material flow post forging, two cross sections of the gear were made through the use of EDM: (i) through the mid-height of the gear, and (ii) through the root of a tooth and the tip of the adjacent tooth in the vertical direction. The cross sections of the 2mm, 4mm and 6mm gears in the horizontal direction are shown in Figure 3.5 below. The cross sections in the vertical direction are shown in Figure 3.6. As can be seen from Figure 3.5, the forging process caused the outer copper ring to be greatly deformed and led to severe thinning on the tooth flanks which caused the material to separate. The lead core flowed through this separation to complete tooth filling. However, thicker rings i.e. 4mm and 6mm do not show signs of this separation which suggests that there is a minimum ring thickness which is necessary to maintain the structural integrity of the gear.

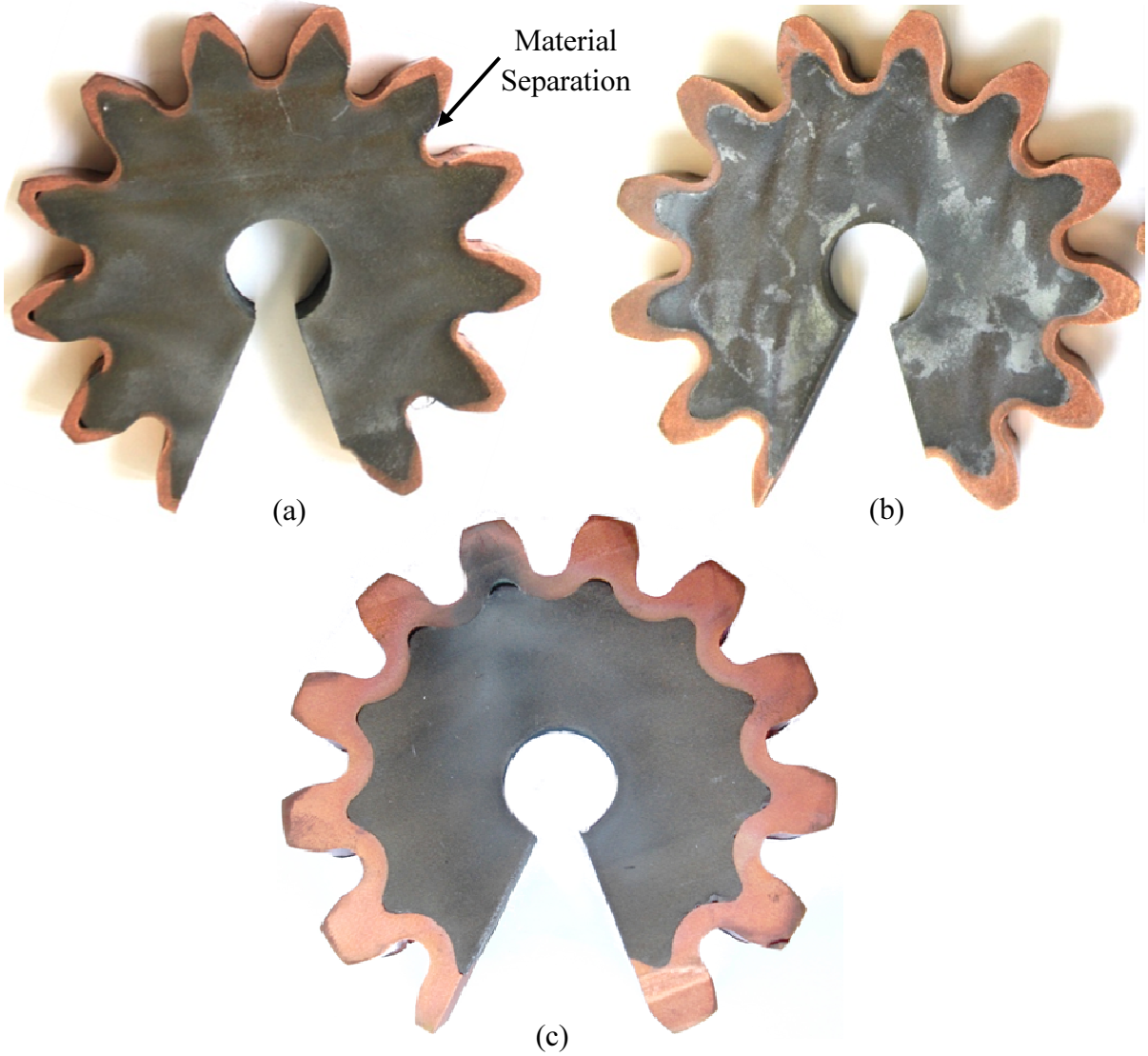
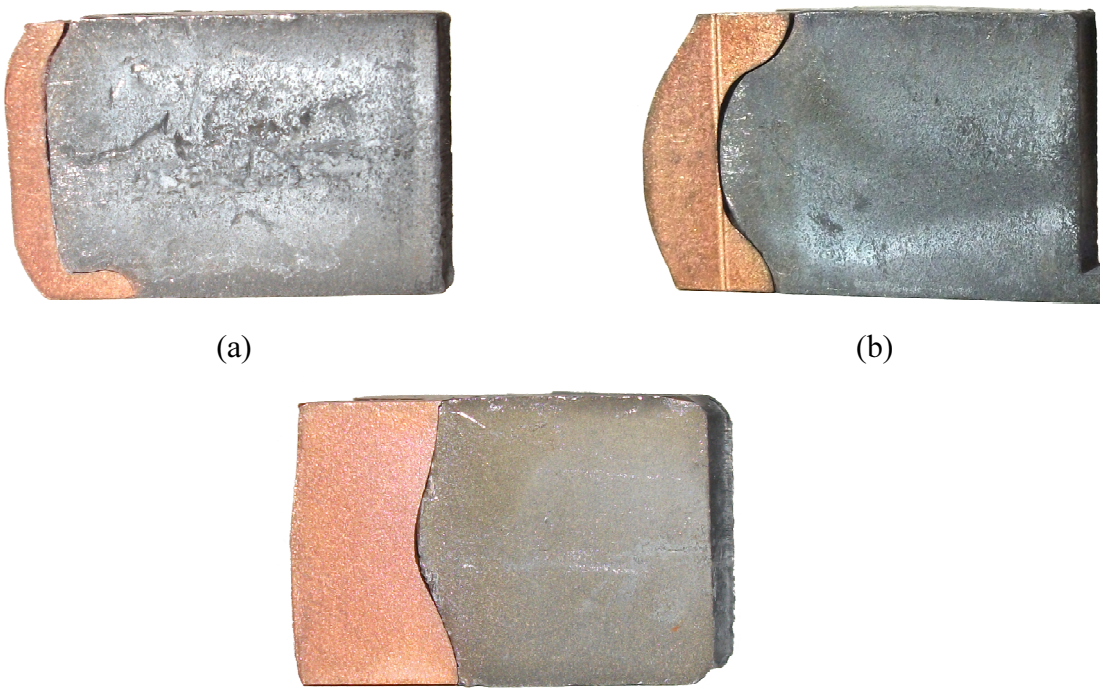


Figure 3.5: Cold forging of lead-copper gears with ring thicknesses: (a) 2mm, (b) 4mm, and (c) 6mm

The vertical cross-section through the midpoint of a tooth is shown in Figure 3.6 below. It can be seen that the ring material folds and contacts the punch and counterpunch as the gear is being forged, hence effectively locking the material in the axial direction. Furthermore, the figure shows that large ring thicknesses resulted in gears with incomplete die filling. The load cell of the Instron 250 ton press showed that forging the 2mm ring gear required over 2.1MN to fill the die, and therefore larger ring thicknesses would require loads exceeding that available from the press.



(a) (b)

(c)

Figure 3.6: Vertical cross section of lead-copper gears for: (a) 2mm, (b) 4mm and (c) 6mm gears

3.5 Hot Forging Multi-Metal Gears from Engineering Alloys

The cold forming tests described above utilised model materials in order to gain an understanding of the material flow during the bi-metallic forging process. However, gears used in real-life engineering applications require engineering alloys capable of withstanding operating conditions. Ideally, the material used as the outer ring material will be steel, or nickel super-alloys such as 16 MnCr5, AISI 4320 and AISI 9310 (Rakhit, 2000) currently used for gears. A low density engineering alloy such as that of aluminium or magnesium can be used as the lightweight core material. However, magnesium has certain negative

characteristics, such as corrosion and potential flammability, when working at high temperatures and requires more investigation as to its suitability. The use of a aluminium and steel combination is particular beneficial in practice, as aluminium has a density and yield strength of 2700kg/m^3 and 265MPa (CES Edupack, 2010) whereas gear steel can have values up to 7850kg/m^3 and 2000MPa (Lucefin Group, 2011; He *et al.*, 2004) resulting in a gear which may be both lightweight and withstand operating loads.

In this research project hot forging tests were performed using two materials: (i) 230M07 mild steel as the ring material, and (ii) Al 6082 for the core material. Mild steel is used for the outer material as opposed to gear steel due to the load limitations of the press. The ring thicknesses of 2mm, 4mm and 6mm were tested achieving weight reductions of approximately 57%, 47% and 38% compared to single material steel gears.

To assist material flow and reduce flow stress during forging, the two parts of the composite billets (cores and rings) were heated to the recommended forming temperatures found in the literature. Graphite lubricant was applied to the external surfaces of the composite billets and tool surfaces to provide effective lubrication at high temperature. Having applied the lubricant, the steel ring was heated to 1150^{o}C (Lucefin Group, 2011; Spittel and Spittel, 2009), whereas the aluminium core was heated to 535^{o}C to be below melting temperature (Aalco Metals Ltd., 2013; CES Edupack, 2010). In order to minimise the heat transferred from work-piece to toolset, the toolset was heated through the use of gas torch to a temperature of 200^{o}C, measured using an infrared thermometer. Once both billets are uniformly heated to the required temperature, determined through thermocouple measurements of secondary samples in each furnace, the steel ring was first removed from the furnace and placed into the die. The core was then positioned inside the ring. Once assembled, the press operated to form the bi-metallic gear in a single step.

In order to perform hot forging, the Wavematrix program was used with a 2 step profile, whereby the speed of the forging was conducted at 10mm/s and for the final 1mm of stroke, the speed was reduced to 1mm/s to reduce the overshoot of the load and prevent damage to the load cell and press. A maximum speed of only 10mm/s could be used as this was the maximum speed available to allow for a two step profile.

Post forging, two cross sections of the gear were made through the use of EDM: (i) through the mid-height of the gear and (ii) through the root of a tooth and the tip of the adjacent tooth

in the vertical direction, as for the cold forming tests described above. The cross sections of the 2mm, 4mm and 6mm gears in the horizontal direction are shown in Figure 3.7 below. Cross sections in the vertical direction are shown in Figure 3.8.

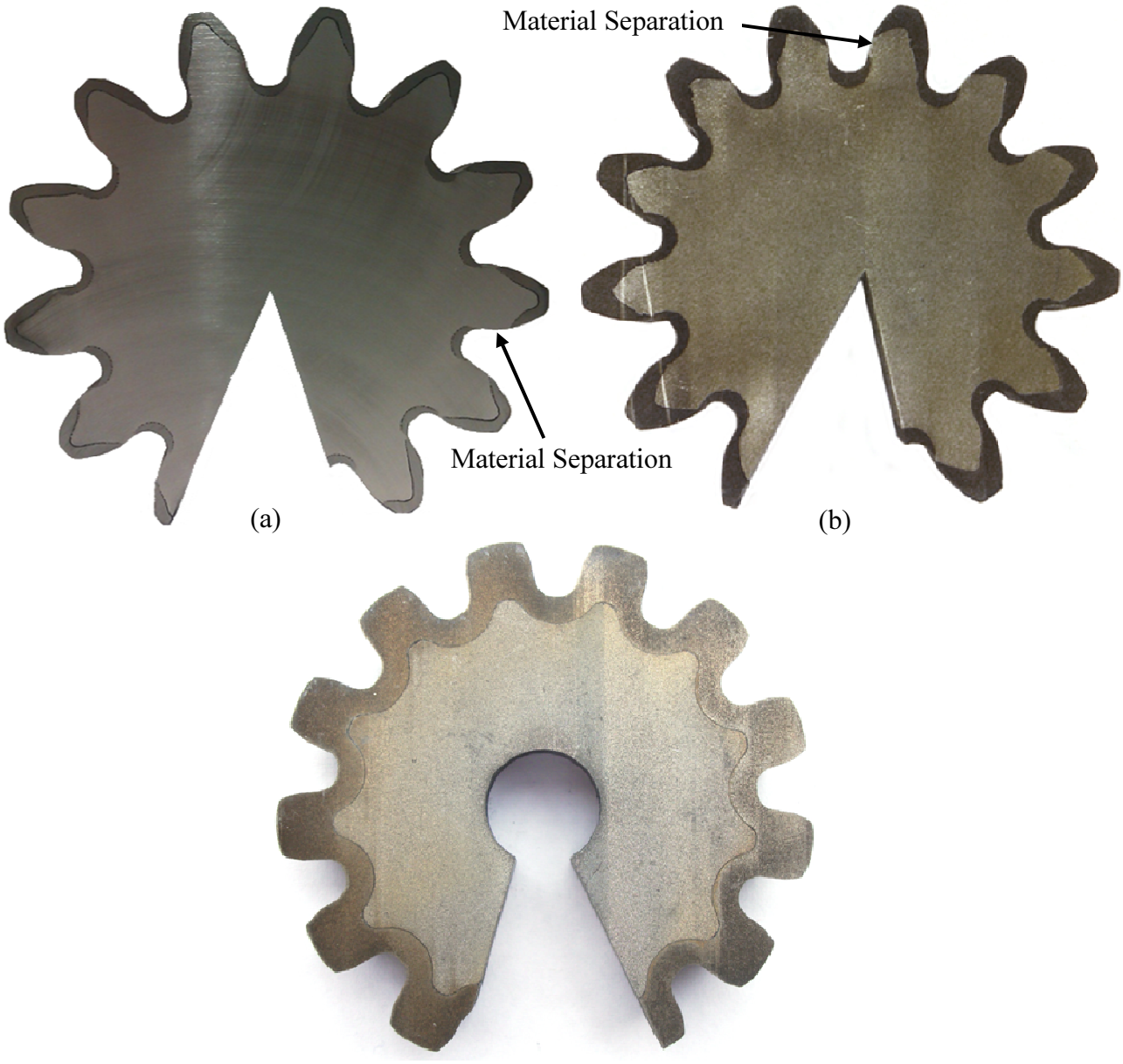


Figure 3.7: Hot forging of aluminium-mild steel gears with ring thicknesses: (a) 2mm, (b) 4mm, and (c) 6mm

As for the cold forming experiments, it can be seen from Figure 3.7a that thinning of the initially thinnest ring has led to separation near and below the pitch line. The aluminium core has flowed to form this region of the tooth flank. Thicker rings reduce the amount of thinning

which takes place, as shown in Figures 3.7b and 3.7c. However, unlike the lead-copper combination, the 4mm ring thickness gear has also suffered from material separation on the ring, which suggests that the minimum ring thickness needed to maintain structural integrity depends on properties (perhaps relative properties) of the work-piece metals. Further tests were attempted to reduce thinning further, in a fully formed tooth cross-section, by using a 6mm steel ring. However, the forging load necessary to form a complete tooth profile, on any section, exceeded the maximum load which can be applied by the Instron press and hence, a completely filled 6mm gear could not be forged.

A vertical cross-section through the midplane of a tooth is shown in Figure 3.8. As for cold forging, the ring material folded, locking the core and ring material in the axial direction.

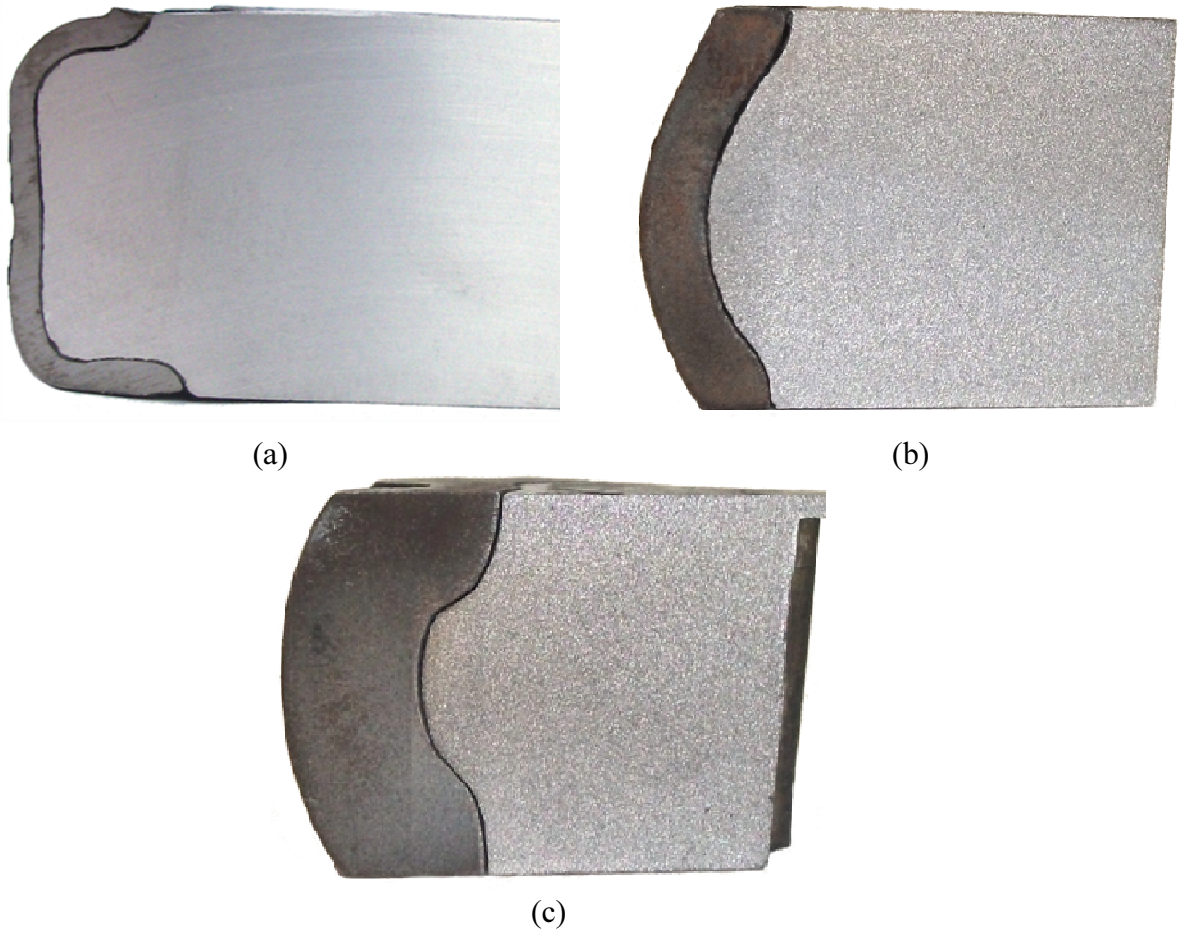


Figure 3.8: Vertical cross section for: (a) 2mm, (b) 4mm and (c) 6mm gears

An effect observed in both hot forging and cold forging is that for rings of thickness 2mm and also for 4mm in the case of hot forging, ring separation tends to occur on only one side of every tooth. It has been observed that there appears to be an effective mirror/symmetry line,

whereby on one side of this line (Figure 3.9) the ring tends to separate on the same side of each tooth and on the other side of this mirror line, the ring tends to separate on the opposite side of every tooth.

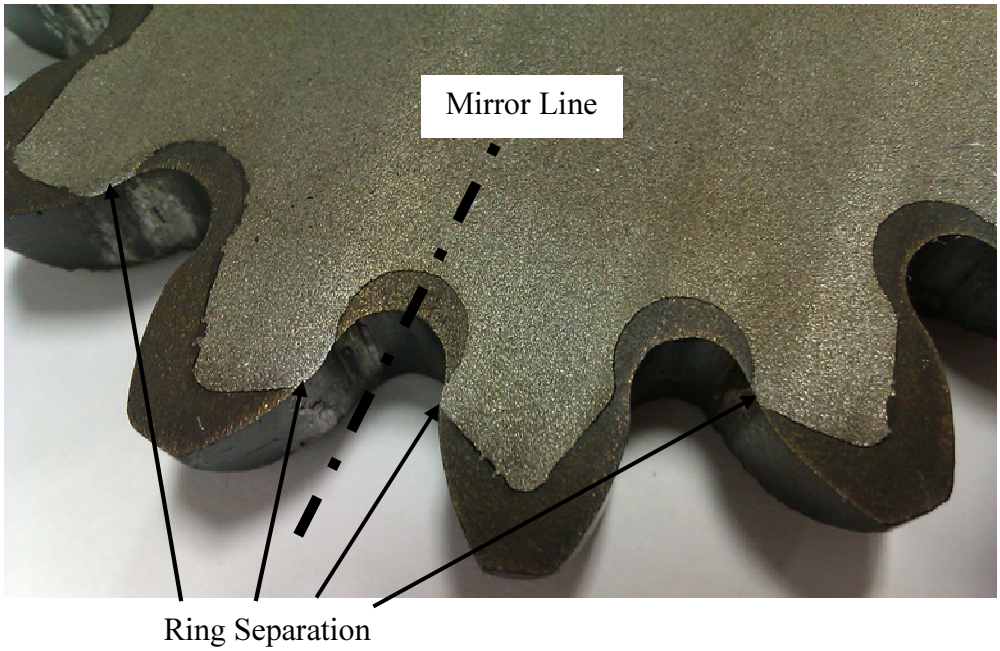


Figure 3.9: **Asymmetric separation**

A possible explanation for this effect could be the misalignment of the ring-core assembly of the gear inside the die. As there is a space between the outer diameter of the ring and the root diameter of the gear profile of the die, it is possible that the ring-core assembly is not positioned precisely concentrically in the centre of the die, and may be touching the root of a tooth on one side, thus leaving a large space between the ring and die on the other side. Where the assembly is closest to the die will be the point at which the line of symmetry passes through. The effect of misaligned work-pieces is described in the literature (Ibhadode and Dean, 1988) which shows that the 'more a billet is located off-centre, the greater the load' as there is 'extra frictional work on the die wall'. This is described as incurring distortion of the work-piece and could be a possible cause for this mirror effect. Further tests will need to be conducted by adjusting the alignment of the work-piece in the die to gain better understanding of this effect.

3.6 Material Locking Mechanisms

A crucial requirement of a multi-metal gear during operation is to ensure that the various metals do not disengage during operation. A number of naturally occurring locking mechanisms between the two parts of a gear were investigated and are discussed below.

3.6.1 Macro-Mechanical Locking

The primary means of preventing the two metals from disengaging is the lock achieved both rotationally and axially due to the metal flow shown in Figures 3.7 and 3.8 above. Rotational locking is caused by the deformation of both materials into the gear tooth shape during deformation, whereas axial locking is achieved by barrelling due to friction. This type of locking mechanism is achieved in both cold and hot forging.

3.6.2 Diffusion Bond Interface

The formation of a diffusion bond between metals is dependent on the combination of pressure, elevated temperature and time and is possible to be formed during hot forging. According to the literature, a diffusion bond is formed when the temperature of the lower melting temperature material reaches between 0.5-0.8 of the melting temperature (Loh *et al.*, 1993). The authors Loh *et al.* (1993) and Cline (1966) state that the formation of a diffusion bond is a two step process, where (i) 'the applied load causes plastic deformation....which reduces the interfacial voids' and (ii) 'the bond develops by diffusion controlled mechanisms such as grain-boundary diffusion and power-law creep'. The literature also states that the quality of surface finish becomes less critical on the bonding of metals with large enough pressures (Yiasemides, 1987).

Therefore, an investigation of a potential diffusion bond was performed on a section of the interface between the two metals by extracting a sample from the 4mm ring thickness gear through the use of EDM, and analysing with Scanning Electron Microscopy (SEM). The sample was extracted from the tooth root, as incomplete die filling and low forming speeds of the press resulted in the specimens substantially cooling down towards the end of the stroke and reduced the likelihood of a diffusion bond being formed at the tooth tip.

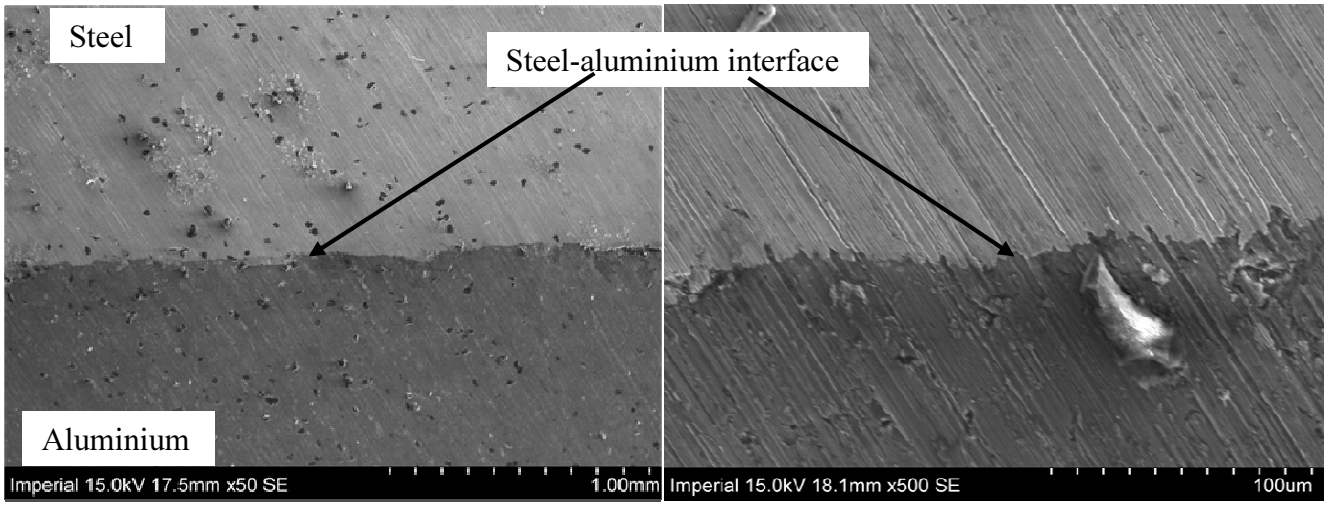
The subsequent specimen was embedding in bakelite using the Struers LaboPress-3 and the surface was grinded with the Metaserv 2000 grinder/polisher, first with coarse 240 grit abrasive paper to remove scratch marks caused by the EDM, followed by finer 600, 800 and 1200 grit abrasive paper. The specimen was then polished to 1μm using a Metaserv universal polisher. An example of the extracted sample is shown in Figure 3.10.



(a) (b)

Figure 3.10: Interface boundary sample: (a) Extracted through EDM from tooth and (b) Mounted in bakelite

SEM photographs of this interface boundary are shown at low and high magnification in Figures 3.11a and 3.11b, respectively. As can be seen, at a high magnification there is no presence of voids although it is difficult to identify an intermetallic phase.



(a) (b)

Figure 3.11: SEM photo of interface between steel and aluminium at: (a) low and (b) high magnification

The difficulty in observing intermetallic compounds of iron and aluminium can be explained by a variety of factors. In the literature, the growth of an intermetallic compound is dependent on the duration at which the specimen is held at elevated temperatures. Rathod and Kutsuna (2004) discuss that holding steel and aluminium at 550^{o}C for a duration of 10s just begins to grow an inter-metallic compound as separate particles. Furthermore, holding for substantial lengths of time such as 100s has the effect of significantly increasing the thickness of any such compound. However, as the hot forging of gears was performed in approximately 10

seconds, and the two metals of the gear were not held at constant temperatures and had cooled throughout the forging process, such intermetallic compounds would be difficult to form. Moreover, as reported by Abdel-Rahman and Dean (1981), a heavy layer of oxide forms on the surface of steel billets when heated to high temperatures such as 1200^{o}C, which when removed by 'knocked off prior to forging, quickly reformed'. Such an oxide layer may have also interfered in the bonding of the two metals. Furthermore, there is the possibility that graphite lubricant used to lubricate the toolset may have seeped into the clearance between the core and the ring, creating a barrier to diffusion bonding.

The determination of elemental compounds in a weld is typically performed through Energy-dispersive X-ray spectroscopy (EDX) analysis, or for higher resolution, transmission electron microscopy (TEM) (Li *et al.*, 2008). An EDX line scan was performed across the interface from steel to aluminium as shown in Figure 3.12a.

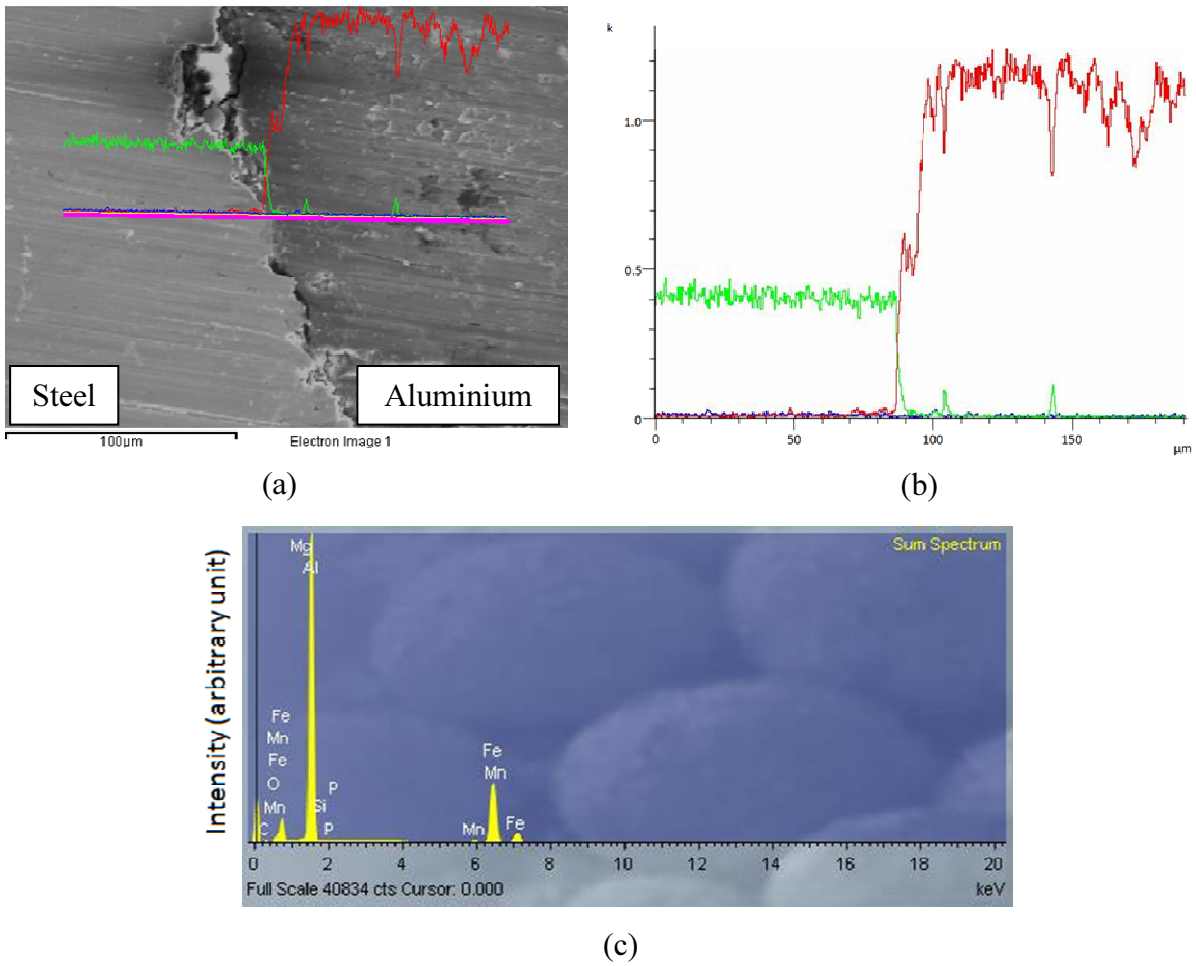


Figure 3.12: EDX analysis of interface region: (a) Line scan of joining zone, (b) Enhanced version of line scan, and (c) Elemental composition chart

As can be seen from Figure 3.12b, there is an abrupt transition from the steel to aluminium with no identifiable inter-metallic zone being formed at the resolution of the equipment used. Furthermore, the elemental analysis of Figure 3.12c, is typically performed in an intermetallic phase region to identify the weight percentage of elements present in the compounds of a clear weld and hence does not indicate a weld being formed. It is anticipated that should forgings be performed at a higher rate in a protective atmosphere, and the issues described earlier are resolved, a more visible and quantifiable diffusion bond will be present.

3.6.3 Micro-Mechanical Locking

Another locking mechanism which has been identified through SEM is micro-mechanical locking. As shown in Figure 3.13, this locking method is achieved through protrusions of one material into another, in this case the steel into the softer aluminium. This form of locking may occur through imperfections on the surfaces of the two metal billets whereby a small scratch or dent on the surface of one component is filled with material from the other.

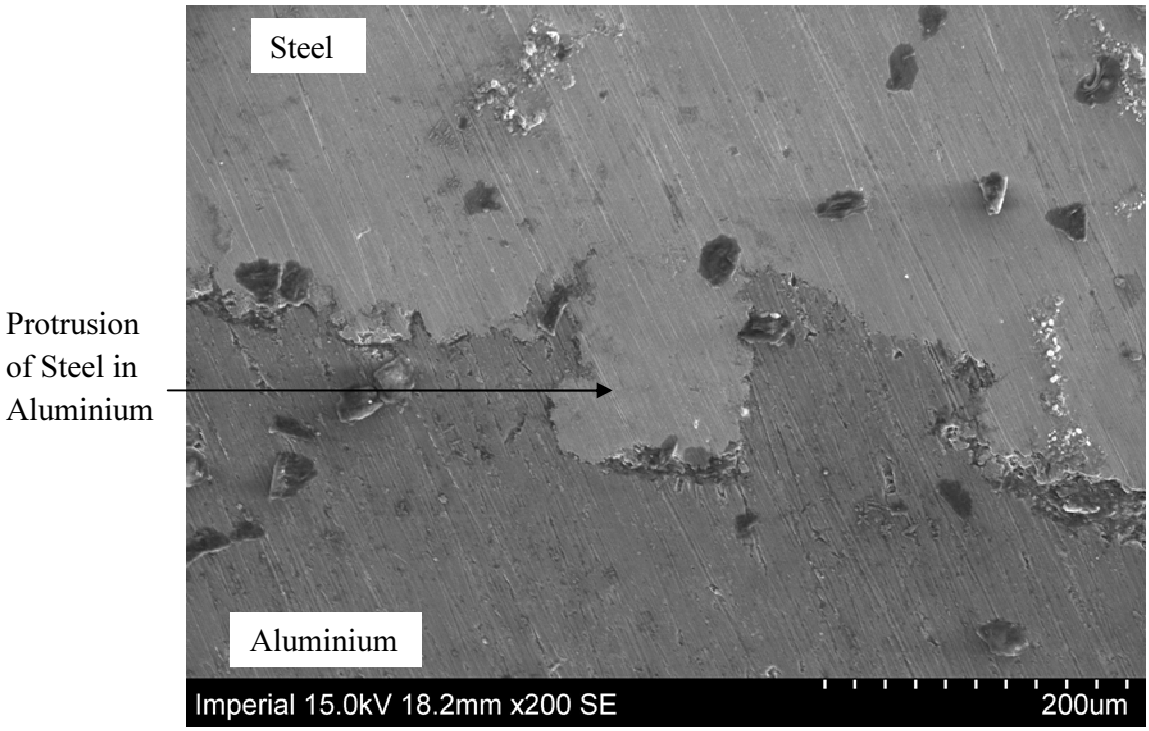


Figure 3.13: SEM photo of protrusion of steel in aluminium in tooth root

Examination of the results has revealed that it is possible for three locking mechanisms to occur during the forging of engineering alloys, which coupled together, probably would prevent the components of a multi-metal gear from disengaging. More experimental work is necessary to determine the strength of these locks.

Chapter 4 Development of Unified Visco-Plastic Constitutive Equations

This chapter describes the constitutive equations which have been used to characterise the behaviour of the metals used in this research, under a range of strain rates and temperatures. Experiments were conducted using a Gleeble 3800 thermo-mechanical testing machine for the alloys Al 6082-O and 230M07, used in the hot forging of bi-metallic gears, as well as the alloy 16MnCr5, to determine the difference in behaviour between mild steel and a typical gear steel. The flow stress-strain data obtained for a range of strain rates and temperatures are fitted through a set of unified constitutive equations to provide an analytical representation of the experimental results.

4.1 General Constitutive Equations

The thermo-mechanical behaviour of a work-piece during the hot forging process affects the load experienced by a forging press as well as the metal flow. In the case of bi-metallic gears for example, the degree of thinning of the ring material during deformation will affect the quality and structural integrity of the forged gear. In order to understand the hot forging behaviour of bi-metallic gears, the variation of flow stress of the work-piece material during variations of temperature and strain rate must be determined in order to accurately determine metal flow. The behaviour of materials during deformation can be described through constitutive equations applicable to the range of operating conditions. This can enable an accurate simulation of the process, to be undertaken.

The constitutive equations identified in the literature (Guo *et al.*, 2005; McQueen, 1993), which are typically used to describe the hot working of metals, are expressed in the forms of a power law, exponential law, and hyperbolic sine law, as shown in equations 4.1 - 4.3, respectively.

$$\dot{\varepsilon} = A^{'}\sigma^{n'}exp\left(\frac{-Q}{R_gT}\right) \qquad Eqn\ 4.1$$

$$\dot{\varepsilon} = A^{''}exp(\beta\sigma)exp\left(\frac{-Q}{R_gT}\right) \qquad Eqn\ 4.2$$

$$\dot{\varepsilon} = A^{'''}(\sinh\alpha\sigma)^{n''}exp\left(\frac{-Q}{R_gT}\right) \qquad Eqn\ 4.3$$

Where: $\dot{\varepsilon}$ is the strain rate, σ is the flow stress, Q is the activation energy for deformation, R_g is the gas constant (R_g = 8.31 J/mol K) and T is the working temperature. The symbols A', A'', A''', n', n'', α and β $(= \alpha n'')$ are constants. The equations shown above may also be found in the literature expressed in terms of the Zener-Hollomon parameter (Z) given by the expression $Z = \dot{\varepsilon} exp\left(\frac{Q}{R_g T}\right)$ (Zener and Hollomon, 1944).

According to McQueen *et al.* (2009), equation 4.1 can be applicable 'across a very broad range (of stress, temperature, and strain rate) but with a variation in n''. However, the authors McQueen *et al.* (2009) state that the power law relationship for predicting $\sigma - T - \dot{\varepsilon}$ behaviour can break down when the exponent n' is required to rapidly rise to model high stresses at high temperatures and hence the use of a single value for this constant would only be applicable 'over a narrow processing range' (McQueen *et al.*, 2009). In other words, the power law 'loses linearity at high stresses' (McQueen and Ryan, 2002). The exponential equation on the other hand (equation 4.2) loses linearity at low stresses and 'breaks down at high T below $1s^{-1}$' strain rates (McQueen and Ryan, 2002). The hyperbolic sine law of equation 4.3 effectively incorporates both of the equations 4.1 and 4.2. This law is used to predict the steady state flow stress for various temperatures and strain rates typically based on the peak flow stress (Valberg, 2010; McQueen and Ryan, 2002). However, the equation is not applicable for the initial low strain behaviour. According to Rieiro *et al.* (2010), constitutive equations must: '(a) characterise flow behaviour in a given strain rate and temperature range, and (b) should reproduce stress-strain curves with high statistical quality'. Thus, these equations are not well suited to simulating the forging of gears, where sections of the billet experience large variations in strain rate and temperature.

In order to predict the material flow behaviour through a large range of strain rates and temperatures, a phenomenologically controlled set of equations described by Foster (2007), Lin and Liu (2003) and Lin *et al.* (2002) have been adapted for gear forging. A phenomenological approach, which involves several variables with physical meaning, allows the mechanical response of the material to be accurately described (Kocks, 1976). The equations used allow for the incorporation of physical parameters, such as stress, plastic strain rate, isotropic hardening, and dislocation density, and are described in the section below.

4.2 Unified Visco-Plastic Constitutive Equations

During the forging of gears, dynamic microstructural changes which occur in the material 'are dependent on strain rate, temperature and the material initial microstructure and composition' (Lin and Dean, 2005; Sellars, 1990). Physical variables such as 'dislocation density, recrystallisation and grain size evolution' occur simultaneously in the material, and the use of traditional constitutive equations described earlier may not adequately represent the forging process. In order to develop a set of equations to model the coupling of these effects, Lin and Liu (2003) first identified 'mechanisms and driving forces for recovery, recrystallisation, grain size evolution' as well as the 'dislocation density and average size of precipitate' (Lin and Dean, 2005). This allowed the modelling of the 'microstructural evolution and visco-plastic flow of metals' (Lin and Dean, 2005) during deformation. The equations developed by this 'mechanism-based approach' (Shi *et al.*, 2010) have been coined as 'physically based unified visco-plastic constitutive equations' (Shi *et al.*, 2010; Lin and Dean, 2005; Lin *et al.*, 2005; Lin and Liu, 2003; Lin *et al.*, 2002).

Stress-strain relationships for metals at low (cold working) temperatures below the recrystallisation temperature, such as temperatures less than $0.4T_m$ are generally described by a strain hardening power law such as equation 4.4 (Altan *et al.*, 2005).

$$\sigma = K\varepsilon_p^N \qquad Eqn\ 4.4$$

Where in this equation, ε_p is the plastic strain, σ is the stress, K is the stress constant and N is the strain hardening exponent constant. However, during hot forming operations at temperatures greater than the recrystallisation temperature ($0.5T_m$), the 'influence of strain rate becomes increasingly important' (Altan *et al.*, 2005) as 'thermally activated processes become significant' (Mohamed *et al.*, 2012). Therefore, a plastic strain rate term $\dot{\varepsilon}_p$ as well as a strain rate hardening exponent (m') are including in the Fields-Backofen equation as shown in equation 4.5 (Cheng *et al.*, 2008; Gronostajski, 2000; Fields and Bachofen, 1957).

$$\sigma = K\varepsilon_p^N \dot{\varepsilon}_p^{m'} \qquad Eqn\ 4.5$$

Visco-plastic flow occurs when the applied stress exceeds the initial yield stress (k) (Altan *et al.*, 2005), and hence the stress can be expressed as $\langle \sigma - k \rangle_+$, 'where only positive values are valid, i.e. stress must exceed the yield point for consideration of visco-plastic flow to be meaningful' (Lin and Dean, 2005; Lin *et al.*, 2002). Furthermore, by removing the isotropic

hardening of the material (R) which occurs at a given plastic strain due to 'dislocation entanglement and pile-ups', the visco-plastic flow stress is represented as $\langle \sigma - R - k \rangle_+$. The visual representation of the effect of these components on the flow stress can be found in the work performed by Foster (2007). Hence, by rearranging equation 4.5 and including these terms, the plastic strain rate can be calculated as shown in equation 4.6:

$$\dot{\varepsilon}_p = \left(\frac{\sigma - R - k}{K} \right)^n \qquad Eqn\ 4.6$$

Where: n is a material constant, and K is a temperature dependent constant. The isotropic hardening variable (R) 'is caused by the build-up of dislocations and is proportional to the square root of dislocation density' (Shi, *et al.*, 2010; Estrin, 1998). Therefore, R can be represented by equation 4.7 below:

$$R = B(\bar{\rho})^{0.5} \qquad Eqn\ 4.7$$

Where: 'B is a temperature dependent material constant and $\bar{\rho}$ is a normalised dislocation density' (Shi *et al.*, 2010). The normalised dislocation density can be written as $\bar{\rho} = 1 - \frac{\rho_i}{\rho}$, where: ρ_i and ρ are the initial and current dislocation density. According to the literature (Shi *et al.*, 2010) the value of $\bar{\rho}$ can vary between 0 and 1 where 0 is the initial state and 1 is the maximum value, or saturated state of a dislocation network. Lin and Dean (2005) state that there are three softening mechanisms included in the $\bar{\rho}$ term, namely: (i) dynamic recovery, (ii) static recovery (annealing) and (iii) recrystallisation. The effect of recrystallisation occurs 'when the normalised dislocation density reaches a critical value, given sufficient time'. As forging experiments are performed in a short period of time, recrystallisation will not have time to occur and is thus ignored. Hence, the dislocation density equation can be reduced to equation 4.8 below:

$$(\dot{\bar{\rho}}) = A(1 - \bar{\rho})\left|\dot{\varepsilon}_p\right| - C\bar{\rho}^{\delta} \qquad Eqn\ 4.8$$

Where: A, C and δ are material constants. The first term 'models both the development of dislocation density due to plastic strain and dynamic recovery of dislocation density', whereas 'the second term is due to the static recovery of dislocation density during the thermal process' (Shi *et al.*, 2010). Finally, during the elastic deformation range, Hooke's law can be applied resulting in equation 4.9 below, where E is the elastic modulus, ε_T is the total strain and ε_p is the plastic strain (Mohamed *et al.*, 2012; Shi *et al.*, 2010):

$$\sigma = E(\varepsilon_T - \varepsilon_p) \qquad Eqn\ 4.9$$

Effects such as damage evolution have been incorporated in the constitutive equations found in the work performed by Mohamed *et al.* (2012) and Foster (2007) to predict 'the decrease in flow stress at later stages of deformation' for tensile tests. However, as the effects of inclusion related damage through micro-cavity growth occur during tensile rather than compression tests (Lin *et al.*, 2005), the damage terms have been removed from the constitutive equations used for gear forging.

The unified visco-plastic constitutive equations 4.6 - 4.9 involve several constants, namely: k, K, B, C, and E which are temperature dependent and can be expressed through Arrhenius relationships as shown in equations 4.10 - 4.14 below (Bai *et al.*, 2013; Foster, 2007):

$$k = k_o exp\left(\frac{Q_P}{R_g T}\right) \qquad Eqn\ 4.10$$

$$K = K_o exp\left(\frac{Q_A}{R_g T}\right) \qquad Eqn\ 4.11$$

$$B = B_o exp\left(\frac{Q_B}{R_g T}\right) \qquad Eqn\ 4.12$$

$$C = C_o exp\left(\frac{Q_C}{R_g T}\right) \qquad Eqn\ 4.13$$

$$E = E_o exp\left(\frac{Q_E}{R_g T}\right) \qquad Eqn\ 4.14$$

Where: k_o, K_o, B_o, C_o, E_o, Q_P, Q_A, Q_B, Q_C and Q_E are temperature independent constants. T is the temperature in Kelvin and R_g is the universal gas constant 8.31 J/mol.K. The values of these constants have been determined by fitting experimental results conducted over a range of strain rates and temperatures as described below.

4.3 Gleeble Compression Tests

In order to determine values of the constants in the above equations, compression tests were performed on samples with dimensions 8mm diameter by 12mm length (Bai *et al.*, 2013; Mohamed *et al.*, 2012) and using the Gleeble 3800 thermo-mechanical testing machine. As the 16MnCr5, 230M07 and Al 6082 were supplied in bar form with outer diameters 63.5mm, 60mm and 60mm respectively, samples of 10mm diameter were extracted from the cylindrical bars through the use of EDM. The samples were then turned down to the required

dimensions for testing. The tests were performed for a 50% reduction in height (Altan *et al.*, 2005) and diametral strains were measured using a C-gauge. Nickel based graphite paste with the commercial name, Thred Gard Anti-Seize & Lubricating Compound and graphite paper with the commercial name Grafoil, of 1mm thickness were used between the surfaces of the sample and the anvils of the Gleeble in order to minimise barrelling and to withstand high temperatures. An example of the experimental setup, and samples before and after compression, are shown in Figures 4.1a and 4.1b, respectively.

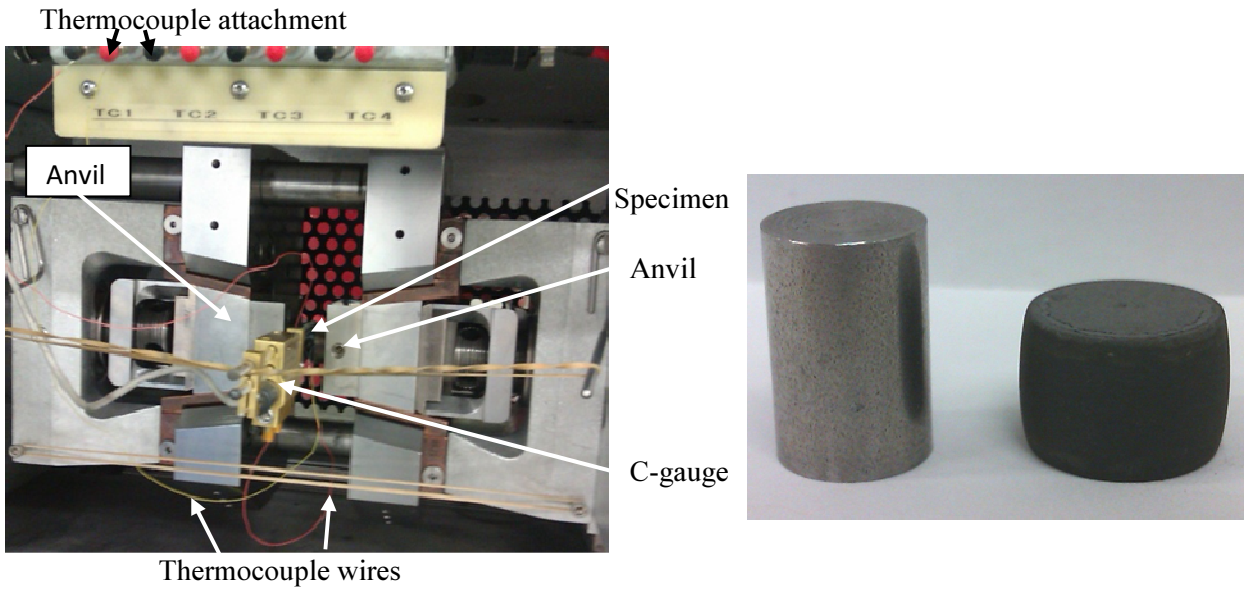


Figure 4.1: Gleeble compression tests: (a) Experimental set-up and (b) Sample before and after compression

Isothermal, constant strain rate tests were performed for three materials, namely: (i) Al 6082-O, (ii) 230M07 mild steel, and (iii) 16MnCr5 gear steel. For each material, tests were conducted for strain rates of $0.1s^{-1}$, $1s^{-1}$ and $10s^{-1}$ over the range of working temperatures which were considered to be adequate to encompass those arising in forging, as shown in the test matrix of Table 4.1. Specimens were resistance heated with the test temperature controlled through an attached thermocouple. Repeat tests were performed for each test condition.

A thermal cycle, as shown in Figure 4.2 was input into the Gleeble 3800 in order to perform the tests at the target temperature. During this cycle, the material experiences 5 stages: (a) heating at $10^{o}C/s$ to a temperature $50^{o}C$ below target temperature, (b) heating at the lower rate of $5^{o}C/s$ to reach target temperature whilst avoiding overshoot, (c) soaking for 60 seconds, (d) deformation and (e) water quenching to room temperature. The thermal cycle of

Figure 4.2 demonstrates the temperature profiles for 230M07 mild steel, with letters A-E representing the 5 stages.

Table 4.1: Compression test matrix

Material	Temperature (°C)	Strain Rate (s^{-1})		
		0.1	1	10
Al 6082-O	550	✓	✓	✓
	500	X	✓	X
	450	X	✓	X
230M07	1150	X	✓	X
	1100	✓	✓	✓
	1000	X	✓	X
	900	✓	✓	✓
16MnCr5	1000	X	✓	X
	950	✓	✓	✓
	900	X	✓	X

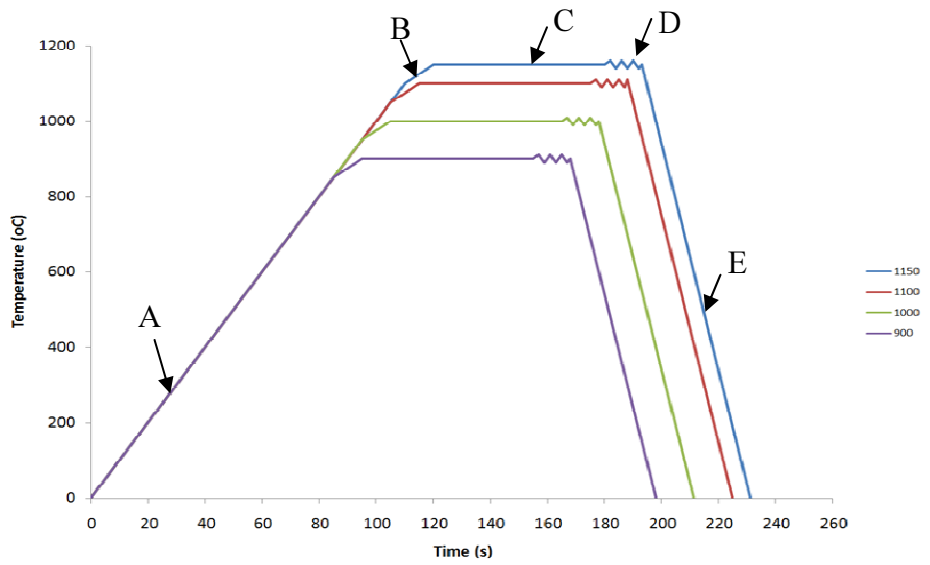


Figure 4.2: Thermal cycle during Gleeble testing for 230M07 mild steel

Sections 4.3.1 - 4.3.3 below present the results obtained from the compression tests.

4.3.1 Al 6082-O Aluminium Alloy Compression Test Results

Tests were first conducted for Al 6082-O at strain rates of $1s^{-1}$ for temperatures of 450, 500 and 550°C which encompassed the temperature 535°C typically specified for forging the alloy. Furthermore, tests were performed at 550°C for a range of strain rates; $0.1s^{-1}$, $1s^{-1}$ and $10s^{-1}$, which were considered likely to occur at various regions of the billet during forging, thus allowing the determination of material behaviour with strain rate. The results of the tests are shown in Figures 4.3a and 4.3b, respectively.

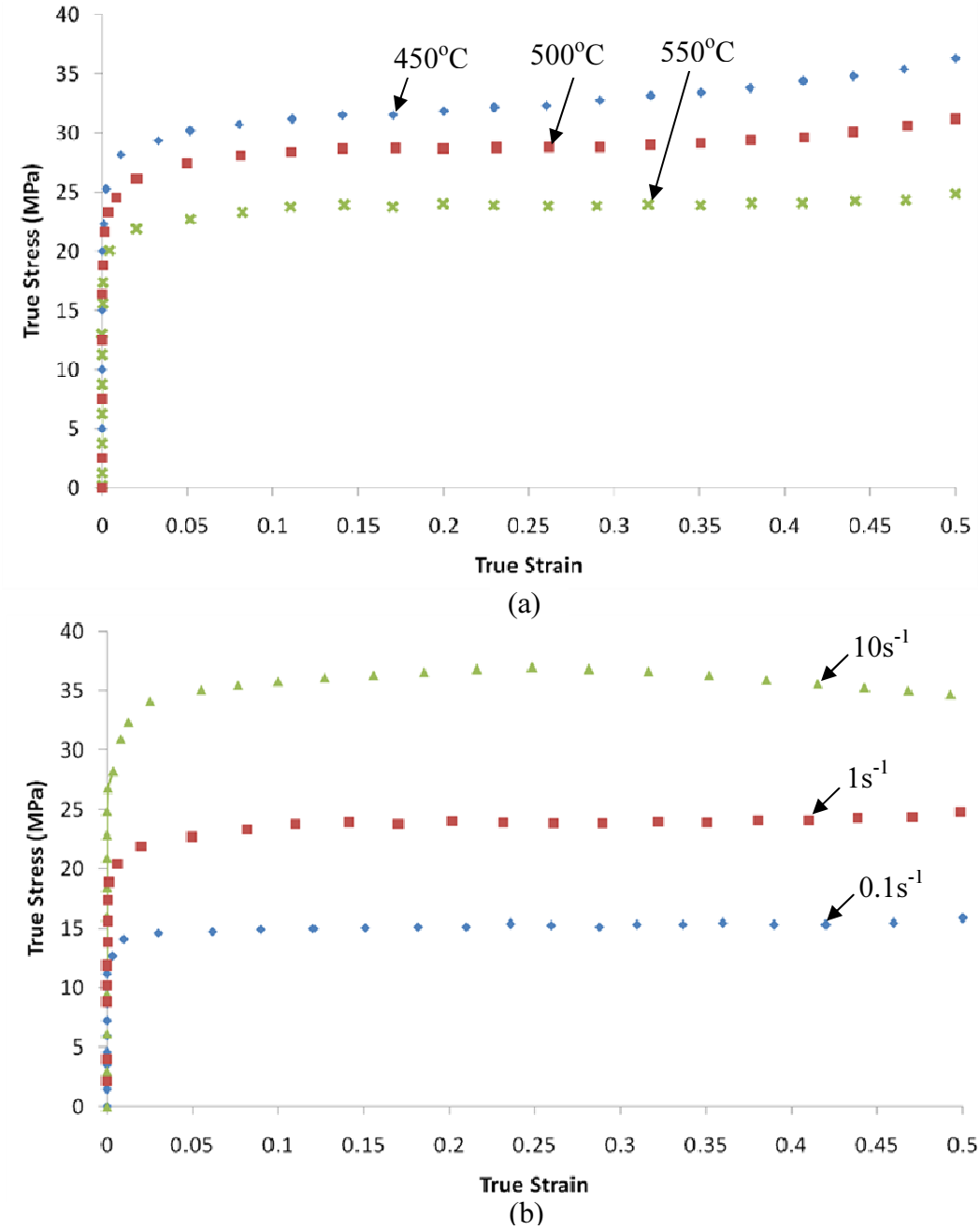


Figure 4.3: Al 6082-O Gleeble test results for: (a) Strain rate of $1s^{-1}$ and (b) Temperature of 550°C

4.3.2 230M07 Mild Steel Compression Test Results

Experiments were performed for the mild steel used as the ring material. As with the aluminium alloy, tests were performed for the range of forming temperatures (Figure 4.4a) and strain rates (Figures 4.4b and 4.4c) as indicated in Table 4.1. For steel, the strain rate effects at a high temperature of 1100°C were tested. Furthermore, to observe the effect of lower temperatures with strain rate, the effect of strain rates of the same values were tested at a lower temperature of 900°C.

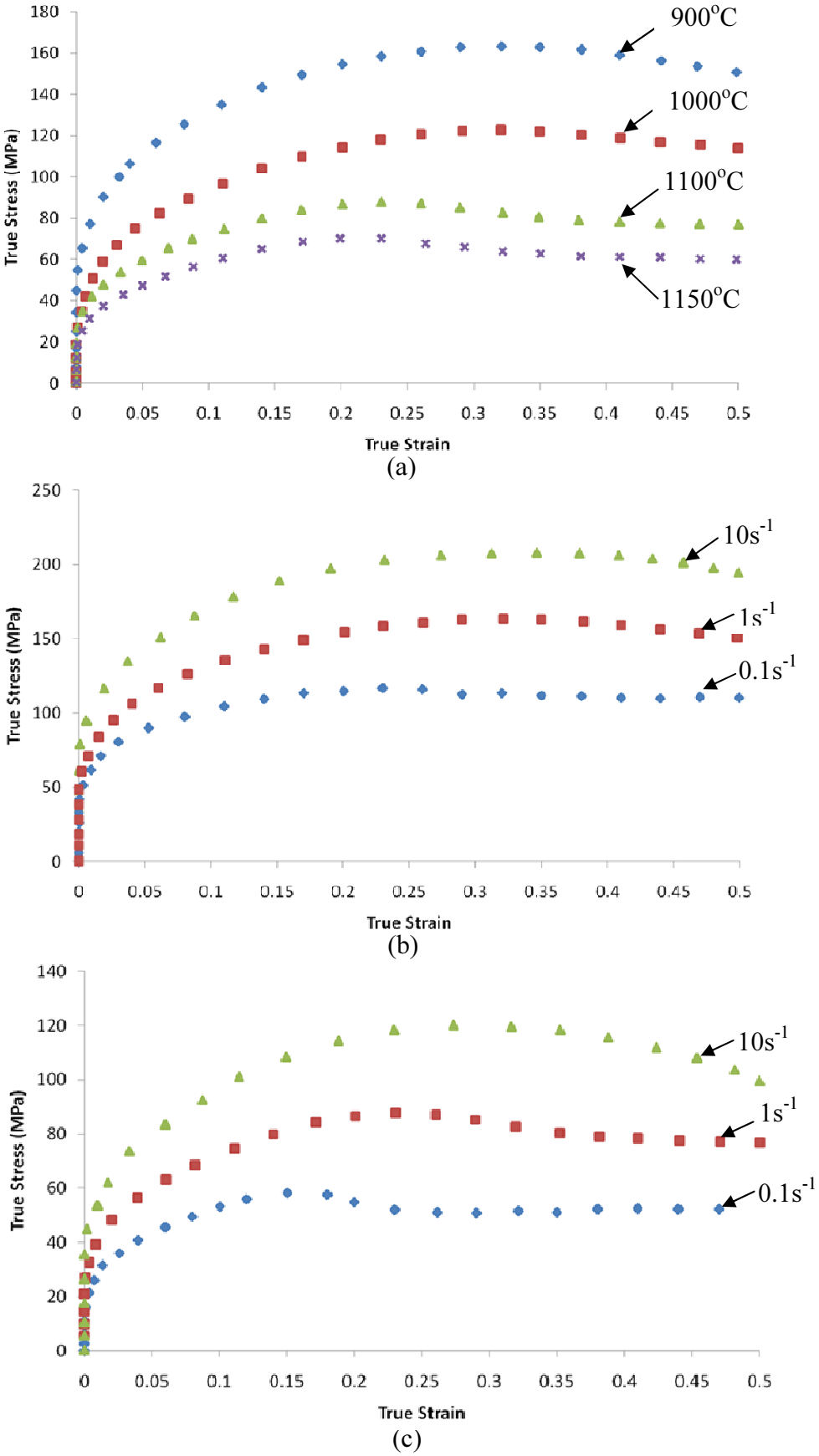


Figure 4.4: 230M07 Gleeble test results for: (a) Strain rate of $1s^{-1}$, (b) Temperature of $900^{o}C$ and (c) $1100^{o}C$

4.3.3 16MnCr5 Gear Steel Compression Test Results

Although the forging of bi-metal gears was not performed with gear steel due to the insufficient load capacity of the press, for forging this high strength steel fully to shape, compression tests were performed at similar temperatures and strain rates as those for mild steel, in order to provide the necessary material data for future work involving gear steels. The results of temperature variations with a strain rate of $1s^{-1}$, as well as the effects of strain rate at a lower temperature of $950^{o}C$ are shown in Figures 4.5a and 4.5b, respectively.

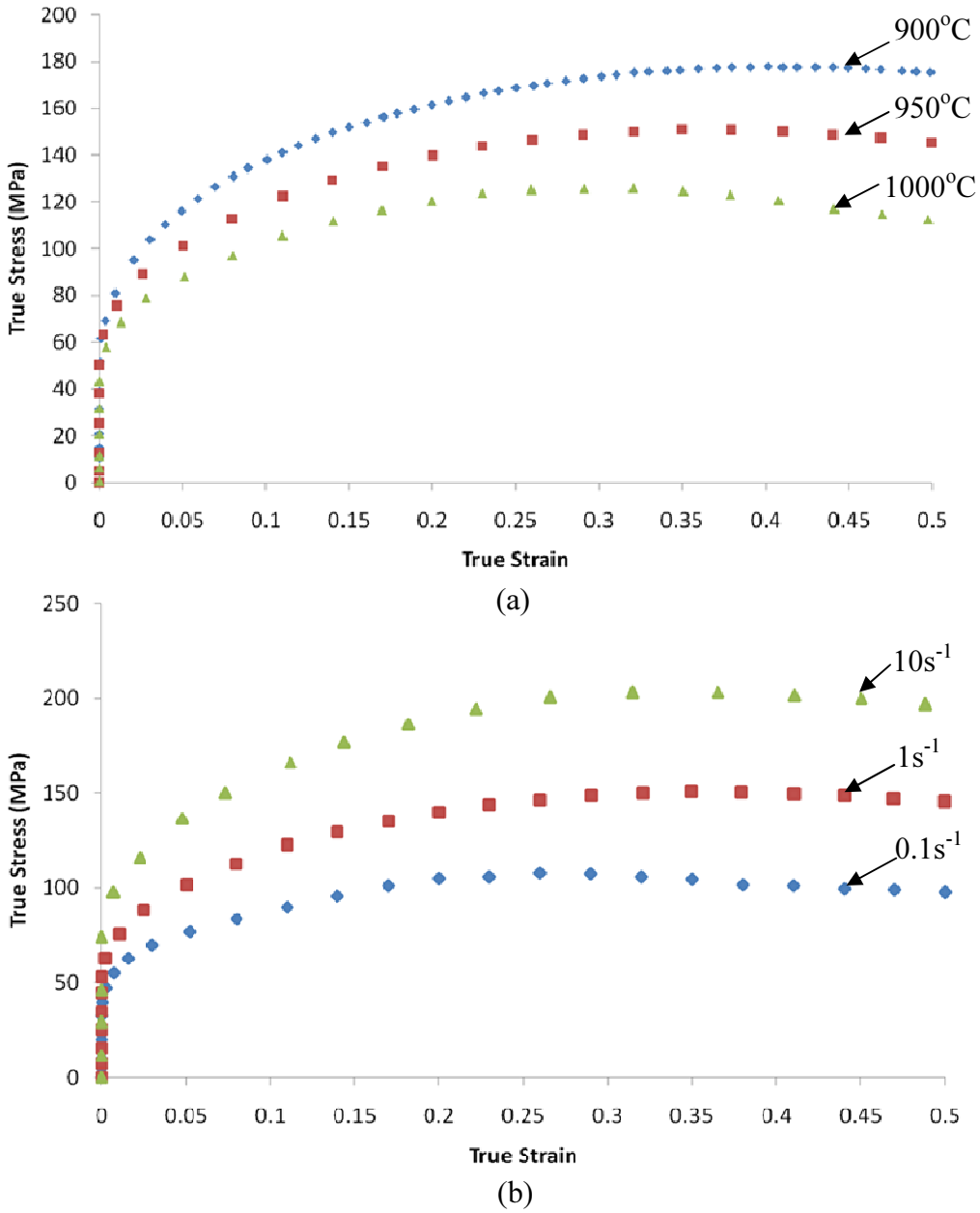


Figure 4.5: 16MnCr5 Gleeble test results for: (a) Strain rate of $1s^{-1}$ and (b) Temperature of $950^{o}C$

4.4 Calibration of Unified Visco-Plastic Constitutive Equations

The set of visco-plastic constitutive equations (4.6 - 4.9) reproduced below, which are used to model the compressive behaviour of the tested materials were calibrated using the experimental data by determining the constants of the equations.

$$\dot{\varepsilon}_p = \left(\frac{\sigma - R - k}{K}\right)^n \qquad Eqn\ 4.6$$

$$R = B(\bar{\rho})^{0.5} \qquad Eqn\ 4.7$$

$$(\dot{\bar{\rho}}) = A(1 - \bar{\rho})\left|\dot{\varepsilon}_p\right| - C\bar{\rho}^{\delta} \qquad Eqn\ 4.8$$

$$\sigma = E\left(\varepsilon_T - \varepsilon_p\right) \qquad Eqn\ 4.9$$

These constants, in kind, are temperature dependent as shown by equations 4.10 - 4.14, which requires the constants, namely: k_o, K_o, A_o, B_o, C_o, E_o, Q_p, Q_a, Q_{aa}, Q_b, Q_c, Q_E, n, and δ to be determined. Algorithms included in the software package developed by the authors Li *et al.* (2002) can be used to determine the material constants for unified creep damage constitutive equations. However, difficulty in practical implementation of this algorithm allows for a trial and error process to be more time efficient.

In order to determine the above constants, the temperature independent constants; k, K, A, B, C, E, n and δ were first found by fitting theoretical and experimental equations over a range of strain rates ($0.1s^{-1}$, $1s^{-1}$ and $10s^{-1}$) for a constant temperature. To assist with this process, the constants for the strain rate of $1s^{-1}$ were first determined and modifications made to adjust strain rate dependent variables to simultaneously fit the $0.1s^{-1}$ and $10s^{-1}$ experimental data.

Having determined the temperature independent constants, temperature dependency can be included by fitting these same constitutive equations to the flow stress data of the remaining temperatures. This resulted in a series of constants representing temperature dependency, for example, for three temperatures, the constants k_1, k_2, k_3, K_1, K_2, K_3 etc. were determined. Each of these temperature dependent constants were then linearly plotted to determine the two remaining constants in the Arrhenius relationships of equations 4.10 - 4.14.

It should be noted that the Young's modulus for the materials could not be determined through the compression tests, as this would require a very high sampling rate over the duration of the tests resulting in large data files, and hence the temperature dependency of the

Young's modulus for each material was obtained from the literature. For aluminium at temperatures of 450°C, 500°C, and 550°C the elastic modulus was found to be 53.5 GPa, 50 GPa, and 45.5 GPa, respectively (Mclellan and Ishikawa, 1987; Ledbetter, 1982) and for steel, the Young's modulus at 900°C, 950°C, and 1000°C is 113 GPa, 100.5 GPa, 88.5 GPa for 16MnCr5 and 106.4 GPa, 94.7 GPa, 83.3 GPa for 230M07, respectively (Spittel and Spittel, 2009; Chen *et al.*, 2006). Therefore, the constants E_o and Q_e were also calculated through linear plots of the Arrhenius relationship.

4.4.1 Al 6082-O Constitutive Equation Calibration

The constants determined for Al 6082-O using the above process are shown in Table 4.2.

Table 4.2: Constants for Al 6082-O

k_o (MPa)	K_o (MPa)	B_o (MPa)	C_o (-)	E_o (MPa)	Q_p (J/mol)	Q_a (J/mol)
0.21827	4.0390	0.16696	405.45	14271	19977	8991.4
Q_b (J/mol)	Q_c (J/mol)	Q_E (J/mol)	A (-)	n (-)	δ (-)	
24897	-27714	7969.3	11	3.8	1.6	

A comparison of the fitted constitutive equations and the respective experimental results for Al 6082-O at 550°C is shown in Figure 4.6 below. In this figure, crosses represent experimental results and solid coloured lines represent the constitutive equations derived through theory with the colours cyan, red and green corresponding to the strain rates of $0.1s^{-1}$, $1s^{-1}$ and $10s^{-1}$ respectively.

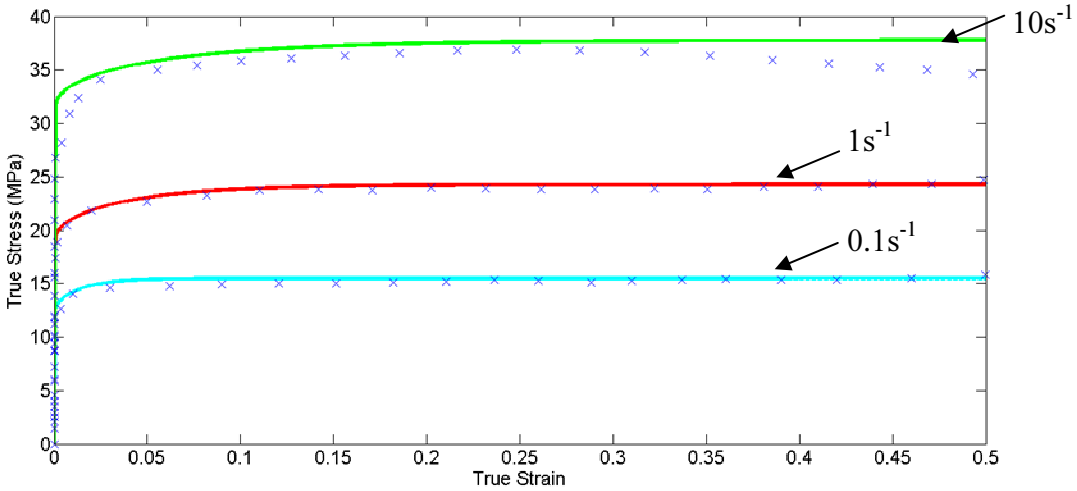


Figure 4.6: Al 6082-O experimental data (crosses) and constitutive equation set results (coloured lines) at 550°C

The effect of temperature on the flow stress of aluminium is plotted for both experimental and constitutive equations in Figure 4.7.

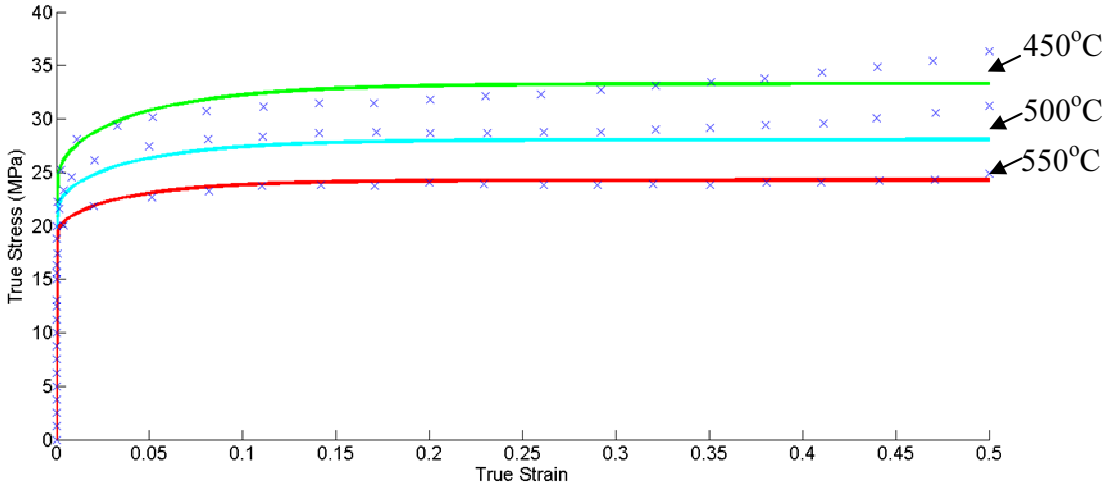


Figure 4.7: Al 6082-O results for different temperatures at 1s^{-1} strain rate comparing experimental data (crosses) with constitutive equations (coloured lines)

4.4.2 230M07 Constitutive Equation Calibration

The constants determined for 230M07 are shown in Table 4.3 below. Through fitting to the experimental data, it was found that the constant A for steel, more than aluminium, is temperature dependent with a closer fit obtained by accounting for this effect. Hence, the constants Q_{aa} and A_o were introduced.

Table 4.3: Constants for 230M07

k_o (MPa)	K_o (MPa)	A_o (-)	B_o (MPa)	C_o (-)	E_o (MPa)	Q_p (J/mol)
0.59690	0.57293	0.22969	8.2896	21.349	2895.8	22487
Q_a (J/mol)	Q_{aa} (J/mol)	Q_b (J/mol)	Q_c (J/mol)	Q_E (J/mol)	n (-)	δ (-)
39514	26825	29467	-19121	35259	3	2

Similar to the aluminium, the experimental and constitutive equation results for 230M07 steel at a constant temperature of 900°C are shown in Figure 4.8.

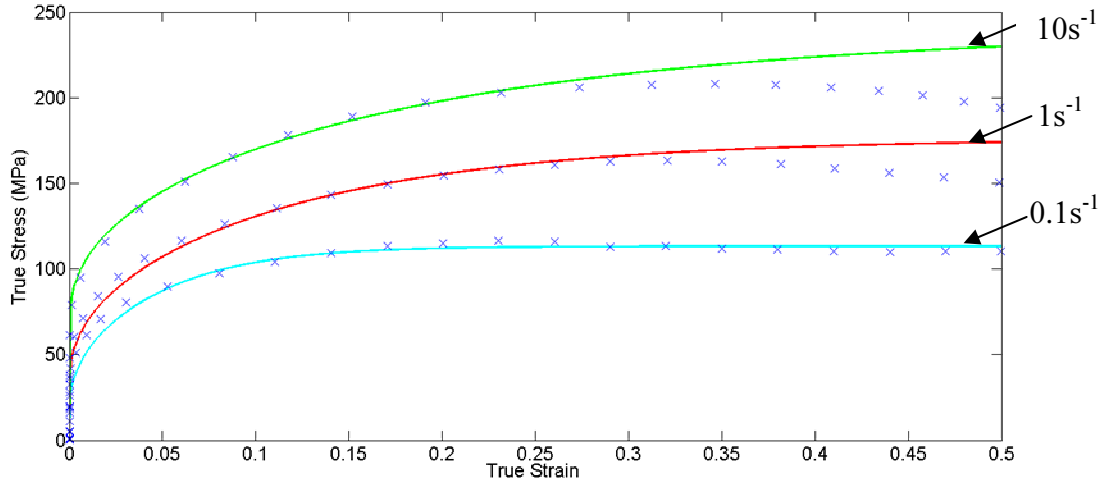


Figure 4.8: 230M07 experimental data (crosses) and constitutive equation set results (coloured lines) at 900°C

The effect of temperature on the flow stress for 230M07 is plotted through both experimental and constitutive equations in Figure 4.9 for a strain rate of $1s^{-1}$.

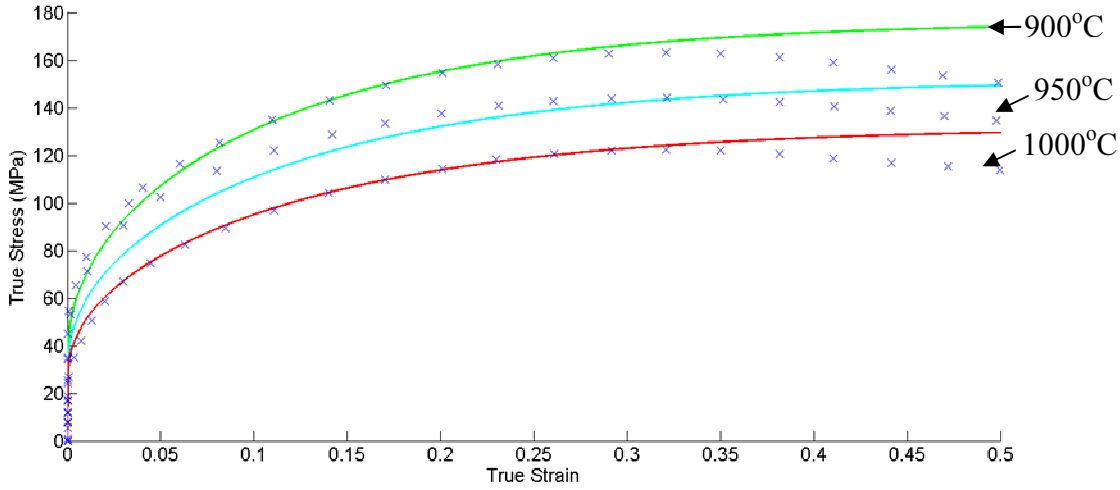


Figure 4.9: 230M07 results for different temperatures at $1s^{-1}$ strain rate comparing experimental data (crosses) with constitutive equations (coloured lines)

4.4.3 16MnCr5 Constitutive Equation Calibration

Finally, the constants determined for gear steel are shown in Table 4.4 below.

Table 4.4: Constants for 16MnCr5

k_o (MPa)	K_o (MPa)	A_o (-)	B_o (MPa)	C_o (-)	E_o (MPa)	Q_p (J/mol)
0.01542	7.3053	0.01662	18.337	1284700	5054.3	63242
Q_a (J/mol)	Q_{aa} (J/mol)	Q_b (J/mol)	Q_c (J/mol)	Q_E (J/mol)	n (-)	δ (-)
17739	53451	20244	-136730	30315	3.2	2

For a temperature of 950°C, the variation of flow stress with strain rate is shown in Figure 4.10. Finally, for a strain rate of $1s^{-1}$ the effect of temperature is shown in Figure 4.11.

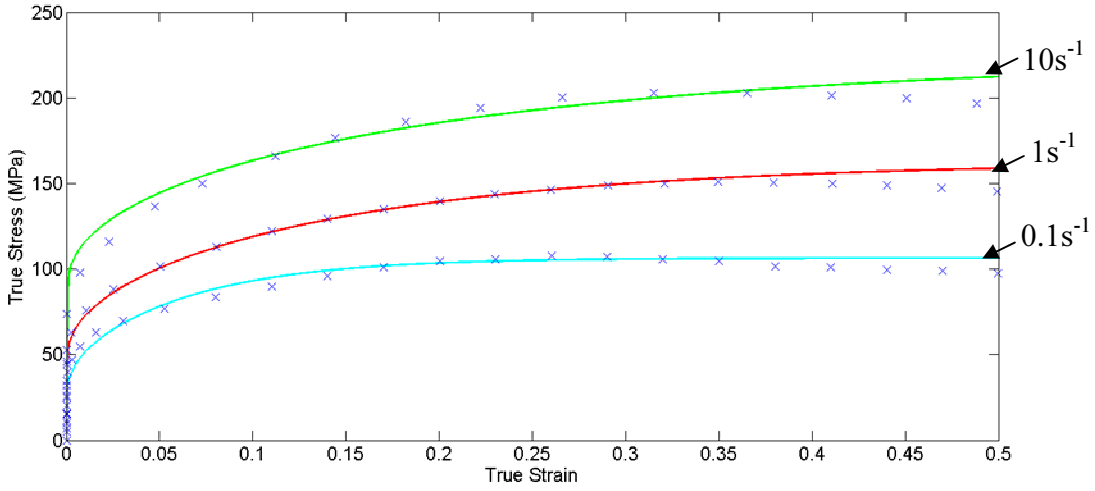


Figure 4.10: 16MnCr5 experimental data (crosses) and constitutive equation set results (coloured lines) at 950°C

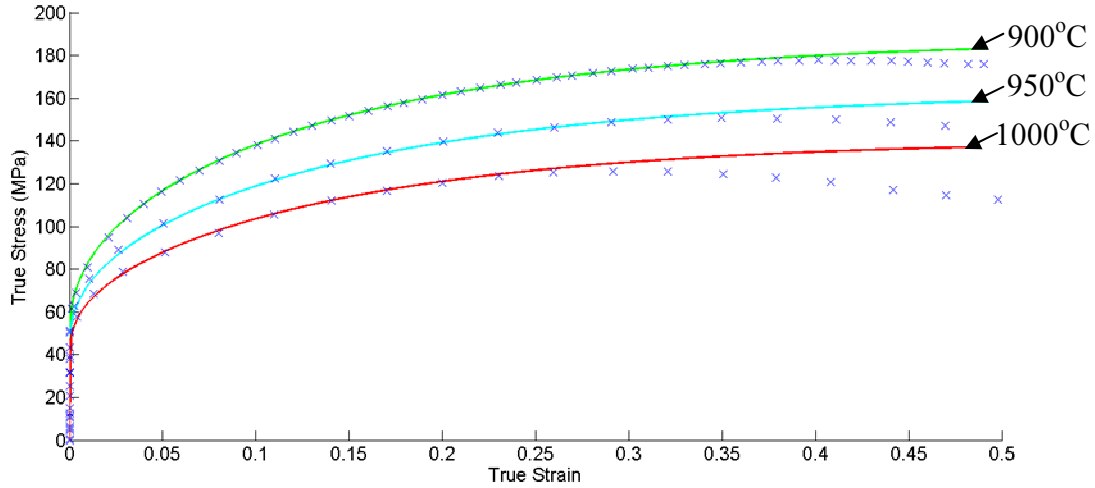


Figure 4.11: 16MnCr5 results for different temperatures at $1s^{-1}$ strain rate comparing experimental data (crosses) with constitutive equations (coloured lines)

As has been demonstrated from the results of the above figures, the constitutive equations and their accompanying constants have been used to model the compressive behaviour of three materials over a wide range of strain rates ($0.1s^{-1}$ to $10s^{-1}$) and over a large temperature range, from 450°C in aluminium to 1000°C in steels. Therefore, the use of phenomenological visco-plastic constitutive equations removes the limitations of traditionally used equations such as the power law, exponential law and hyperbolic sine law resulting in a more realistic representation of material behaviour during deformation.

Chapter 5 Finite Element Simulation of Forging Bi-Metallic Gears

This chapter describes the modelling work performed to study material flow during the forging of bi-metallic gears, the experimental trials of which were described in Chapter 3. An FE model has been established to determine the effect of several forging parameters on the ring thickness distribution of a gear, which in turn can be used to determine the performance and structural integrity of a gear. A cold forging model was created to simulate the copper-lead gear forging process, allowing for a comparison to be made with experimental results. The effect of friction on material flow was studied to determine its effect on ring thickness distribution. Simulations were also conducted assuming perfectly plastic material combinations of inner core and outer ring components, specifically, steel (ring material), copper (ring and core material) and lead (core material) to analyse the effect of yield strength ratios to ring thickness distribution. Finally, a simulation to model the hot forging of aluminium core and steel ring gears is discussed.

Analytical methods such as the upper bound, which is based on obtaining 'power dissipation rates in a deforming body' (Kim and Chitkara, 2001) through kinematically admissible velocity fields, although capable of estimating load-displacement behaviour for gear forging (Choi *et al.*, 1998a; Choi *et al.*, 1998b); are not suitable for analysing material flow behaviour such as ring thickness variations during forging. Therefore, FE simulation, which provides realistic detail of a deforming body, is required to perform this analysis.

5.1 Numerical Procedures for Cold Forging

To understand the bi-metal forming process and simultaneous flow of the two materials during forging, a model was created using Abaqus 6.11 CAE, for a single tooth to take advantage of the symmetry and hence reduce overall simulation time. This model, and a segment of the ring and core, is shown in Figure 5.1. For this 3D analysis, the toothed die and mandrel of the model were defined as 3D rigid shells. The punch and counterpunch were modelled as discrete rigid components. Symmetry boundary conditions were applied to the edges of the core and ring where two rigid planes defined by radii from bore to tooth mid-roots marked planes of flow symmetry between adjacent teeth. The mass and rotary inertia values of each component were input based on the dimensions of the tool set used in experimental trials. In assembling the components, surface-to-surface contact between

contacting surfaces allowed for the input of Coulomb friction (Perez-Castellanos and Rusinek, 2012), coefficients discussed later in this chapter.

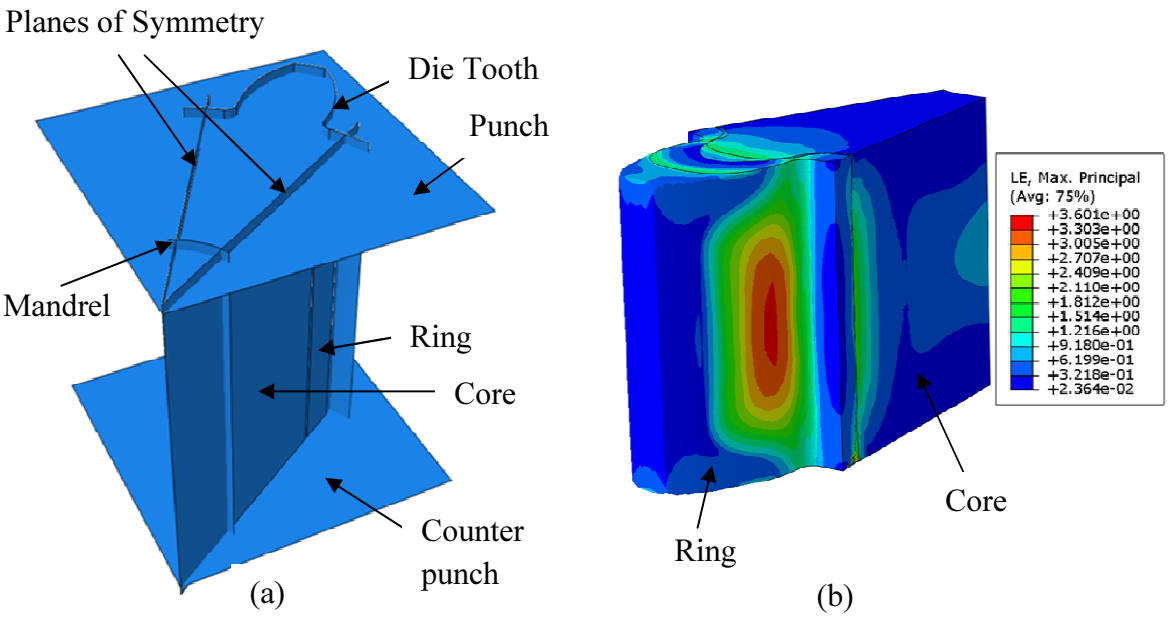


Figure 5.1: FE model of bi-metal gear forging: (a) Die and work-piece segment and (b) Strain for 2mm ring gear

The simulation was conducted using the Explicit Finite Difference Solver, rather than the standard solver due to the large strains and number of complex contacts involved. Initial simulations were performed using a hexahedral mesh of C3D8R elements for both ring and core components. However, it was found that using a combination of linear hexahedral C3D8R, and linear wedge C3D6 elements resulted in reduced simulation time, as a higher concentration of elements was applied to critical regions such as the tooth root, while avoiding an excessive number of elements in non-critical regions such as the gear centre. A mesh convergence study was carried out and it was found that 140,000 linear hexahedral elements in the ring and 119,450 linear wedge and 70,000 linear hexahedral elements in the core were sufficient to achieve a convergent solution. Enhanced Hourglass control was applied to the elements to provide an artificial torsional stiffness to the elements with a single integration point, thus preventing the elements from warping and flowing through the die (Dassault Systems S. A., 2011). The involute profile to generate the gear profile was plotted using equations 5.1 and 5.2 shown below (Litvin and Fuentes, 2004).

$$x_i = r_b(\sin\theta - \theta \cdot \cos\theta) \qquad Eqn\ 5.1$$

$$y_i = r_b(\cos\theta + \theta \cdot \sin\theta) \qquad Eqn\ 5.2$$

In these equations the constants are as follows: r_b = radius of the base circle, and θ = angle of rotation in rolling motion.

5.2 Instron Tests to Determine Material Properties

To perform the simulations, the true stress-strain data for the copper (C101) and commercially pure lead were obtained from compression tests using Instron 250kN and 50kN universal testing machines. Experiments were also performed for mild steel (230M07) at room temperature to demonstrate the large reduction of flow stress when using model materials. Bluehill 2 software was used to control speed and displacement. Dimensions of the test specimens used were 8mm diameter and 12mm high. The upper and lower surfaces of the specimens were polished to a 1 micrometer roughness in order to reduce the friction between the platen and the specimen. FEP film and Mobil Grease 28 were used for these surfaces to minimise barrelling during the test. Each test was performed three times, resulting in a maximum variation between tests of approximately 6.5%. An average of the values for the true stress and strain were obtained and are shown in Figure 5.2.

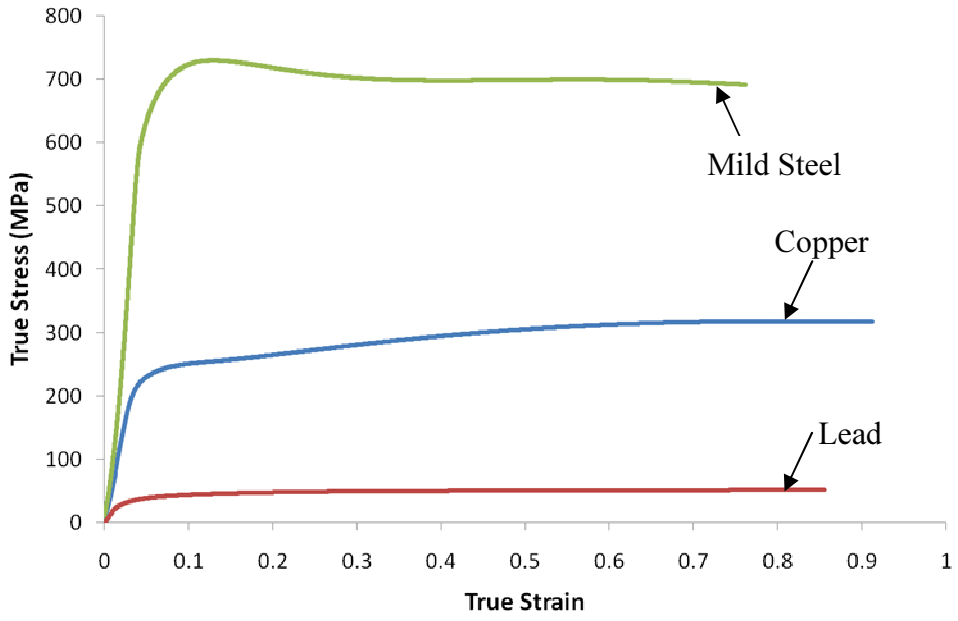


Figure 5.2: True stress versus true strain data for the ring (copper) and core (lead) materials compared to mild steel

5.3 Results

Using this material data in Abaqus software, forging simulations were performed for an initial billet height of 34mm and ring radial thicknesses of 2mm, 4mm and 6mm, as used in

the experimental forgings. As in the experiments, compression displacement from beginning to end of the simulation was 14mm, thus creating a completed gear with a final height of 20mm. An example of a 2mm copper ring simulation through the different stages of compression is shown in Figure 5.3, where s is the current compressive displacement and s_f is the final compressive displacement of 14mm. In Figure 5.3, a friction coefficient of 0.1 was used between work-pieces, punch and counterpunch, which although dependent on factors such as lubricant and metal composition, is an estimated typical value for a cold forming operation (Camacho *et al.*, 2009). Friction values between the interface of the mandrel and core, ring and core, as well as between the ring and die were set to 0 to see the effect that only the punch and counterpunch friction coefficients have on metal distribution. Figure 5.3 shows a cross section of the gear tooth in both the vertical and horizontal directions. The vertical cross section was taken through the centre of the gear tooth whereas the horizontal cross section was taken mid-height through the completed gear.

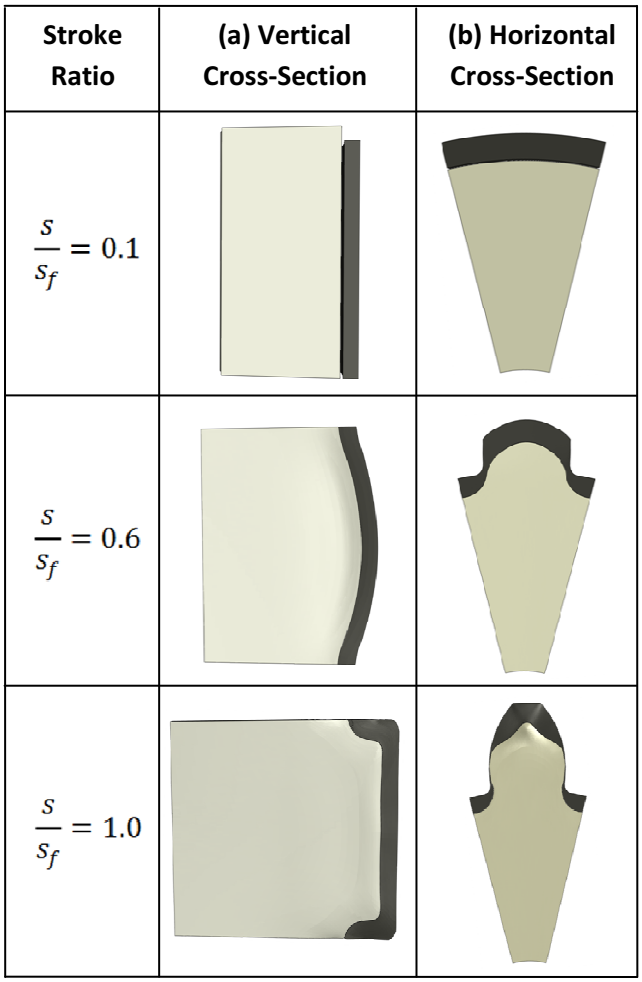


Figure 5.3: Predicted die filling for 2mm ring from: (a) Vertical and (b) Horizontal directions, where μ=0.1 on the punch and counterpunch and s_f=14 mm

5.3.1 Vertical Cross Section

The effect of ring thickness on the distribution of material in the vertical direction is discussed below. A comparison between experimental and simulated results for ring thicknesses of 2mm, 4mm and 6mm is shown in Figure 5.4. For the simulations, a friction coefficient of 0.1 was applied only to the punch and counterpunch, other surfaces being set as frictionless, as the effect these friction coefficients have on material flow distribution are discussed in later sections. The assumption of having only these two friction coefficients results in an axisymmetric ring thickness distribution about the mid-height of the gear, which differs from the experimental results. A cross-section of the experimentally forged gears was made through the centre of a tooth in the vertical direction using EDM.

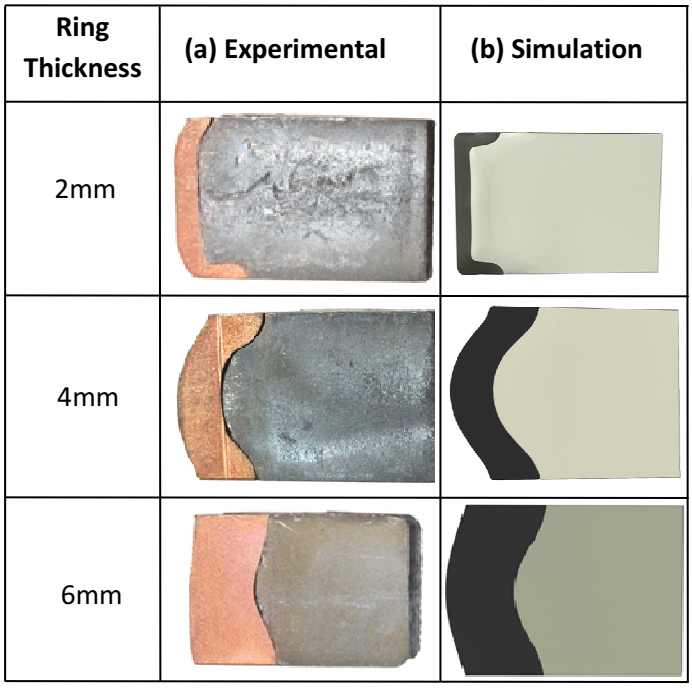


Figure 5.4: Comparison of tooth filling: (a) Experimental and (b) Predicted for different ring thicknesses, where μ=0.1 on the punch and counterpunch

As can be seen from the Figure, a large ring thickness results in incomplete die filling. From the experiments performed on the Instron 250 ton press, the load-cell has shown that the 2mm ring gear requires loads in excess of 210 tons to completely fill the die, and therefore larger ring thicknesses would require loads exceeding that available from the press. Hence, to compare to the experimental results, the final heights of the incomplete gears were measured, and a comparison was made with the Abaqus CAE model at this same height.

In order to compare experimental and simulated gears, measurements of the ring thickness in the direction normal to the vertical were made in 20 increments of 1mm down the vertical cross section, as shown in Figure 5.5. The simulation results are shown as solid lines, whereas experimental results are shown as symbols. As can be seen from Figure 5.5, the 2mm simulation and experimental results correlate closely. For positions 2 to 17, the experimental and simulation results are very similar with the experimental results being consistently slightly greater compared to simulated ones. Simulated and experimental values vary considerably for positions 0 and 1 and 18-20, with the simulation output being symmetrical about the mid-height position whereas the experimental results are asymmetrical. A possible explanation for this asymmetry is the difficulty in applying adequate lubricant to the teeth of the die. Furthermore, the greater filling which has occurred at the bottom compared to the top of the gear is due to the kinetics of the tooling (Sadeghi and Dean, 1994). As revealed by the literature, the movement of the die relative to the work-piece and interface friction tends to move material flow downwards, hence filling the tooth corners near the counterpunch before the punch.

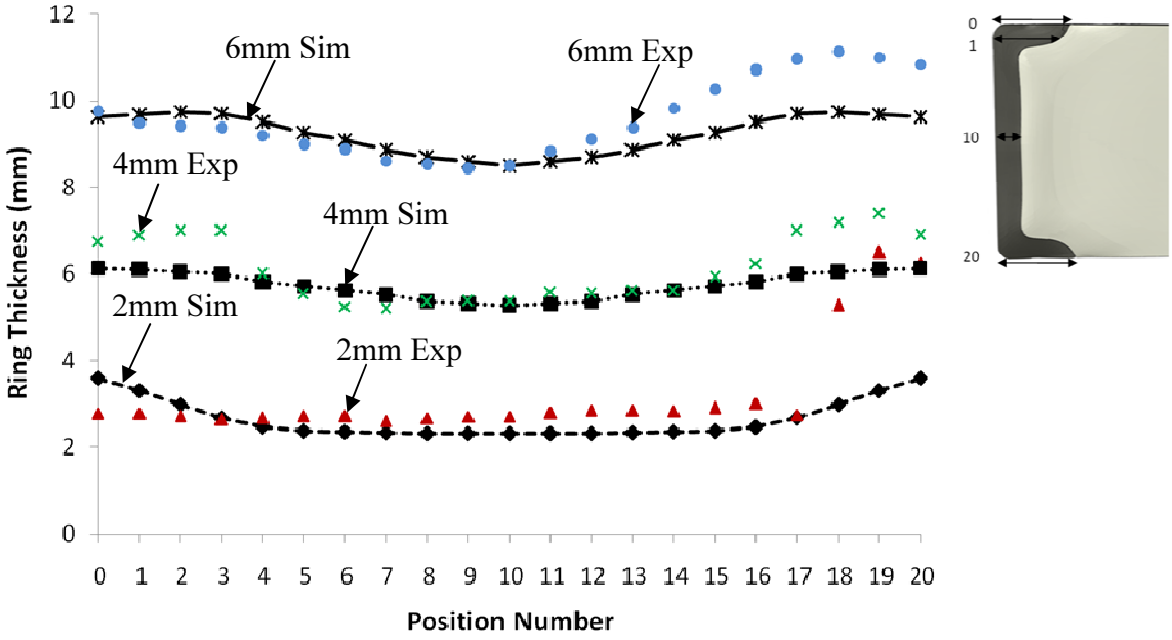


Figure 5.5: Comparison of computed (solid curves) and experimental (symbols) ring thicknesses in the vertical direction for different ring thickness, where μ=0.1 on punch and counterpunch

The simulation results depicted in Figure 5.5 show that all gears experience an increased ring thickness at the punch and counterpunch surfaces (positions 0 and 20, respectively) of the gear. The reason for this is that during the forming process, the ring material is restrained on

the punch and counterpunch surfaces due to friction which causes material from the outer diameter of the ring to fold and come into contact with the punch and counterpunch. Hence, by retarding radial flow, the friction has caused ring material to build up on the punch and counterpunch surfaces. This effect provides a benefit for forged bi-metal gears as the folding of the ring provides an axial lock between the two materials, hence inhibiting relative axial movement between them. A further feature evident from Figure 5.5 is that thicker rings, such as the 6mm ring, exhibit a lower rate of change of ring thinning between the punch to mid-height of the gear and counterpunch to mid-height of the gear (positions 0-10 and 20-10) compared to the 2mm and 4mm rings, which show an abrupt thinning within the first 5mm depth of the gear. Moreover, it is shown that for thicker rings, the region in the centre which has a uniform ring thickness, i.e. positions 5-16 for the 2mm thick ring and positions 8-10 for the 6mm thick ring, reduces significantly.

In order to compare the behaviour of different ring thicknesses accurately, normalised thickness values t/t_o (measured/initial thickness) are plotted against position number for both the simulated and experimental results in Figure 5.6. As can be seen, ring thickness at every position, for all rings, is larger than original ring thickness as they lie above t/t_o=1. The reason for this is that the ring material experiences thinning in other regions of the tooth as shown in the horizontal cross-sections of Section 5.3.2.

By averaging the normalised experimental results from Figure 5.6 at positions 0 and 20, it can be seen that the thickness for the 2mm (t/t_o=2.26) is greater than for the 4mm (t/t_o=1.71) and 6mm (t/t_o=1.72) cases. The simulation results which had friction coefficients of 0.1 applied on only the punch and counterpunch surfaces and a friction coefficient of zero at the die surface demonstrated a similar comparison between the thicknesses i.e. t/t_o=1.81 for the 2mm ring, t/t_o=1.53 for the 4mm ring and t/t_o=1.6 for the 6mm ring thickness. The experimental results show that at the mid-height ring thickness (position 10), as ring thickness increases, the t/t_o value increases. For example t/t_o=1.16 for the 2mm ring, t/t_o=1.32 for the 4mm ring and t/t_o=1.42 for the 6mm ring. The simulation ring thicknesses for position 10 are t/t_o=1.35, 1.35 and 1.42 for ring thicknesses of 2mm, 4mm, and 6mm respectively. This shows that the simple approximation of non-zero friction applied only on the punch and counterpunch have produced reasonably accurate results.

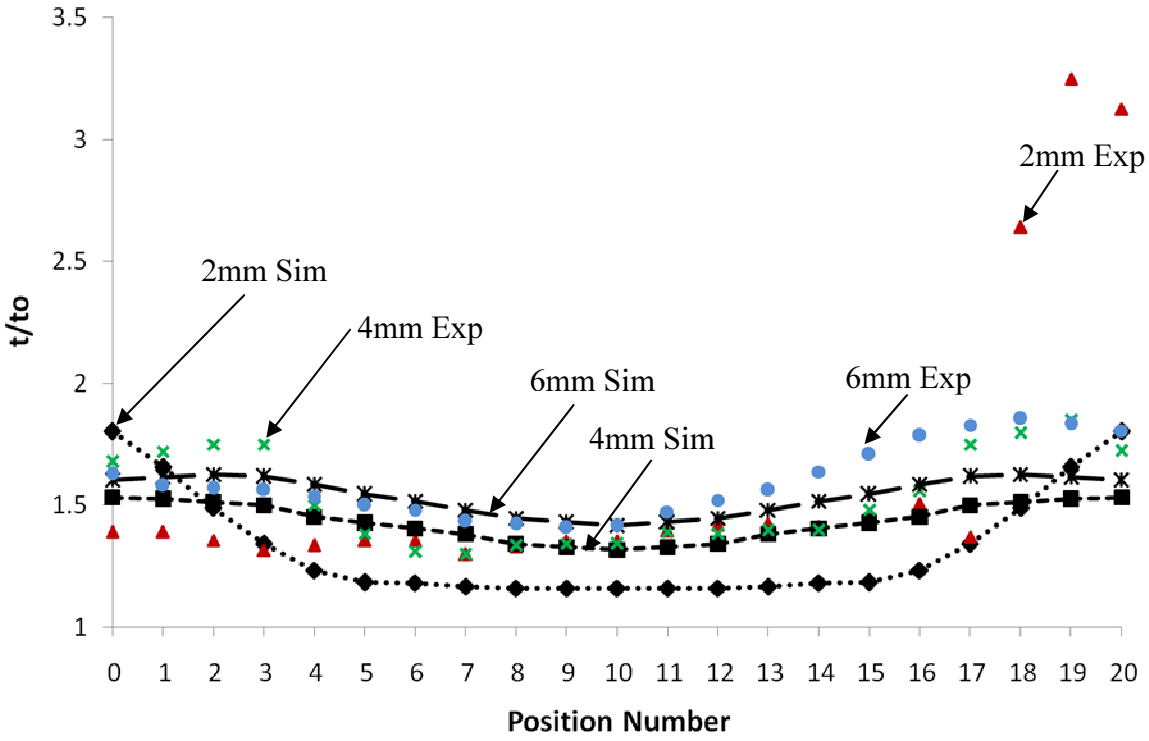


Figure 5.6: Comparison of computed (solid curves) and experimental (symbols) die filling in the vertical direction for different ring thickness (normalised thicknesses)

Both experimental and simulation results for the vertical cross section through tooth tips have demonstrated that the ring thickness at all positions is greater than that of the original ring thickness (t/t_o>1). Therefore there must be regions in a gear which experience ring thinning (t/t_o<1) that may reduce the overall performance of a gear. In order to understand the ring thinning effect, a horizontal cross-section was taken at the mid-height of the formed gear. The results of this analysis are presented in Section 5.3.2 below.

5.3.2 Horizontal Cross Section

In this section a comparison is made between the forged gears and simulated gears with a friction coefficient of 0.1 applied on only the punch and counterpunch. In order to compare the horizontal cross sections, EDM was used to slice the gears at mid-height. A comparison between experimental and simulation results is shown in Figure 5.7.

As shown in Figure 5.7a, in the experiment, flow of the 2mm ring into the tooth cavity was not symmetric and it was severed on one side exposing a large region of the lead core. This asymmetric filling occurred on every tooth of the 2mm ring gear. Furthermore, it can be seen

that at the centre of the tooth tip, the lead material is pointed where it contacts the copper ring compared with the rounded curve of the core in thicker ring gears.

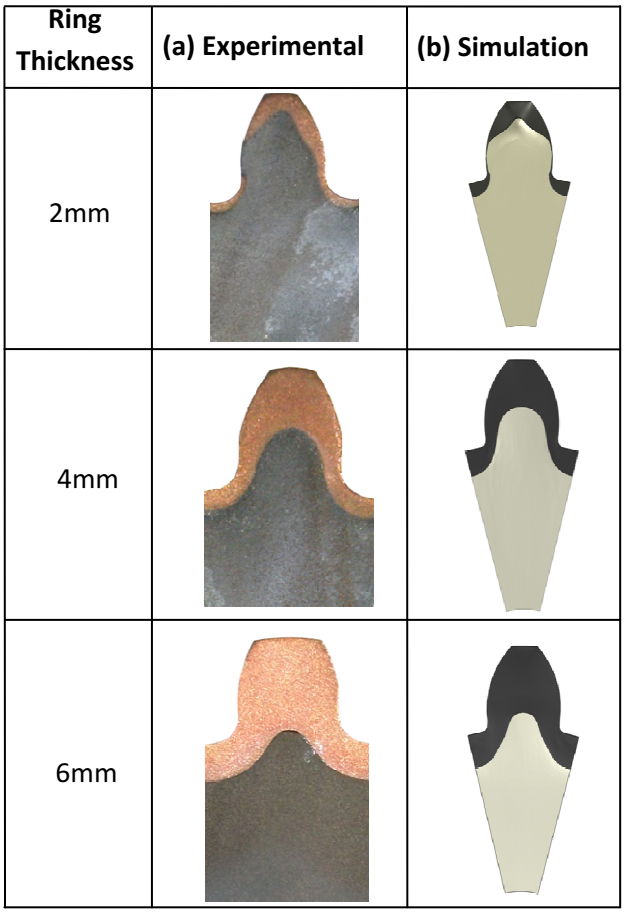


Figure 5.7: Comparison of thickness variations on the cross-section of: (a) Experimental and (b) Simulation for different ring thickness, where μ=0.1 on the punch and counterpunch

The flow of the 4mm thick ring is essentially symmetric. A solid copper tooth has been formed from the tip to about the pitch-circle position and the thickness of the copper outer layer decreases the closer it is to the tooth root. No separation has occurred. Less flow of lead into the tooth occurs with the 6mm ring and a solid copper tooth has been formed from tip to root radius. Measurements of the ring thickness were taken at 12 different locations, from tooth tip to root at mid-height, for all 13 teeth of each gear. Ring severance is considered to be a thickness of zero, and the average thickness was found. The experimental values are compared to the simulation results as shown in Figure 5.8.

As can be seen from Figure 5.8, the experimental and simulation results are similar. However, it can be seen that positions 10 and 11 differ from the experimental results. A possible explanation for this effect could be the value of friction coefficients that were used,

as a friction of μ=0.1 has been applied on only punch and counterpunch, with a frictionless condition applied between the ring and die, core and ring and mandrel and core. The effect of varying some of these friction coefficient values is discussed in the following sections. Furthermore, it can be seen that the most severe thinning occurs between positions 7-9 for the 2mm and 4mm gears, whereas this occurs at positions 8-10 for the 6mm gear. At this position, the 2mm ring has thinned substantially, which indicates that severance of the copper material at this location is likely due to the extreme deformation.

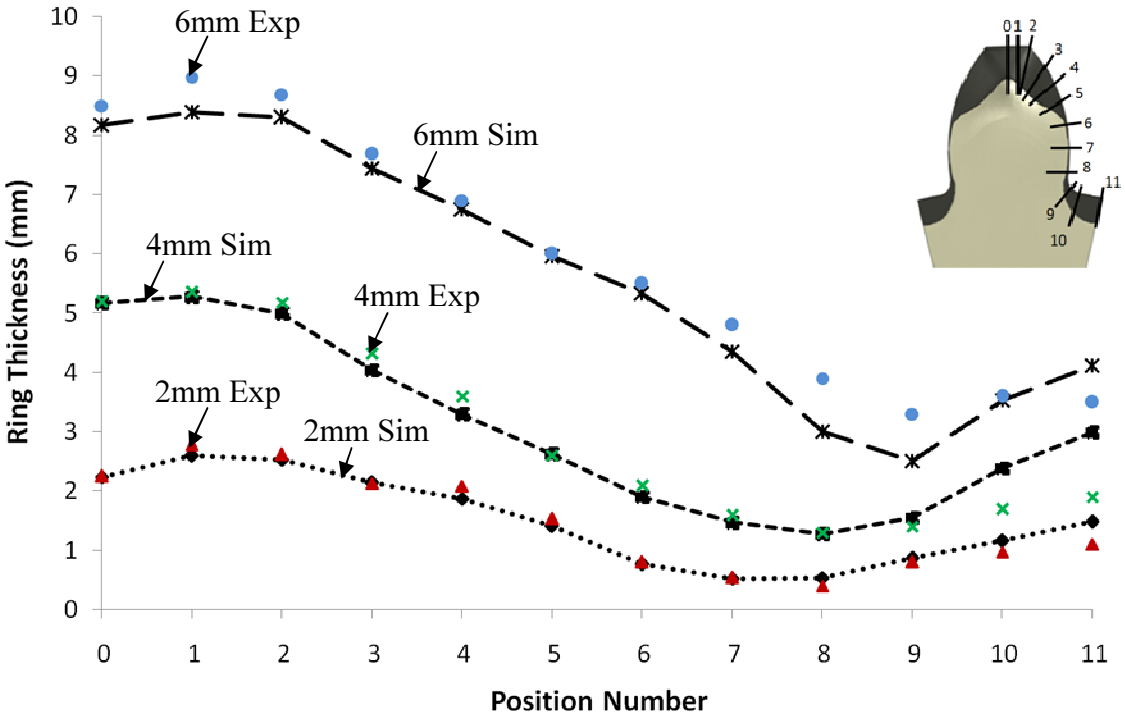


Figure 5.8: Comparison of computed (solid lines) and experimental (symbols) thickness variation for the formed tooth for different ring thicknesses. Cross-sections were taken at the mid-height of each gear. μ=0.1 on punch and counterpunch for simulations

Figure 5.9 shows the normalised thickness results, with the dark horizontal line representing t/t_o=1. As can be seen, ring thickness at the centre of the tooth tip (position 0) is larger than the original. However, for ring thicknesses of 2mm and 4mm, positions 4 onwards experience ring thinning, with positions 7-8 being the thinnest. Moreover, for a ring thickness of 6mm, ring thinning occurs from position 5 onwards with the thinnest material being located at positions 8-10.

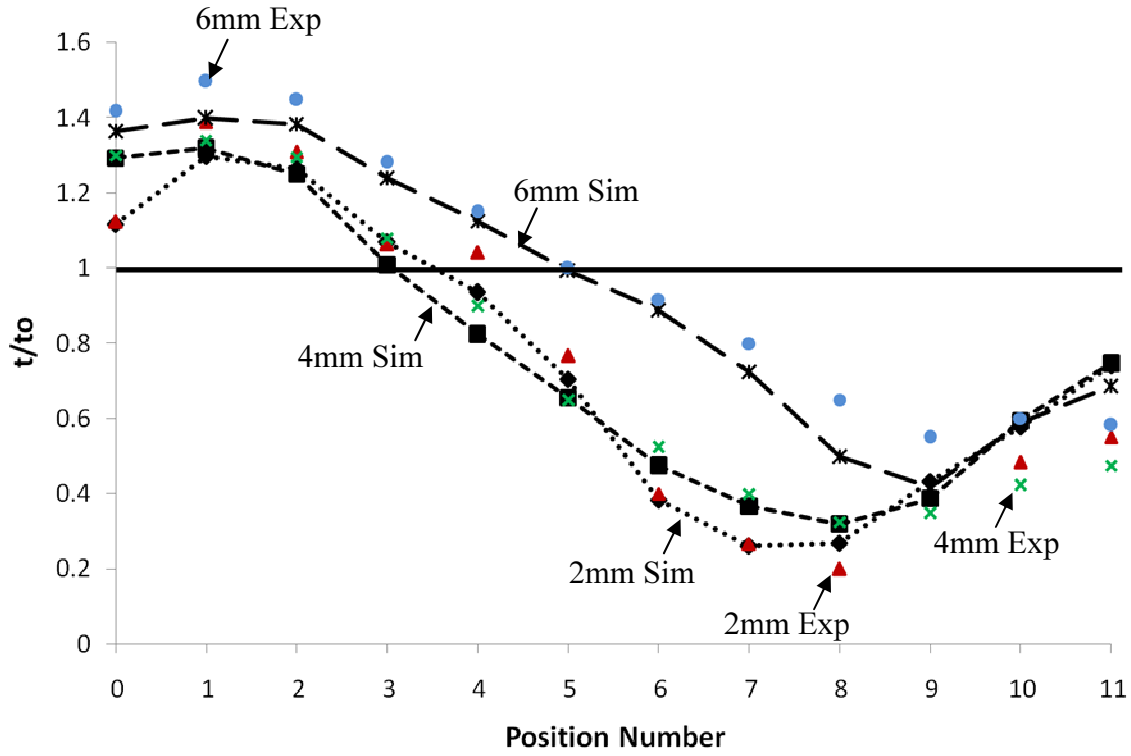


Figure 5.9: Comparison of computed (solid lines) and experimental (symbols) thickness variation for the formed tooth for different ring thicknesses shown as normalised thickness

The reason for the variation between the 6mm and the 2mm and 4mm results is the incomplete tooth filling of the 6mm gear during forging, where the tooth tip did not quite reach the tip of the die. Overall, it can be seen that ring thickness affects material distribution in the horizontal direction, where a larger level of thinning in proportion to the initial value is experienced near the tooth root for thin rings, increasing the likelihood of the ring to fail in this region.

5.3.3 Punch and Counterpunch Frictional Effects

In addition to ring thickness, friction is a variable that affects material flow in bi-metal gear forging. In order to investigate the frictional effect at punch and counterpunch on material flow, simulations were performed for a fully forged 4mm ring with friction coefficients of μ=0.0, 0.1, 0.2 and 0.3 between work-piece, punch and counterpunch. The friction coefficients at the ring-die, core-ring and core-mandrel were set to zero to remove their influence on the material flow, as some of these are investigated in Section 5.3.4.

A vertical cross-section through the tooth tip (Figure 5.10), shows that a low friction coefficient, μ= 0.1, produces a smooth distribution of material throughout the depth of the gear compared to a high friction coefficient, μ= 0.3, for which a large amount of material accumulates on the punch and counterpunch surfaces (positions 0 and 20) and causes a large gradient towards the central region. This results in the ring thickness of the central region (positions 5 to 15) to be substantially reduced for high friction coefficients. However, it is seen that even for a high friction coefficient of 0.3, the t/t_o ratio does not fall below unity.

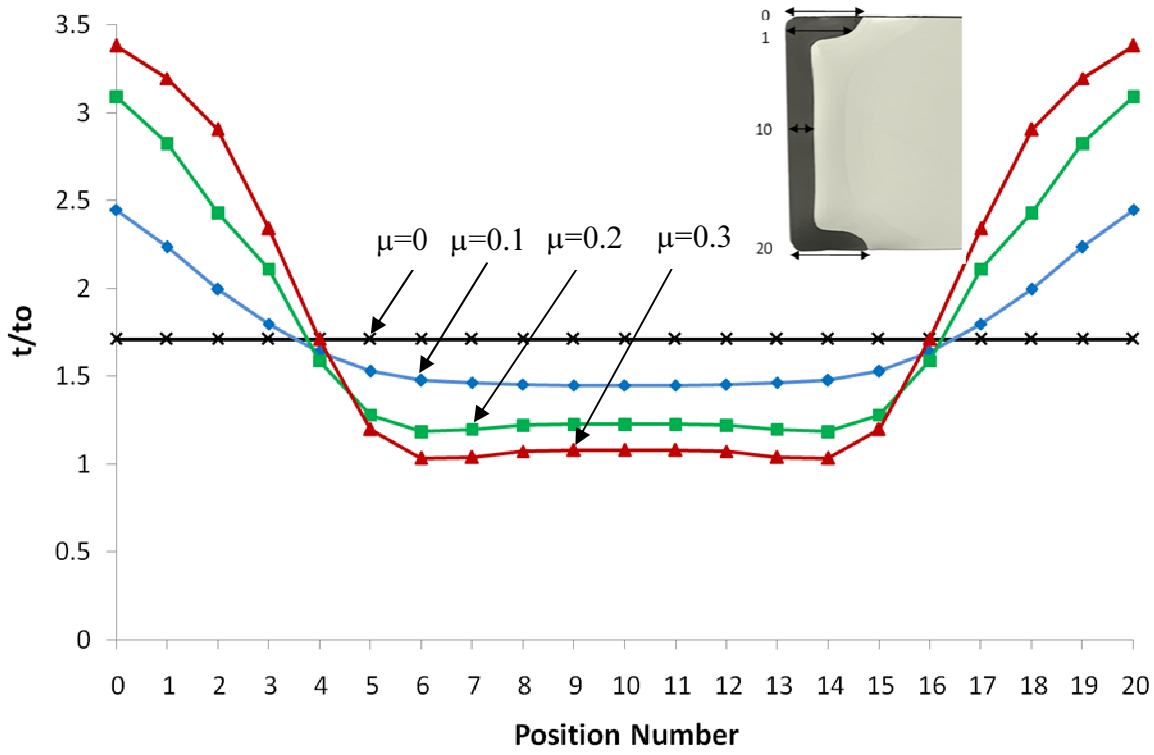


Figure 5.10: Effect of friction on the thickness variations in the vertical direction for the ring thickness of 4mm

Simulations of horizontal flow in the mid-height cross-section (Figure 5.11) show that an increasing friction coefficient generally reduces ring thickness. It is shown that varying the friction coefficient varies the positions where the material thins below t/t_o=1. For example the friction coefficient μ=0 causes thinning from position 4 onwards whereas the high friction coefficient μ=0.3, experiences thinning in many more positions (position 2 onwards). Moreover, it is seen that low friction coefficients cause a large accumulation of ring material at the tooth tip, whereas for the high friction coefficient μ=0.3, the t/t_o ratio does not increase far above unity. Therefore, reducing the friction of the punch and counterpunch has the effect of increasing material flow towards the tooth tip whilst reducing material accumulation at the punch and counterpunch surfaces.

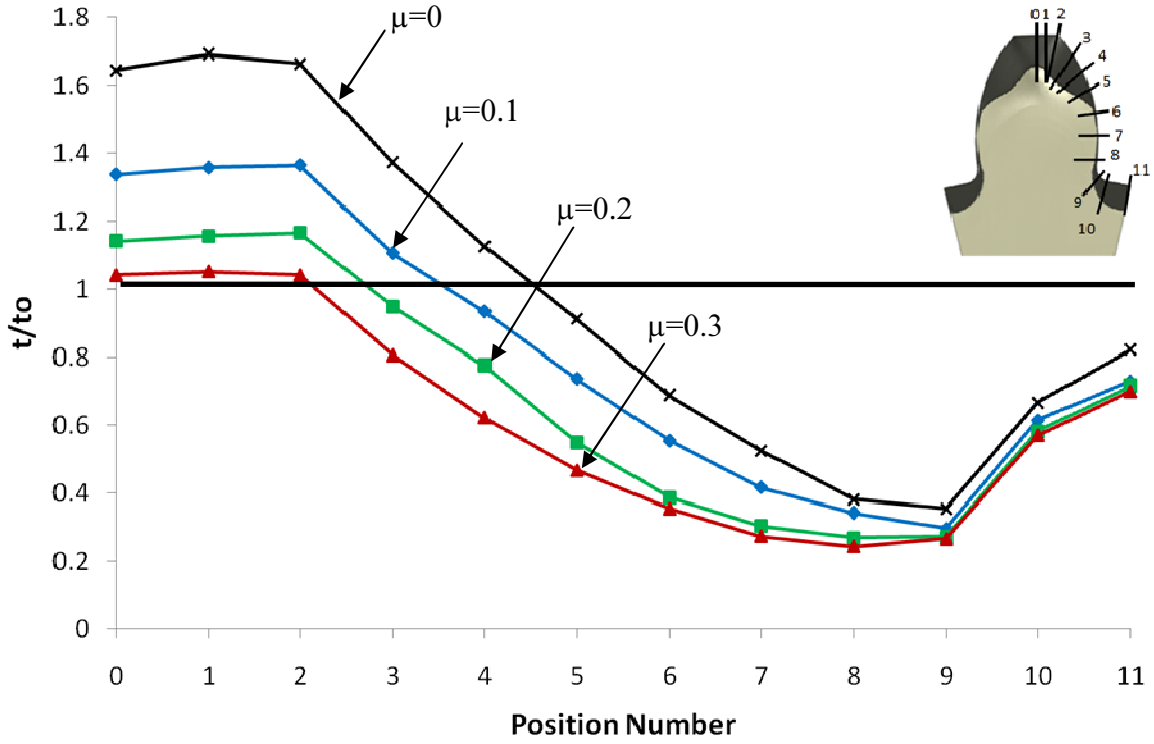


Figure 5.11: Effect of friction on the thickness variations in the horizontal direction for the ring thickness of 4mm

5.3.4 Material Interfacial Friction

In the following section, the effect of interfacial friction between the core and ring is investigated. Simulations were conducted for a 4mm ring with a friction coefficient of 0.1 on punch and counterpunch surfaces and an assumed friction coefficient of 0.2 between the ring and die and core and die to improve model accuracy, as per Chitkara and Bhutta (1996). The effect of the friction between the core and ring was analysed for the two extreme cases, with values of μ = 0 and μ = 0.577 (Grzesik, 2008). Figures 5.12 and 5.13 show the ring thickness distribution in the vertical and mid-height horizontal direction, respectively.

As can be seen from Figure 5.12, the effect of zero interfacial friction between the core and ring, and with a 0.2 friction coefficient at the die has the effect of increasing the asymmetry of the ring thickness distribution about position 10 (mid-height) of the gear. However, it can be seen that the die frictional effect is countered by the inter-component friction to create a more symmetric ring thickness.

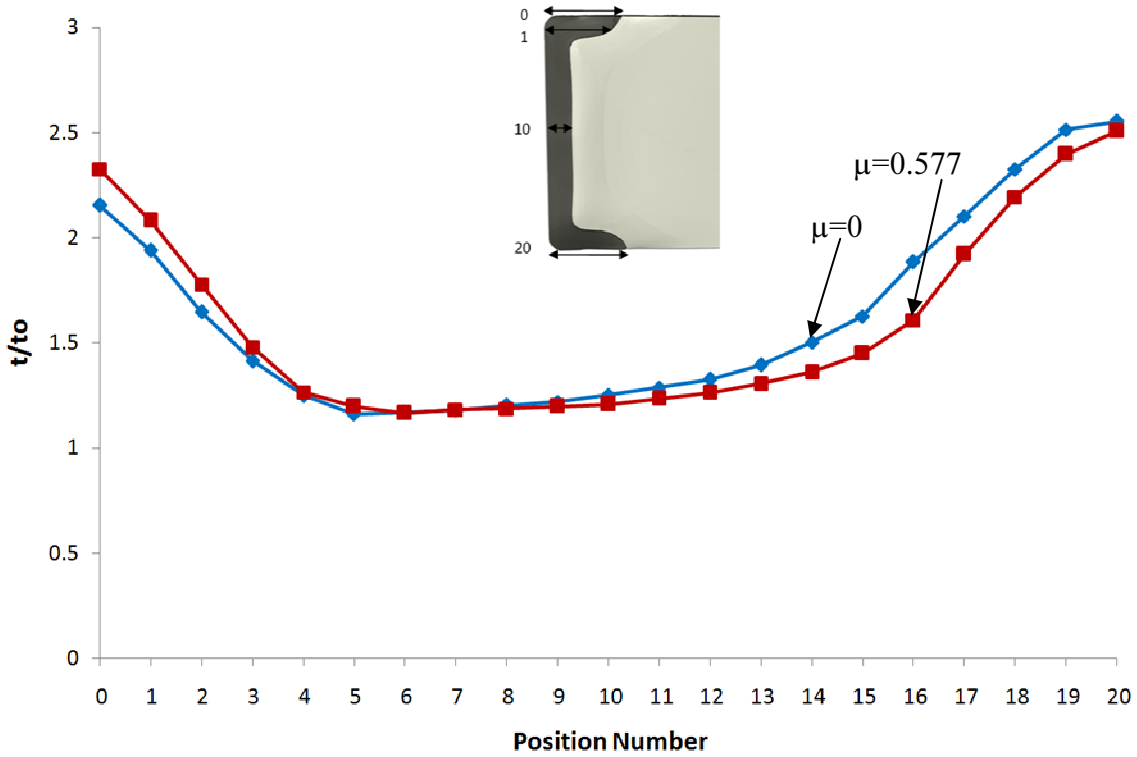


Figure 5.12: Effects of material interfacial friction on thickness variations in the vertical direction for μ=0 and μ=0.577 for an initially 4 mm thick ring. Computations are carried out using tool/work-piece interfacial friction coefficient of 0.2

As mentioned earlier, the reason for this asymmetry is due to the kinetics of the tool, whereby the die fills earlier on the counterpunch surface compared to the punch surface (Tuncer and Dean, 1988; Tuncer and Dean, 1987). Increasing the interfacial friction coefficient (μ=0.577) of the two materials can be seen to have the effect of increasing the ring thickness near the punch (position 0) and decreasing the material thickness towards the counterpunch surface (position 20), i.e. for a given die friction, an increasing interfacial friction has the effect of causing the material to be more symmetrical about the mid-height.

Figure 5.13 indicates that a larger interfacial friction has the effect of increasing the tooth root thickness, as can be seen between positions 6 and 8. However, between positions 9 and 11 it appears to result in a thinner root thickness. Therefore, it can be seen that by combining multiple frictional effects of the tool surfaces, the distribution of ring material can be off-centred in the gear in the vertical direction in conjunction with tool kinetics and can affect thickness of the ring at the tooth flanks and tooth root.

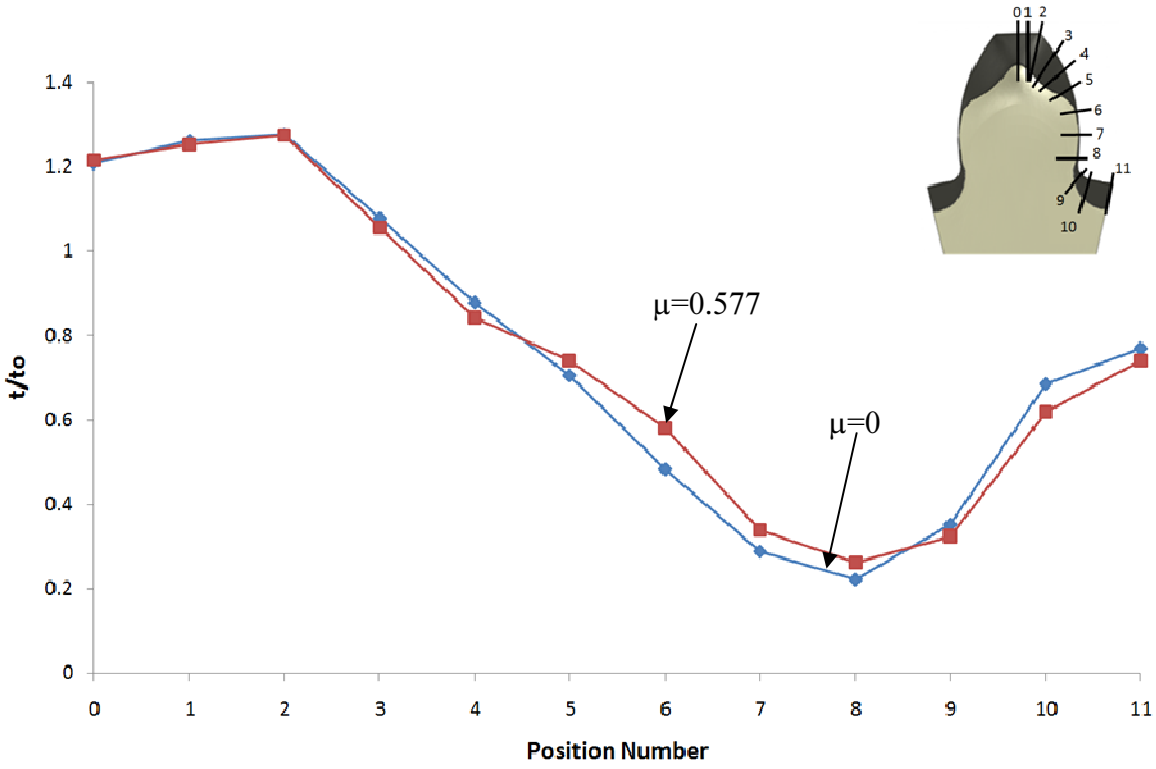


Figure 5.13: Effects of material interfacial friction on thickness variations in the horizontal direction for μ=0 and μ=0.577 for an initially 4 mm thick ring

5.3.5 Alternative Material Combinations

A further variable that would affect the material flow in the tooth profile is the combination of materials used. In order to assess this effect, three simulations were performed for a 4mm ring by applying a friction coefficient of 0.1 only on the punch and counterpunch. The three core-ring material combinations used were lead/mild steel, lead/copper and copper/mild steel. The yield strengths were obtained from compression tests at a 0.2% proof stress. The simulations were performed assuming perfectly plastic materials, whereby the yield strength ratios of the combinations are: (i) 0.05 for lead/mild steel, (ii) 0.14 for lead/copper, and (iii) 0.35 for copper/mild steel. The normalised ring thickness distribution, for the vertical and horizontal cross-sections, is shown in Figures 5.14 and 5.15 below.

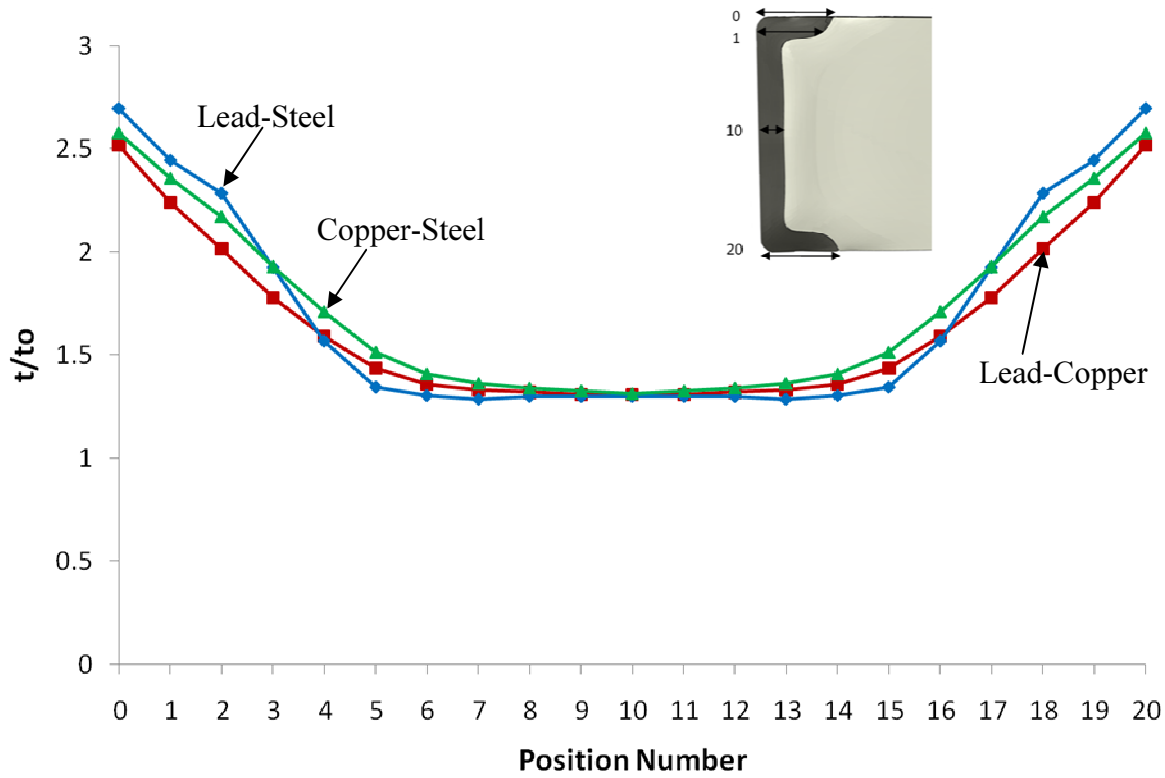


Figure 5.14: Effect of material property difference on ring thickness variations in the vertical direction. Computations are carried using ring thickness of 4mm

As can be seen from Figure 5.14, the lead/steel combination results in the largest material build-up at positions 0 and 20 with a ratio of t/t_o=2.7 compared to t/t_o=2.58 for copper-steel and 2.52 for lead-copper. Furthermore, it can be seen that at the mid-height of the tooth (position 10), all three materials exhibit a similar t/t_o ratio; lead/steel is 1.3, copper/steel is 1.32 and lead/copper is 1.45, which at a maximum difference of 11%, could be within experimental variation. However, it can be seen that the lead-steel curve exhibits a large rate of change between positions 2-5 compared to the other material combinations, but overall, it can be assumed that material distribution in the vertical direction is not significantly affected by the differing yield strength ratios.

It can be seen from Figure 5.15 that all three material combinations show similar thickness ratios between positions 3 and 8. However, the thickness distributions differ at the tooth tip and tooth root with the lead/steel combination having the largest tooth thickness whereas the copper/steel combination has the largest tip thickness. In particular, at the tooth root (position 11), the thickness ratios of the lead/steel, lead/copper and copper/steel are t/t_o=0.86, 0.73 and 0.65 respectively. At the tooth tip, this ratio is t/t_o=1.45, 1.32 and 1.29 for the copper/steel, lead/steel and lead/copper combinations respectively. A clear trend is observed whereby a

higher yield stress ratio results in lower ring thinning near the root. Furthermore, a higher yield stress ratio has the effect of increasing the ring thickness at the tooth tip. Therefore, a large root thickness can be achieved by having two metals of substantially different yield strengths.

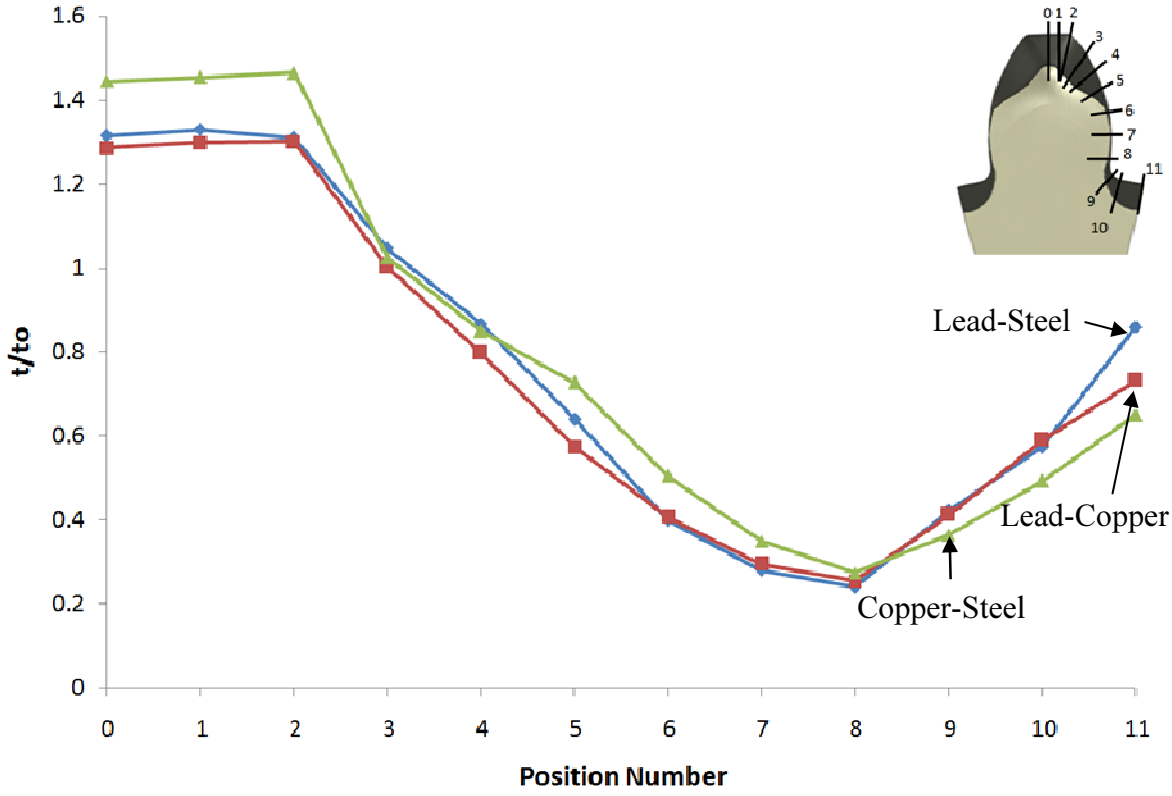


Figure 5.15: Effect of material property difference on ring thickness variations in the horizontal direction. Computations are carried using ring thickness of 4mm

Therefore, it can be seen that the relative mechanical properties of ring and core affect ring thickness distribution around the periphery of a tooth. The use of materials with a large disparity between their material properties will influence the material distribution and hence performance of the gear. Careful material selection as well as simulation analysis is required to ensure that the material flows in the expected manner.

5.4 Numerical Procedures for Hot Forging

A preliminary hot forging simulation to model an aluminium-steel gear of ring thickness 6mm was developed by recreating all the components such as die, punch and counterpunch as 3D deformable bodies rather than discrete or analytically rigid components to allow the effect of temperature on these tool components. Furthermore, the elements used for all components

were modified to allow for the effect of temperature. The temperatures of all heated components before forging, as was discussed in Chapter 3, were used as input to the simulation. Specifically, the toolset was heated to 200^{o}C, the aluminium core to 535^{o}C and the steel ring to 1150^{o}C. An 'inelastic heat fraction' of 0.95 was also included in the material properties, as during the forging process, 'approximately 90 to 95% of the mechanical energy is transformed into heat' (Li *et al.*, 2006; Altan *et al.*, 2005; Farren and Taylor, 1925).

5.4.1 Implementation of Constitutive Equations Using VUMAT

The constitutive equations of the 230M07 steel ring and Al 6082-O core, the constants of which were determined in Chapter 4, were included in the simulation to allow for temperature and strain rate dependent behaviour based on strain rate, stress, dislocation density and isotropic hardening to be accounted for in the simulation. To implement the constitutive equations into Abaqus, a Variable User Material (VUMAT) subroutine was used (Foster, 2007). To include the effect of temperature, the specific heat capacity and thermal conductivity of the ring, core, and tool components were incorporated, with values of specific heat capacity of 460 J/kg.K, and thermal conductivity of 24.3 W/m-K for tool steel (Matweb, 2013a); 481 J/kg.K and 55 W/m-K for mild steel (Matweb, 2013b; PXPrecimet S.A., 2012); and 900 J/kg.K and 172 W/m-K for Al 6082 (CES Edupack, 2010; Mohammed *et al.*, 2012). Furthermore, the variation of heat transfer coefficient with contact pressure for tool steel as presented by the authors Tondini *et al.* (2011) and Caron *et al.* (2013); and for aluminium as presented by Foster *et al.* (2008) were incorporated into the component contact properties of the simulation. By incorporating this data for a 6mm ring thickness simulation, it was found that by the end of the forging, the interface temperature between ring and core at the tooth tip had reduced to 415^{o}C. This large temperature reduction coupled with the relatively short forging time period of 10s is not conducive to promoting a diffusion bond between ring and core and may explain the difficulty in the formation of a diffusion bond shown in Chapter 3. As this simulation was for the largest ring thickness of 6mm, it is expected that the lower ring thicknesses of 2mm and 4mm will exhibit greater ring temperature reduction, thus increasing the difficulty in the formation of a diffusion bond between the core/ring interface. Suggested methods of resolving this are discussed in the recommendations of future research section of Chapter 7.

Chapter 6 Finite Element Simulation of Contact Performance of Multi-Metal Gears

The work performed in this chapter presents the FE model constructed using Abaqus CAE, to assess the stress distribution of bi-metallic aluminium-steel gears in comparison with single material steel gears, under running conditions. Variables such as lubricant, film thickness and surface temperature which require solving lubricant viscosity variations with pressure, bulk surface temperature variations and heat flux (Wang and Cheng, 1981; Wang and Cheng, 1980) were considered to be beyond the scope of this work and are hence not included in the analysis.

In order to assess the validity of the FE model, an analysis using both the empirical American Gear Manufacturers Association (AGMA) and British Standard (BS), was performed to determine tooth contact stresses and root stresses of a solid steel gear to compare them with values found from FE analysis. Having verified the validity of the model, simulations were performed for uniform ring thicknesses of 1mm, 2mm, 4mm and 6mm to estimate the contact stress, root stress and stress distribution within a bi-metal tooth, and a comparison was made with a single material tooth to identify significant changes in behaviour. Finally, simulations were performed for thinned ring profiles of 2mm, 4mm and 6mm, whose profile was determined in Chapters 3 and 5 and the stress distribution during gear meshing was compared with the uniform ring thickness simulations. This allows for the mechanical performance of the forged bi-metal gears to be evaluated.

6.1 Analytical/Empirical Estimation of Tooth Stresses

As stated in the introduction, gears transmit power from one rotating shaft to another by the repeated rolling and contact of the teeth between the gears (Chacon *et al.*, 2010). The conjugate action of an involute profile provides a constant angular velocity throughout the contact of two mating teeth. Extensive work has been performed throughout the years (Hwang *et al.*, 2013; Dean, 1974; American Gear Manufacturers Association, 1966; Buckingham, 1949; Lewis, 1892; Hertz, 1881) in determining the fatigue and mechanical performance of gears through analytical, experimental, and more recently numerical methods, which has allowed them to be used effectively, and with predictable performance. In order for multi-metal gears to be accepted in an operating environment, the performance of these gears

must be analysed and compared with conventional gear performance, and variations between these two must be determined.

Conventional gear theory such as the Hertz contact theory (Hertz, 1881), and the Lewis (Lewis, 1892) and Buckingham (Buckingham, 1949) equations have provided analytical equations to estimate the bending and contact stresses (Sfakiotakis *et al.*, 2001) of the tooth. However, these equations have limitations; for example, Hertz contact theory assumes frictionless contact of two long cylinders to represent gear teeth, whilst making it difficult to account for the geometry of the tooth. Moreover, the Lewis equations are based on the assumption that a tooth is a cantilever beam. More accurate approximations can be made from equations published in documents by the AGMA (American Gear Manufacturers Association, 1966) and the British Standards Institution (BS ISO Standard, 2006a) which assist both manufacturers and end users to estimate gear performance. However, according to the literature, the complex nature of 'time varying stress fields' (Sfakiotakis *et al.*, 2001) due to the 'rolling and sliding action associated with gear teeth meshing' (Chacon *et al.*, 2010) requires the use of computer models to obtain an 'accurate prediction of these stresses experienced by the load carrying teeth' (Sfakiotakis *et al.*, 2001), free of the simplifying assumptions of analytical methods. Several studies such as those performed by Vijayarangan and Ganesan (1993), Ramamurti and Ananda Rao (1988) and Wallace and Seireg (1973) have analysed the dynamic bending stresses of the tooth loading. Moreover, studies performed by Refaat and Meguid (1995) and Arikan (1991) have accounted for the distribution of contact stresses in gears.

The stresses experienced by the tooth root, particularly at the tooth fillet region are 'mainly responsible for tooth breakage' (Sfakiotakis *et al.*, 2001; Dolan and Broghamer, 1942). The tooth bending strength was first presented by Lewis (1892), who stated that the gear tooth can be modelled as a parabolic cantilever beam. He estimated the bending stress at the tooth fillet using equation 6.1, where, σ_L= tooth bending stress at tooth fillet, F_t = tangential load at tooth tip, b = tooth width, y = tooth form factor, p = circular pitch of the gear, and K_t = stress concentration factor.

$$\sigma_L = \frac{F_t}{byp} K_t \qquad Eqn\ 6.1$$

The maximum contact stress was calculated by Buckingham (1949, 1935) using equation 6.2, where, σ_B = maximum Hertzian contact stress, F_n = normal contact force, d = gear pitch

diameter, Q_g = gear ratio factor ($2N_n/(N_r + N_n)$), K_m = material factor ($1/E_r + 1/E_n$), and φ = pressure angle. For the gear ratio factor Q_g, N_r represents the number of teeth in driver gear, N_n the number of teeth in driven gear, and E is the Young's modulus of the gear (Sfakiotakis *et al.*, 2001).

$$\sigma_B = \sqrt{\frac{F_n}{dbQ_g K_m \sin\varphi}} \qquad Eqn\ 6.2$$

These equations offered early estimates for determining gear stresses. More recently, gear standards found in the British Standards Institution and the AGMA handbook are used to provide more accurate estimates for values such as gear contact stresses and bending stresses. The British Standards BS ISO 6336 (BS ISO Standard, 2006a, 2006b, 2006c) as well as the AGMA standards (American Gear Manufacturers Association, 1966) are used in this chapter in order to calculate the contact and root stress for two meshing steel gears of dimensions similar to the forged gears described in previous chapters. These estimates are also used to provide a value to compare with those produced by FE simulations presented in later sections of this chapter.

6.1.1 Contact Stress Calculations

The estimation of contact stress is important as it plays a significant role in affecting the 'scoring and surface cracking failures' (Sfakiotakis *et al.*, 2001) in gears. Tooth contact stress can be determined from equation 6.3 below, which is found in the AGMA standards (Childs, 2003; American Gear Manufacturers Association, 1966).

$$\sigma_c = Z_e \left(W_t K_{OF} K_v' K_s \frac{K_H}{Fd} \frac{Z_R}{Z_I} \right)^{0.5} \qquad Eqn\ 6.3$$

The constants of the equation above are as follows: σ_c = absolute contact stress; Z_e = elastic coefficient taking into account the effect of material properties such as Young's modulus and Poisson's ratio; W_t = transmitted tangential load; K_{OF} = overload factor; K_V' = dynamic factor; K_s = size factor; K_H = load distribution factor; F = face width; d = pitch diameter of pinion; Z_R = surface condition for pitting resistance, and Z_I = geometry factor for pitting resistance. As mentioned in previous chapters, the dimensions of the forged gears are as follows: φ = 20° pressure angle, m = 5mm module, F = 20mm facewidth, N_t = 13 teeth, and d = 0.065m pitch circle diameter. Furthermore, it is assumed that the gear will be subjected to

a torque of T_q = 150Nm, as this is a reasonable estimate for an automotive transmission, and the analysis is a quasi-static analysis as performed in the literature (Rameshkumar *et al.*, 2010; Wang and Cheng, 1981). Moreover, the calculations have been performed for a transmission ratio of 1, whereby the pinion and gear are of the same dimensions. The detailed calculations of the AGMA contact stress can be found in Appendix B.1. The calculated value for the contact stress is found to be $\sigma_c = 1{,}374.67MPa$. According to the literature (Saarstahl, 2004; Davis, 1996), gear steels such as 16MnCr5 can have yield strengths between 1000 to 1400MPa, with some steels even exceeding 2000MPa (He *et al.*, 2004), and therefore at the calculated contact stress for the specified torque and tooth geometry, plastic deformation will not arise for steels exhibiting higher yield strengths. The contact stress calculated from the AGMA methods can be compared to that found from the British Standards (BS ISO Standard, 2006a, 2006b, 2006c), which, although similar, introduce additional factors that must be considered in gear calculations in order to provide a second empirical value to compare with FE simulations. According to the British Standards (BS ISO Standard, 2006b), the tooth contact stress ($\sigma_{H1,2}$) can be found from equations 6.4 and 6.5 below, where, σ_{HO}, defined as 'the nominal contact stress at the pitch point' (BS ISO Standard, 2006b), must first be calculated before calculating the 'contact stress at the inner point of single pair tooth contact' (BS ISO Standard, 2006b) written as $\sigma_{H1,2}$.

$$\sigma_{HO} = Z_H Z_E Z_\varepsilon Z_\beta \sqrt{\frac{F_t}{d_1 b} \cdot \frac{u+1}{u}} \qquad Eqn\ 6.4$$

$$\sigma_{H1,2} = Z_B \sigma_{HO} \sqrt{K_A K_v K_{H\beta} K_{H\alpha}} \qquad Eqn\ 6.5$$

The constants of equation 6.4 are defined as: Z_H = zone factor taking into account flank curvatures at pitch point, Z_E = elasticity factor taking into account material properties such as Young's modulus and Poisson's ratio, Z_ε = contact ratio factor taking into account overlap ratios on the surface load, Z_β = helix angle factor taking into account the influence of a helix angle of helical gears, u = gear ratio, F_t = tangential force, d_1 = pitch diameter and b = facewidth. The constants in equation 6.5 represent: Z_B = single pair tooth contact factor, K_A = application factor for variations of input or output torque, K_V = dynamic factor, $K_{H\beta}$ = face load factor and $K_{H\alpha}$ = transverse load factor. The detailed calculations of the contact stress using the British standards method can be found in Appendix B.2. From these calculations, the tooth contact stress can be calculated as being $\sigma_{H1,2} = 1{,}415.33MPa$, which is

approximately 3% higher than the AGMA estimated value and greater than the 1400 MPa yield strength for 16MnCr5 gear steel, which demonstrates that an 150Nm torque is the upper limit to avoid yield for the current tooth geometry using a typical gear steel. Therefore, the average contact stress value from the standards can be calculated as being 1395 MPa for single material gears.

6.1.2 Root Stress Calculations

As described earlier, the Lewis equation can be used to approximate the bending stress at the tooth fillet. The Lewis form factor, which is a factor taking into account geometry of the tooth, for the prescribed tooth dimensions is found from the literature (Childs, 2003; Mitchener and Mabie, 1982) as being Y = 0.24317. A calculation of the estimated bending stress can be found in Appendix B.3, where it is calculated as being approximately σ_L = 190MPa. However, as explained by Dolan and Broghamer (1942), the Lewis equation under-predicts the fillet stress as 'the sharpness of the fillet radius which greatly influences the maximum stress developed in the fillets' (Dolan and Broghamer, 1942) is not considered and it assumes the tooth as a constant cross-section cantilever beam without factoring the change in cross-section of the tooth profile. A more accurate estimate can be obtained from the AGMA handbook. According to the literature (Childs, 2003; American Gear Manufacturers Association, 1966) the bending stress can be calculated from equation 6.6:

$$\sigma_{BE} = W_t K_{OF} K_V^{'} K_s \frac{1}{Fm} \frac{K_H K_B}{Y_J} \qquad Eqn\ 6.6$$

The constants of the above equation represent: σ_{BE} = bending stress; W_t = transmitted tangential load; K_{OF} = the overload factor, taking into account additional external loads to the tangential load; K_V' = dynamic factor, taking into account the increase in load during operation at high speed; K_s = size factor, which accounts for non-uniformity in material of large dimensions; F = face width; m = module; K_H = load distribution factor, which accounts for non-uniform distribution of load across the line of contact; K_B = rim thickness factor; and Y_J = geometry factor for bending strength. Detailed calculations of this stress can be found in Appendix B.4, where the bending stress is calculated as being σ_B = 250MPa.

6.2 Numerical Procedures

A finite element model was created using Abaqus CAE 6.11 for two meshing gears in order to determine the variation in stress distribution for various ring thickness gears under

operation. A quasi-static 2D planar elastic model was created through the standard solver as opposed to a dynamic simulation using a dynamic explicit analysis, to reduce the overall computational time, whilst obtaining comparative results for low speeds (Ajmi and Velex, 2005; Kahraman *et al.*, 1990). The simulation of bi-metal aluminium-steel gear meshing required the specification of the Elastic Modulus, and Poisson's ratio (Chacon *et al.*, 2010; Rameshkumar *et al.*, 2010). Specifically, the properties used were E = 210GPa and υ = 0.3 for 16MnCr5 steel (SteelSS, 2011) and E = 72GPa and υ = 0.33 (CES Edupack, 2010) for Al 6082 aluminium.

The gear profile used in the simulation was similar to the forged gear profile described in earlier chapters. The involute profile to generate the gear teeth was plotted using the involute profile equations of Chapter 5. For the model, a 2D plane strain simulation was created (Rameshkumar *et al.*, 2010; Hsieh *et al.*, 1992) as this approximation can be made for a high face width to tooth height ratio (Beghini *et al.*, 2004). In order to model the operation of the gears, both the driver and the driven gear were modelled as having the same dimensions, hence simulating a transmission ratio of 1. Both driver and driven gears were simulated with only three teeth in order to reduce the total number of elements and solving time. The contact between two meshing gear teeth was set as frictionless contact, with hard normal contact behaviour allowing separation after contact, as 'the effect of the sliding friction is found to be rather limited' (Kahraman *et al.*, 2007), with only a 5% increase in contact stress 'when the friction coefficient is increased from 0 to 0.3' (Vijayarangan and Ganesan, 1994). Furthermore, the two gears were connected to individual analytically rigid shaft components where the torque was applied. The gear teeth were partitioned in 10 regions as shown in Figure 6.1 in order to allow for varying element density and hence obtain a representative stress profile whilst reducing the total number of elements per tooth (Litvin and Fuentes, 2004).

The elements used for the tooth were of the quadrilateral type CPS4R with reduced integration and hourglass control. The mesh was created by assigning edge seeds and automatically generating the mesh using the top-down free meshing technique and medial-axis meshing algorithm. A convergence test was performed for single material steel gears of torque T_q = 150Nm as used in the analytical and empirical analyses, where tooth contact stress value was recorded for varying node/element numbers and compared with the empirical value calculated using the AGMA and British Standards. As can be seen from

Figure C1 in Appendix C, the result of the convergence study tends towards a von Mises contact stress of 1235 MPa and a principal stress of 1271MPa which is 9% lower than the empirically calculated value of 1395 MPa.

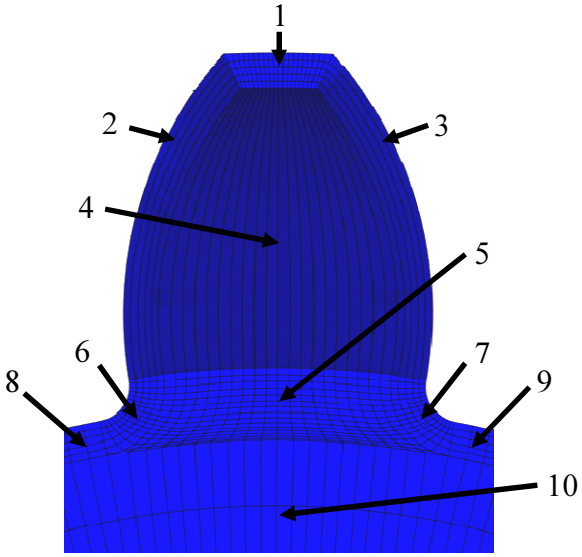


Figure 6.1: Discretised regions for meshing

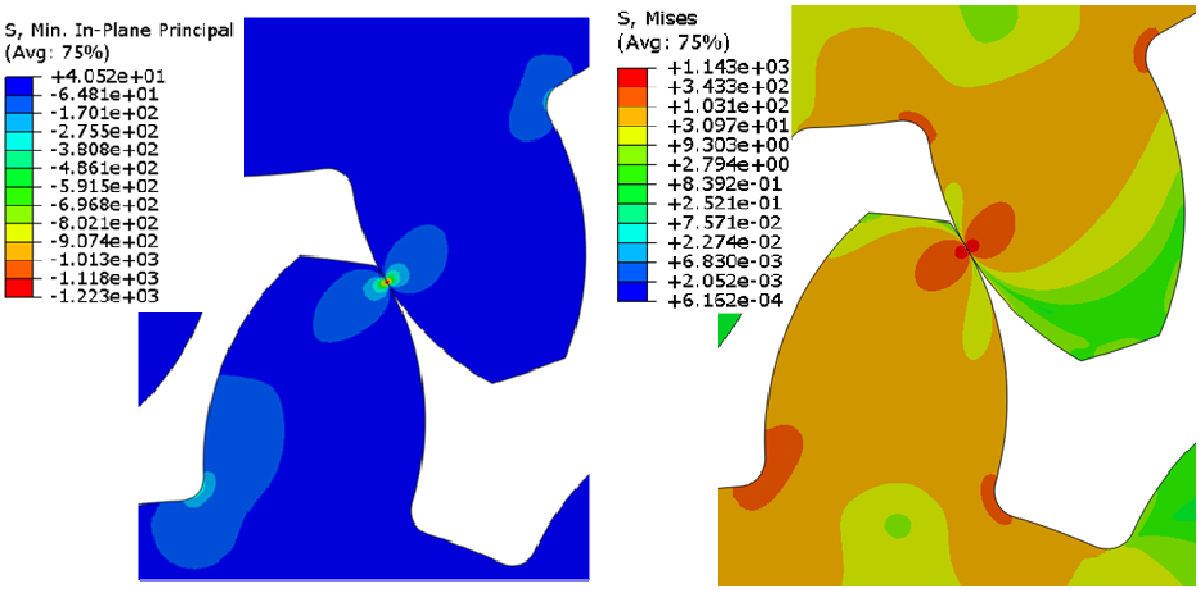
The difference between these values can possibly be explained by the extensive assumptions and approximations made in determining various constants in the analytical and empirical equations, as demonstrated in Appendix B. Furthermore, FE models tend to predict lower contact stresses than the analytical calculations, as the models allow for elastic tooth deformation with 'contact zones with greater area, and therefore lower pressures' (Chacon *et al.*, 2010). In order to reduce computational time, the number of nodes used per tooth was fairly low (42738), thus predicting a von Mises contact stress of 1143 MPa or 8% lower than the 1235 MPa but with a 5 fold reduction in computational time compared to the more detailed runs in the convergence test. Hence, further simulations have been performed with this node value.

Bi-metal simulations were performed by creating individual ring and core parts and applying the material properties of steel and aluminium to these parts respectively. Simulations were performed for uniform ring thicknesses of 1mm, 2mm, 4mm and 6mm. The ring thinning gears of 2mm, 4mm and 6mm have been simulated by using the final thinned profile of the forged ring from Chapters 3 and 5 and applying this geometry to the ring and core parts of these simulations. These simulations are presented in Sections 6.3.2 and 6.3.3, respectively.

6.3 Stress Distribution in a Gear Tooth

6.3.1 Steel Tooth Stress Distribution

A single material steel gear was first simulated in order to compare to the analytical and empirical results calculated earlier. An example of the principal stress and von Mises stress distribution obtained from the single material steel gear simulation at first contact is shown in Figure 6.2 below. The stress distribution at first contact is analysed as 'the most severe load conditions is found when a single pair of teeth assume the full burden' (Chacon *et al.*, 2010). Furthermore, as can be seen from the figure, the stress is greatest at the contact point and 'decreases in the normal direction to the surface' (Vijayarangan and Ganesan, 1994) and along the surface.



(a) (b)

Figure 6.2 Steel stress distribution: (a) Principal stress and (b) von Mises stress

According to the literature (Vijayarangan and Ganesan, 1994), the stress at a depth of 0.5 mm perpendicular to the contact surface reduces to approximately a half of the contact stress value for the module 10mm gear analysed in the literature. The simulation of Figure 6.2 has found that the stress indeed reduces from a value of 1143 MPa at the point of first tooth contact to a value of 539.2 MPa at a depth of 0.5 mm. Moreover, the root fillet stresses, which are 'evaluated at the middle points of fillet arcs' (Dolan and Broghamer, 1942) of the compressive and tensile root fillets were found to be 297.1MPa on the compressive and 223.2MPa on the tensile fillets. During disengaging of the tooth, the compressive and tensile stresses reduced to 175.1MPa and 172.3MPa, respectively, where it can be seen that the root

stress on the compressive fillet is once again greater than the tensile fillet. This has been demonstrated in the literature where the authors Dolan and Broghamer (1942) have found that 'the maximum stress on the fillet in compression was often larger than that at the fillet in tension' although this can vary depending on load direction and tooth geometry. As the simulation for single material gears was found to be validated by the literature, the model of bi-metal gear meshing was developed, based upon this single-material model.

6.3.2 Uniform Ring Thickness Stress Distribution

As described earlier, aluminium-steel gears in service, were simulated by creating separate components for the steel ring and aluminium core. The first bi-metal gear meshing simulation was conducted for a uniform ring thickness of 1mm with an applied torque of T_q = 150Nm, whose stress distribution at first tooth contact is shown in Figure 6.3. As can be seen from Figure 6.3, the stress distribution within the tooth varies significantly from a single steel material tooth shown in Section 6.3.1. The Figure shows that the high stress values not only occur normal to the contact point, but are found to be distributed around the aluminium core and along the majority of the steel ring. This is due to the ring material having a greater stiffness than that of the core material, and thus provides the majority of the rigidity and structural integrity when transmitting torque.

The simulation shown in Figure 6.3 has demonstrated that the von Mises stress perpendicular to the contact point decreases as in the single material tooth, up to a point, where the stress value then increases towards the inner side of the ring. However, when evaluating the von Mises stress at the outer surface of the aluminium core, it is found to be substantially less than on the adjacent inner surface of the ring (position A). This is shown graphically in Figure 6.7 at the end of this section for clarity, where the Mises stress on the inner surface of the steel ring is 256MPa and that of the outer surface of aluminium core is 148MPa. As the yield stress for aluminium is σ_y = 265MPa (CES Edupack, 2010), the aluminium core will avoid plastic deformation. Moreover, the maximum stress experienced at the compressive root fillet of the steel (position B) is 483.8MPa, whereas on the inner surface of the steel (position C) it is 86.0MPa and 71.3MPa on the outer surface of the aluminium surface. On the tensile root fillet (position D), the stress on the outer surface of ring is found to be 317.6MPa, whereas the inner surface of the ring (position E) experiences 46.3MPa. The outer surface of the aluminium experiences 39.8MPa.

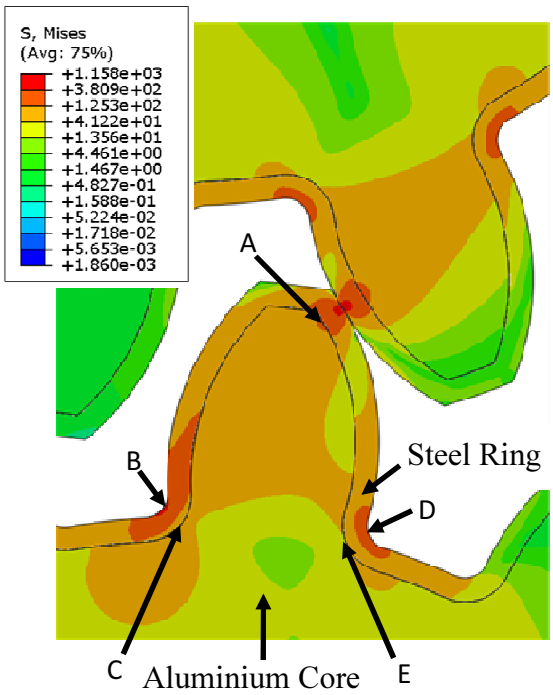


Figure 6.3: 1mm ring stress distribution

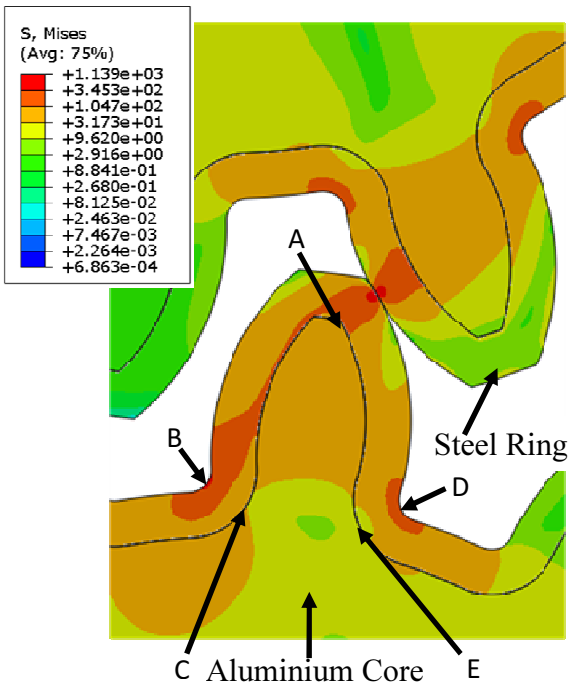


Figure 6.4: 2mm ring stress distribution

A similar analysis was conducted for a 2mm uniform ring thickness as shown in Figure 6.4. The Figure shows that the stress experienced at the contact point at a value of 1139 MPa is similar to the 1158MPa experienced for the 1mm ring. A large stress is also experienced around the steel ring periphery and is reduced substantially on the outer surface of the aluminium core. The stress variation with depth normal to the contact point is again shown in Figure 6.7 for clarity. For example, at first tooth contact, the von Mises stress on the inner surface of the steel (position A) is found to be 149.5MPa, whereas the on the outer surface of the aluminium it is 80 MPa. Hence, the increased ring thickness has substantially reduced the stresses at the interface by 46% compared to the 1mm ring. Furthermore, the maximum stress on the compressive tooth fillet (position B) is 408MPa on the steel ring, whereas the inner surface of the ring and outer surface of the aluminium experience 40.8MPa and 36.5MPa, respectively (position C). The stress on the surface of the tensile root fillet (position D) for the steel ring is 282.3MPa, whereas the inner side of steel and outer surface of the aluminium are 30.1 MPa and 24.6MPa, respectively (position E).

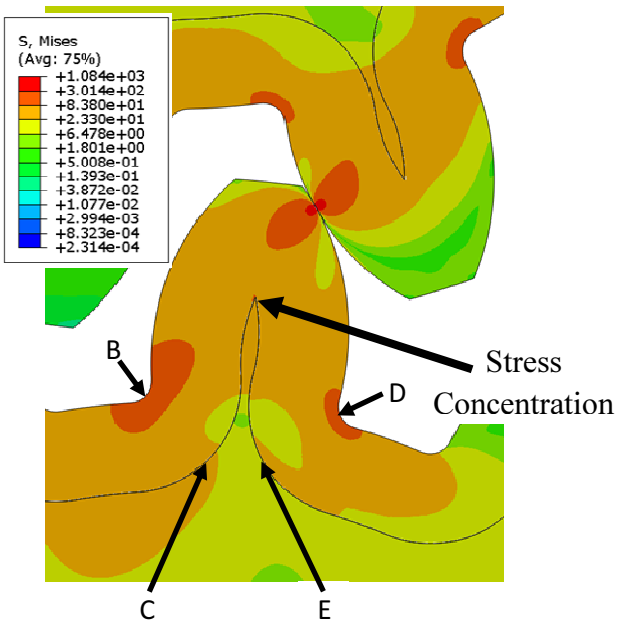
The 4mm uniform ring thickness simulation results are shown in Figure 6.5. As can be seen, a uniform ring thickness throughout the tooth results in core material protruding radially outwards in a thin, sharp profile. Although this would be difficult to manufacture in practice, it allows for a comparative analysis with uniform ring thicknesses examined earlier. Firstly, it can be seen from Figure 6.7 that a 4mm ring thickness appears to be large enough to remove

the significant variation in stress distribution between bi-metal and single material gears. It can also be seen from Figure 6.5 that the sharp protrusion of core material into the ring creates a region of stress concentration whereby the stress increases substantially when compared to the surrounding material within the tooth. This demonstrates that any multi-material gear should be comprised of rounded geometry at the material interface to minimise stress concentration and hence the risk of an internal fracture during operation. The results of this 4mm uniform ring simulation have shown that the maximum root stress is found to be 337.2MPa and 234.0MPa on the compressive (position B) and tensile (position D) fillets, respectively. In the normal direction on the compressive fillet, the stresses are 28.4MPa on the inner surface of the ring and 24.1MPa on the outer surface of the core (position C). Similarly, normal to tensile fillet, the stresses are 30.3MPa and 21.1MPa on the inner surface of ring and outer surface of core, respectively (position E).

The final uniform ring thickness simulation was conducted for a 6mm uniform ring resulting in a tooth comprised entirely of steel material with minimal protrusion of aluminium of only 1.83mm into the steel profile, as shown in Figure 6.6. Due to the large ring thickness, the gear teeth behave as in the solid steel gear of Section 6.3.1. The prevention of aluminium core material flowing into the tooth allows for the existing AGMA and British standards to be used in predicting tooth contact and root stresses, hence greatly reducing the complexity of analysis. These results are summarised in Table 6.1.

Table 6.1: Summary of stresses through different regions of gear tooth (uniform ring profiles)

Ring Thickness (mm)	Tooth Fillet Type	Surface Stress (MPa)	Inner Steel Stress (MPa)	Outer Al Stress (MPa)
1	Compressive Fillet	483.8	86.0	71.3
	Tensile Fillet	317.6	46.3	39.8
2	Compressive Fillet	407.8	40.8	36.5
	Tensile Fillet	282.3	30.1	24.6
4	Compressive Fillet	337.2	28.4	24.1
	Tensile Fillet	234.0	30.3	21.1
6	Compressive Fillet	309.1	-	-
	Tensile Fillet	223.4	-	-
Single Steel	Compressive Fillet	297.1	-	-
	Tensile Fillet	223.2	-	-



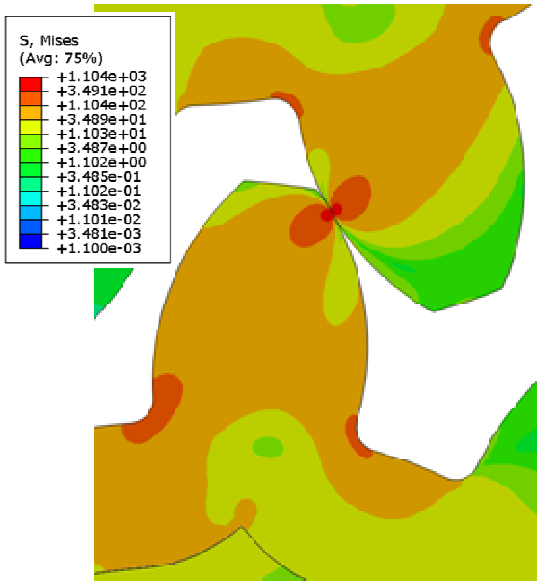


Figure 6.5: 4mm ring stress distribution **Figure 6.6: 6mm ring stress distribution**

A comparison of stress along a path normal to the point of first contact is shown graphically in Figure 6.7 for all uniform ring thicknesses as well as for a single material steel gear. For clarity, the stress is shown on a logarithmic scale. As can be seen, all gears experience an exponential reduction in stress where the contact stress declines 80% within the first millimetre of material. In fact, it has been found that as long as the contact stress at the ring remains below the yield stress of steel, for this gear geometry, the stress experienced by the aluminium core remains below its yield stress. Furthermore, for ring thicknesses of 1mm and 2mm, it can be seen that there is a large variation in stress across the transition from ring to core material at 1mm and 2mm respectively, and this transition variation is also present on the other side of the tooth. As discussed earlier, the transition from ring to core results in the von Mises stress increasing towards the inner surface of the ring before sharply declining when measured on the outer surface of the core, where the stress changes from 256MPa to 148MPa or 42.2% for the 1mm ring. Similarly, for the 2mm ring, this behaviour is again observed with a change from 149.5 to 80MPa or 46.5% at the interface of the two materials. Therefore, it can be seen that for both of these thin rings, the stress experienced at the surface of the core is approximately half of that experienced on the inner surface of the ring. Moreover, at measured depths of approximately 5mm and 6mm into the tooth, the stress again sharply increases when measuring across the core-ring boundary, where the stress of the core is 49.6% of the ring for the 1mm ring and 55.5% for the 2mm ring. Large ring

thickness teeth of 4mm and 6mm experience no transition from steel to aluminium in the measured direction, as all measurements are taken within the ring material. This results in a stress profile similar to the single material tooth. It should be observed from Figure 6.7, that single material teeth and large ring thickness gears experience a greater stress at measured depths between 2-5mm when compared to the 1mm and 2mm gears where the aluminium experiences a lower stress at this depth. A possible reason for this is that a generally higher overall stress is experienced throughout the entirety of the stiffer thin ring profile, which may reduce the stress propagated through the less stiff aluminium core. Finally, from the perspective of the measured direction, the 4mm, 6mm and solid steel teeth values overlap which shows that at certain thicknesses, the complexities of a steel-aluminium transition can be avoided, with bi-metal gears behaving similar to a single material gear.

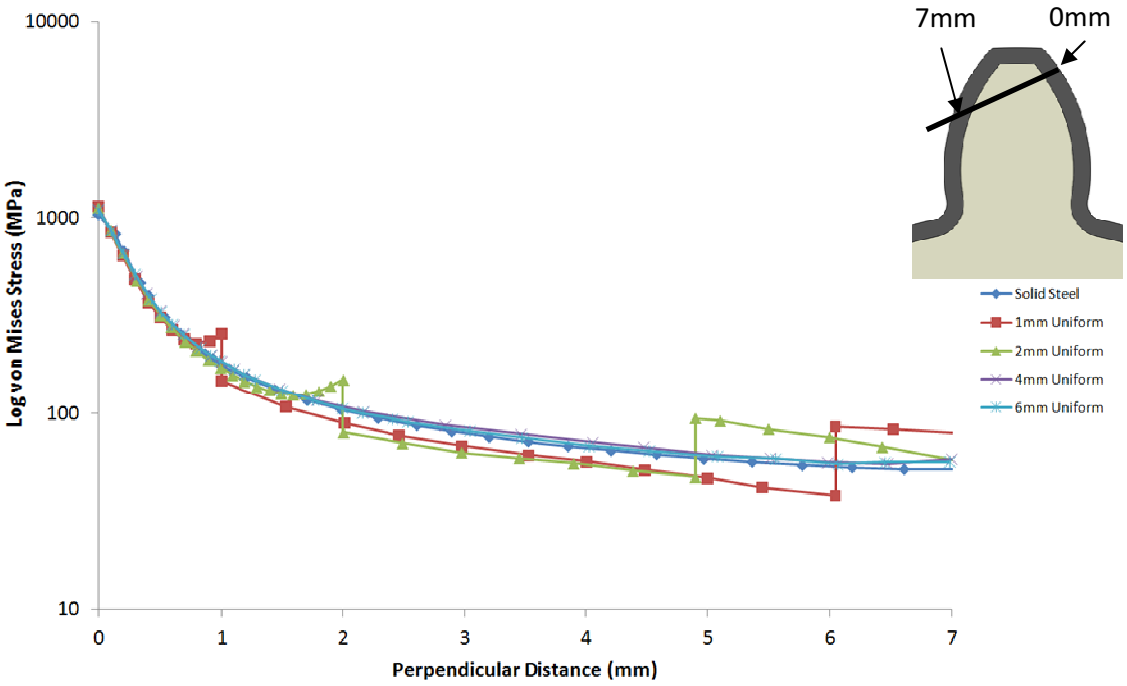


Figure 6.7: Stress perpendicular to contact point (first contact) for uniform ring gears

Although contact stresses are the greatest stresses experienced during gear meshing, the tooth fillet region must be examined and the fillet stresses compared with single material teeth in order to determine differences in operational behaviour. The stress evaluated at the mid-point of both the compressive and tensile root fillet for single material and uniform ring thickness teeth are shown in Figures 6.8 and 6.9, respectively. As shown in Figures 6.8 and 6.9, the stresses are plotted against rotational angle, with 0 rad being the point of first contact and

0.45 rad the point of disengagement of the gear, with these rotation angles being labelled 'Position A' and 'Position B', respectively. The single material steel tooth shows the lowest compressive fillet stress at 300MPa differing by 20% from the AGMA equation or 32% from the Lewis equation, which is within the variation band of 20-120% found in the literature (Dolan and Broghamer, 1942). Nevertheless, a clear trend is shown in both Figures 6.8 and 6.9, where the maximum stress is experienced when the load is applied 'at the tip of the tooth' (Dolan and Broghamer, 1942) due to the large moment arm and reduces exponentially as the gear tends to disengage.

Furthermore, as can be seen from Figures 6.8 and 6.9, thin rings experience a far greater stress at the tooth fillets than single material gears, as the overall stiffness of the tooth is lower whilst supporting the same load from the applied torque. Furthermore, Figures 6.8 and 6.9 show that increasing the ring thickness tends towards single material tooth behaviour. It can be seen that ring thicknesses of 4mm and 6mm have similar compressive and tensile fillet stresses as a single material steel tooth with the difference being 13.5% and 4.8% for the 4mm ring and 4% and 0.1% for the 6mm ring, respectively. Moreover, as has been found in the simulations and confirmed by the literature, 'higher values of stress are obtained for the fillet on the compression side of the tooth' compared to the tensile side (Dolan and Broghamer, 1942).

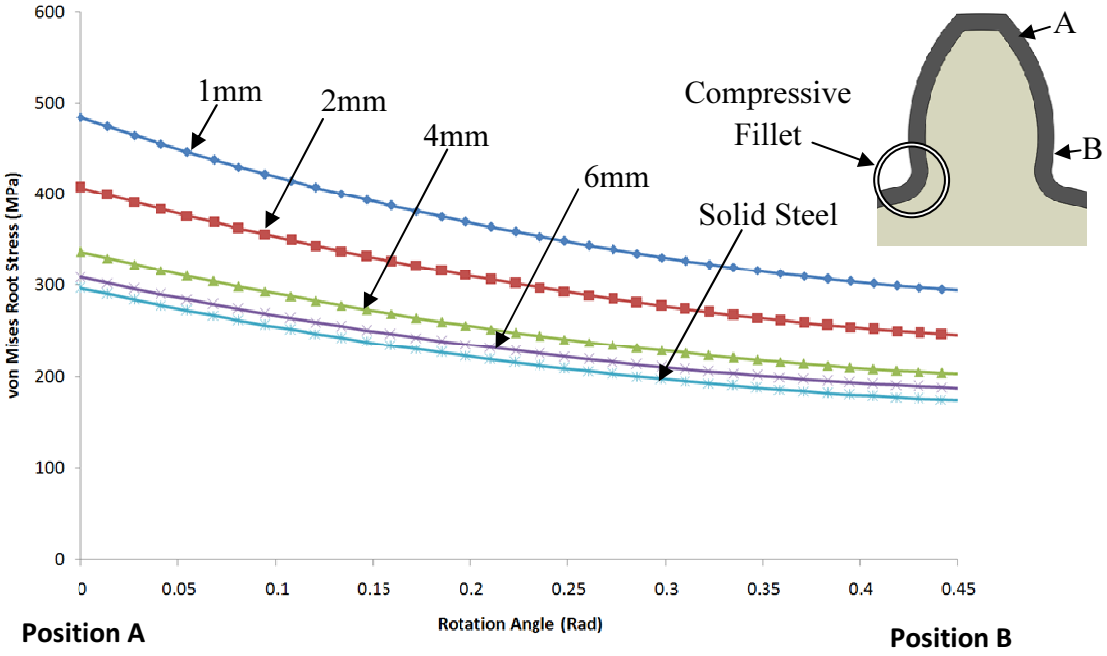


Figure 6.8: Compressive surface root stress comparison for uniform ring thickness

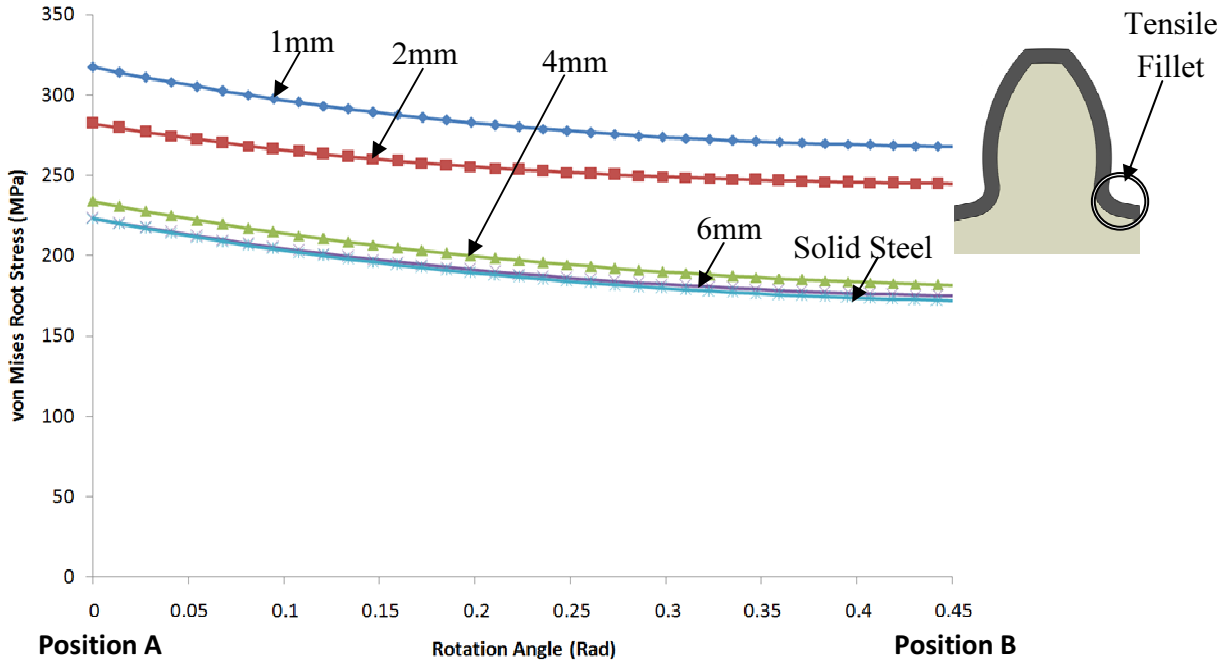


Figure 6.9: Tensile surface root stress comparison for uniform ring thickness

6.3.3 Forged Ring Profile Stress Distribution

Previous simulations presented in Section 6.3.2 were conducted for the case of a uniform ring thickness around the entirety of the tooth. However, during the forging process, it has been shown in Chapter 3 that extensive ring thinning is present. Hence, the operational performance of these forged/thinned gears must be simulated and any differences with uniform ring thickness gears identified. The simulations presented in this section involve the use of the thinned ring profiles determined at mid-thickness from the forged gears and applying these profiles to the core and ring components.

The 2mm ring profile shown in Figure 6.10a has experienced substantial thinning during forging towards the tooth root and flanks and a protrusion has been formed towards the tooth tip, resulting in a significant variation of stress distribution compared to a 2mm uniform ring profile. For example, the thinning of the tooth root and flank has led to a high stress being experienced in the aluminium core. Furthermore, the protrusion of the aluminium into the ring at the tooth tip has created a region of stress concentration.

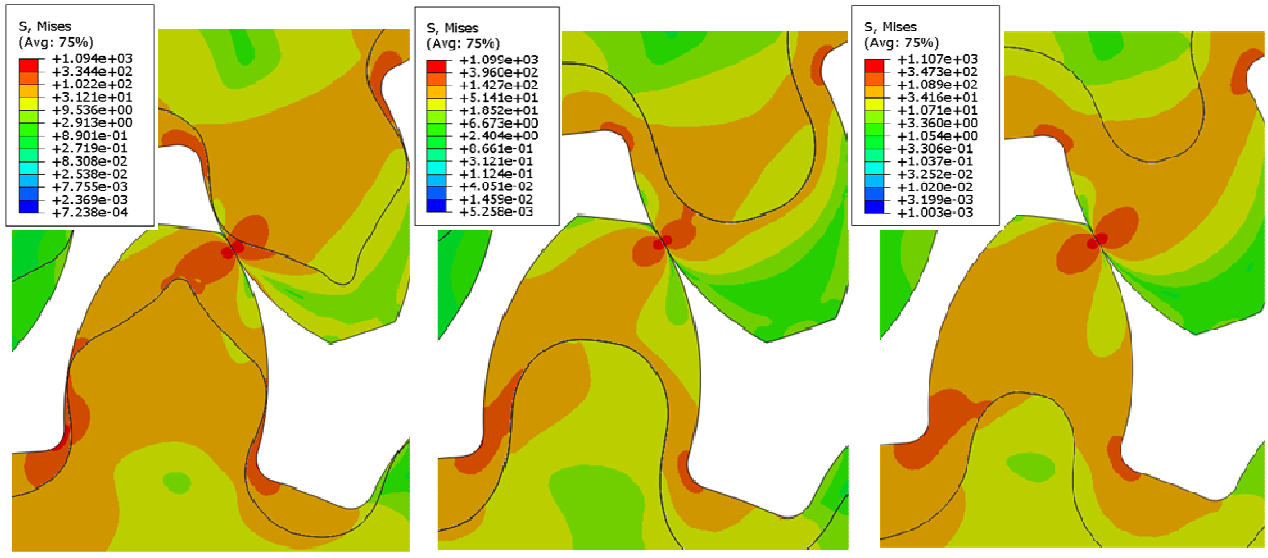
The post forged 4mm profile under gear meshing is shown in Figure 6.10b. It can be seen that the ring has a rounded profile towards the tooth tip when compared to the 2mm ring profile mentioned previously, hence removing the region of stress concentration. The high stresses experienced by the ring material near the tooth root and flank appear to be distributed through

the ring material with substantially lower stresses experienced by the aluminium core. This is further seen in the post forged 6mm profile (Figure 6.10c) where the ring comprises the majority of the material of the tooth. This again shows that the majority of the high stresses are confined to the higher stiffness ring material and, as in Figure 6.10b, alter the stress distribution around the tooth flank to flow around the aluminium core.

The results of the compressive and root fillet stresses at the tooth surfaces, as well as the inner surface of the steel ring and outer surface of the aluminium core measured in the normal direction to the midpoint of the root are shown in Table 6.2. The von Mises stress measured in the direction normal to the point of first tooth contact is shown in Figure 6.11.

Table 6.2: Stresses through regions of gear tooth (thinned ring profiles)

Ring Thickness (mm)	Tooth Fillet Type	Surface Stress (MPa)	Inner Steel Stress (MPa)	Outer Al Stress (MPa)
2	Compressive Fillet	504.5	147.7	69.5
	Tensile Fillet	347.7	90.3	47.9
4	Compressive Fillet	406.3	75.1	39.4
	Tensile Fillet	269.5	34.0	24.5
6	Compressive Fillet	363.7	37.5	25.3
	Tensile Fillet	237.8	21.1	18.4



(a) (b) (c)

Figure 6.10: Gear meshing stress distribution for thinned ring profiles for: (a) 2mm, (b) 4mm and (c) 6mm rings

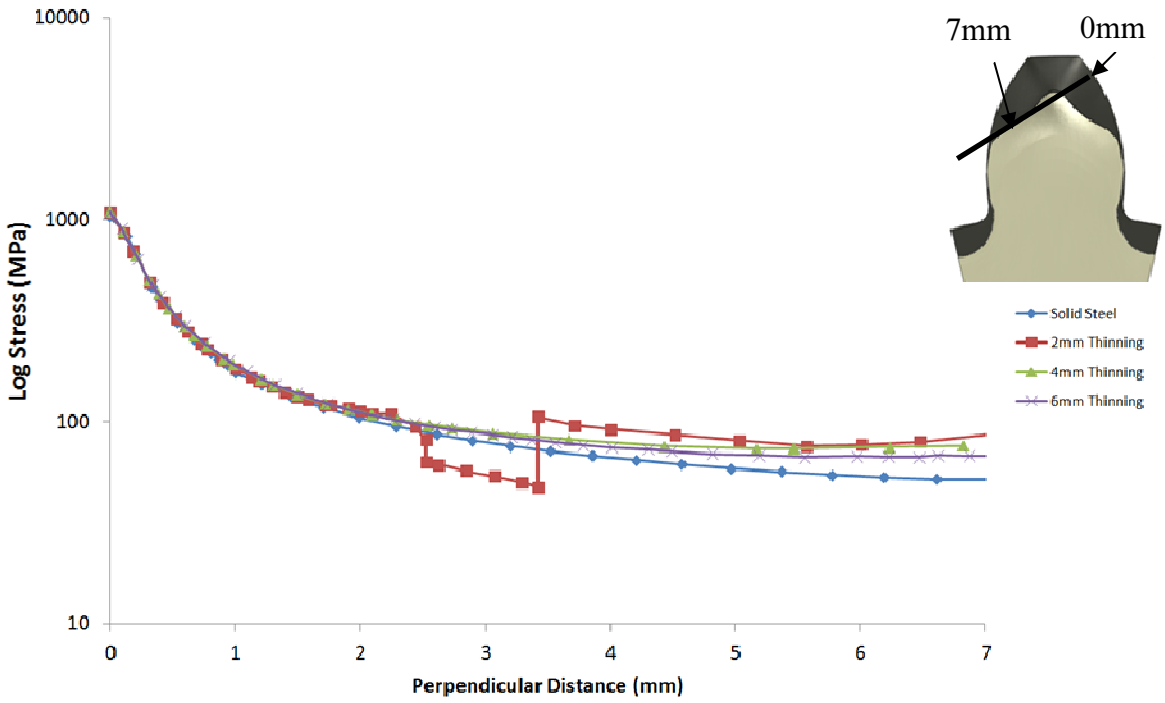


Figure 6.11: Stress perpendicular to contact point (first contact) for thinned rings

The effect of a thinned ring profile on the root surface stresses at the compressive and tensile root fillets, from the point of first tooth contact to point of tooth disengaging are shown in Figures 6.12 and 6.13. The Figures compare the 2mm, 4mm and 6mm thinned ring profile to a single material steel gear tooth. It can be seen that unlike the uniform ring thickness cases presented in Figures 6.8 and 6.9, the large ring thickness (4mm and 6mm) appear to result in root stresses significantly larger than those of the solid steel gear tooth. That is because the ring thickness of these profiles near the root are substantially lower than their uniform counterparts, where, for example, at the tooth root, the 4mm and 6mm rings are in fact 1.6mm and 2.5mm thick, respectively (i.e. a reduction of 60% and 58%).

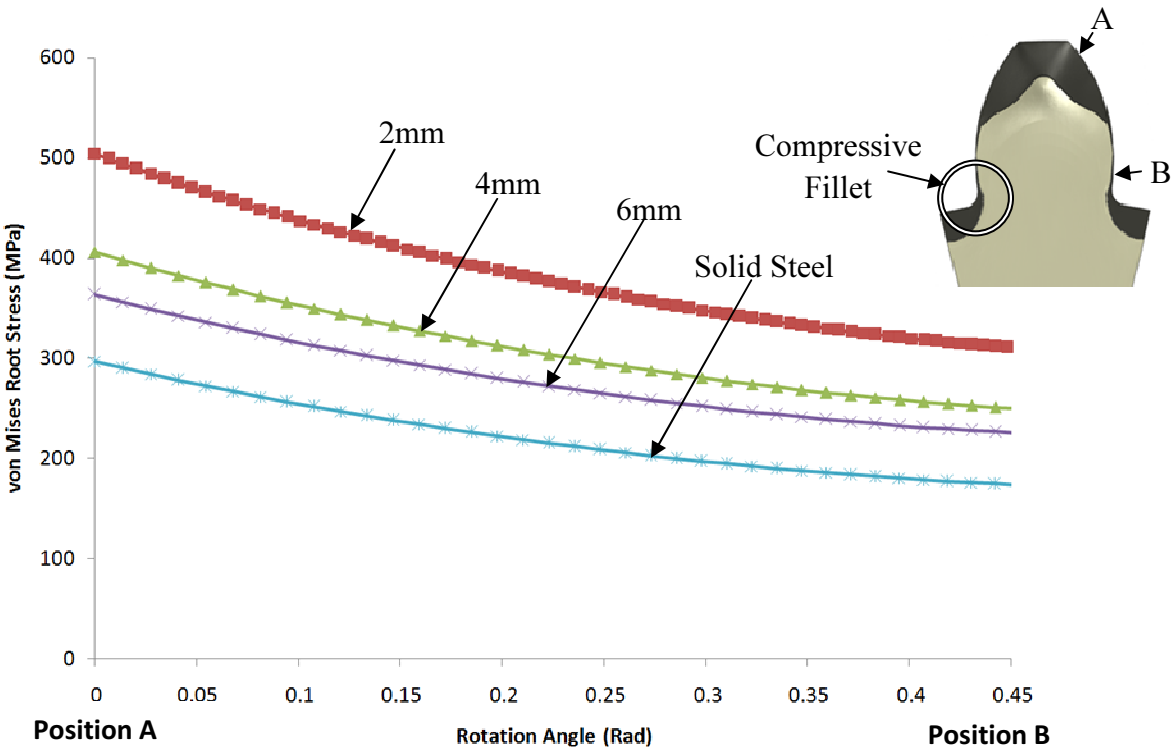


Figure 6.12: Compressive surface root stress comparison for thinned rings

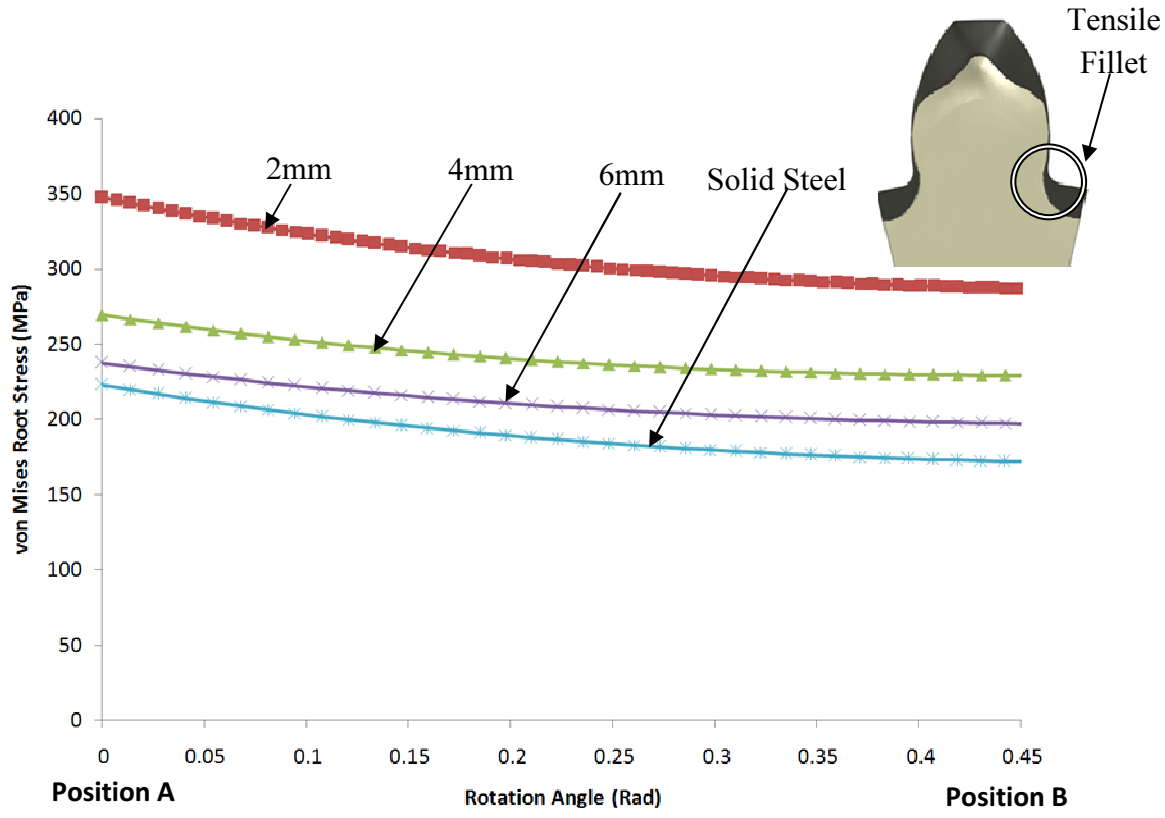


Figure 6.13: Tensile surface root stress comparison for thinned rings

The determination of maximum stresses experienced by the ring and core materials through FE simulation allows for an estimation of the fatigue life of the gear based on the S-N fatigue data available from the literature. For example, for a 1mm uniform ring thickness at 150Nm torque, the maximum stress experienced in the steel is 1143MPa and in the aluminium is 148 MPa. For gear steel 16MnCr5, which has a fatigue limit of 900 MPa as wrought material or 1340MPa with a shot peening surface treatment (Curtis Wright Surface Technologies, 2010), the determined stress lies below the fatigue limit of the material, and thus the ring should not fail due to fatigue. Aluminium Al 6082 however, does not experience a fatigue limit, and hence the stress of 148MPa falls within the 100 cycles life (CES Edupack, 2010). However, for the increased uniform ring thickness of 2mm, the aluminium fatigue life lies in the range of 100,000 to 12 million cycles (CES Edupack, 2010), thus indicating that a small change in ring thickness significantly improves the fatigue life of the tooth.

The fatigue life prediction for multi-metal gears may be simplified through the use of a lightweight material which also experiences a fatigue limit. An example of one such lightweight metal is magnesium alloy AZ31, where the authors Avedesian and Baker (1999) have shown that the S-N curve appears to show a constant fatigue stress of approximately 100MPa.

Chapter 7 Conclusions and Suggestions for Future Research

The following chapter summarises the key findings from the experimental and simulation work performed in this thesis. Conclusions from these findings are drawn and recommendations are made for areas requiring further investigation to allow the application and utilisation of multi-metal forged gears in practice.

7.1 Conclusions

In this research a process for the production of multi-metal gears utilising the forging method has been proposed with the focus of reducing the overall mass of a gear while maintaining operational performance properties. To study the forging of multi-metal gears, the focus of the research was on the experimentation and simulation of bi-metallic gears constructed by the simultaneous forging of a lower strength and density cylindrical core material positioned concentrically within a high strength and density ring component. To facilitate the experimental work, a tool-set was designed and manufactured for the forging of spur gears by adapting several tool concepts identified in the literature. The following conclusions can be drawn from the investigation:

- An innovative method for manufacturing tailored gears was developed, specifically for the production of lightweight gears using the forging process. Through this technique, a gear can be constructed from multiple metals, whereby high strength, high density materials are located in regions of high stress concentration, such as the gear teeth, and lower strength, lower density materials are located at less critical regions, such as the central region of the gear. A patent has been filed for the production process.
- Through the proposed process, multi-metal gears, specifically bi-metallic gears were produced and investigated from two components: a lower strength lightweight centre (core) and high strength outer material (ring). The pre-forms are forged in a single step into the shape of the gear. Through this process, the material flow between the metals locks/binds them together to form the completed gear.
- Experimental forgings for bi-metallic gears were performed under cold and hot forging conditions. Model materials namely copper C101 (tooth ring material) and commercially pure lead (core material) were used for cold forging. Engineering alloys

230M07 (ring material) and Al 6082 (core material) were used for hot forgings allowing for the production of a lightweight gear. Ring thicknesses of 2mm, 4mm and 6mm were tested to observe the effect of ring thickness on the material flow of the two metals during forging. These ring thicknesses for the steel-aluminium combinations achieving weight reductions of approximately 57%, 47% and 38% for the 2mm, 4mm and 6mm rings, respectively compared to single material steel gears.

- Material flow for these ring thicknesses was analysed through two cross sections of the gear: (i) through the mid-height of the gear on a horizontal plane and (ii) through the root of a tooth and the tip of the adjacent tooth on a vertical plane. It was observed that the forging process caused the outer ring material to be greatly deformed leading to severe thinning and separation on the tooth flanks, specifically for the 2mm copper ring and 2mm and 4mm steel rings. This results in core material flowing through this separation to fill the tooth cavity. However, rings of greater thickness do not show signs of this separation suggesting that there is a minimum ring thickness which is necessary to maintain the structural integrity of the gear.
- Cross-sections identified an effective line of symmetry where ring material consistently separates on the same side of the tooth, whereas across this mirror/symmetry line, the effect is reversed.
- Three locking mechanisms were possible during forging, namely: (i) macro-mechanical locking, (ii) diffusion bonding and (iii) micro-mechanical locking, which when coupled together, are expected to prevent the two components of the bi-metal gears from disengaging during operation. Investigations identified the presence of two locking mechanisms. The first, macro-mechanical locking involves the rotational and axial lock due to metal flow. Axial locking is achieved by barrelling due to friction and the ring folding to contact the punch and counterpunch. Rotational locking is caused by the deformation of both materials into the gear tooth shape during deformation. The second, micro-mechanical locking is also achieved through protrusions of asperities on one material into another. The steel protruded into the softer aluminium. Diffusion bonding is the subject of future investigation.
- Stress-strain behaviour for the metals copper C101, commercially pure lead, mild steel 230M07, aluminium alloy Al 6082 and the gear steel 16MnCr5 were obtained through compression tests. Thermo-mechanical tests were performed for Al 6082, 230M07 and 16MnCr5 over a wide range of strain rates ($0.1s^{-1}$ to $10s^{-1}$) and

temperatures (900^{o}C – 1150^{o}C for steel and 450^{o}C – 550^{o}C for aluminium alloy). A phenomenologically controlled set of unified visco-plastic constitutive equations, incorporating the physical parameters stress, plastic strain rate, isotropic hardening and dislocation density were calibrated using experimental data. This allowed the characterisation of material behaviour whilst avoiding the limitations of traditional equations such as the power law, exponential law and hyperbolic sine law, hence replicating the forging process.

- A mathematical material model was constructed and FE simulation of cold forging of lead and copper bi-metallic gears was undertaken. The simulation of forging with ring thicknesses of 2mm, 4mm and 6mm, allowed for comparison with experimental gear cross sections on vertical and horizontal planes. The effect of friction coefficient on various tool and work-piece surfaces was studied to determine its effect on ring thickness distribution of a gear tooth and hence the quality and structural integrity of the gear. An approximation of friction coefficients acting only between the work-piece and the punch and counterpunch surfaces resulted in ring thickness distributions representative of those obtained through experimentally forged gears whilst simplifying the analysis of the problem.
- Friction on the punch and counterpunch of the toolset causes the ring material to fold onto these surfaces, thus providing an axial lock. Increasing friction on the punch and counterpunch causes more material to fold onto these surfaces with the effect of reducing the material thickness of the tooth tip towards the mid-height of the gear. Furthermore, increasing friction on the punch and counterpunch causes a greater amount of ring material in the tooth to thin, thus potentially affecting the structural integrity of the gear.
- Material flow in bi-metal gear forging is affected by the difference in value of flow stress between the two metals. The lead/steel combination, which had the greatest disparity of flow stress, resulted in the largest proportion of ring metal folding onto punch and counterpunch surfaces. Furthermore, larger disparity combinations led to thicker ring material in the tooth root.
- By embedding the constitutive equations in a hot forging model of aluminium and steel, it was shown that by the end of the forging, the interface temperature between ring and core at the tooth tip had reduced to 415^{o}C, from the initial 1150^{o}C for a 6mm thick ring and 535^{o}C for aluminium core. This large temperature reduction coupled

with the relatively short forging time period of 10s results in unfavourable conditions for the formation of a diffusion bond.

- FE simulations were conducted to simulate gear contact during meshing operation in service, for a combined gear steel (16MnCr5) and lightweight core (Al 6082). The simulations show that a significant reduction of stress occurs, of the order of 80%, within the first millimetre from the contact point for the examined tooth geometry. The stress distribution for uniform ring thicknesses of 1mm, 2mm, 4mm and 6mm was found and the behaviour compared to the thinned ring profiles of 2mm, 4mm and 6mm determined experimentally to evaluate differences in operational behaviour. Complex transition behaviour across the ring-core boundary was also observed, where the core material experienced approximately half of the von Mises stress of the ring material at this transition point.
- It was found that for all uniform ring thicknesses assessed for this tooth geometry, as long as the contact stress at the ring remains below the yield stress of steel, the stress experienced by the aluminium core remains below its yield stress. Furthermore, for large ring thicknesses, such as the uniform 6mm thickness, the von Mises stresses at the compressive and tensile fillet closely resemble those of a single material steel gear.
- Thinned tooth profiles obtained from forging demonstrated that the thinning of the ring substantially degrades performance, with root stresses greater than those of a solid steel gear tooth for all tooth profiles. That is because the ring thickness of these profiles near the root are substantially lower than their uniform counterparts, where, for example, at the tooth root, the 4mm and 6mm rings are in fact 1.6mm and 2.5mm (reduction of 60% and 58%, respectively).

7.2 Recommendations of Future Research

The work performed in this thesis is a preliminary investigation in the forging of multi-metal gears through the simultaneous forging of separate components. Several limitations to the present study are noted and recommendations for further investigation are made below, in order to continue the development and solve the challenges of the forging process to apply multi-metal gears in practice.

- Forging Press: The forging press used in the present study was a hydraulic press with maximum speed of 10mm/s and load of 2.5MN. This has prevented the complete

filling of gear teeth corners and hence has limited the ring thicknesses and materials which could be tested. A mechanical or press with greater load capacity and ram speed may be used in future studies to obviate this limitation.

- Pre-form Design: The use of a uniform annular ring profile has resulted in the thinning and eventual separation of the material during forging. This limitation may be avoided by altering the profile of the ring material for example from the current annular shape to a wave profile of varying thickness. In this way, a larger thickness of material may be located in regions which will be formed into the tooth flanks, thus forging a more uniform ring profile. In terms of industrial application this would require more complex pre-forms potentially produced through an extrusion process.
- Work-piece Alignment: The misalignment of the work-piece within the die may explain the mirror line present in the thinning of the ring material, where the ring tends to separate on the same side of each tooth and separates on the opposite side of every tooth across this line. Further tests regarding the positioning of the work-piece within the die may gain further understanding of this effect. Furthermore, FE simulations on a 3D full gear forging may be performed to assess the effect of misaligning the ring core assembly within the die.
- Billet/Tool Heating: In order to heat the toolset and reduce heat transfer, a propane gas torch was used. However, during forging it was removed to provide an accessible area to position the work-piece within the die. Moreover, the heating of the core and ring materials was performed in two separate furnaces before being individually transferred to the die for forging. This resulted in difficulties in transferring both materials to the die by a single operator whilst avoiding heat loss. Furthermore, heat loss occurs as a result of the slow forging process. The combined effect of these temperature loses substantially reduces the interface temperature of the two materials where the likelihood for the formation of a diffusion bond is greatly reduced. The use of heating elements integrated into the tool-set, for example induction heating, may substantially reduce the heat transfer to the toolset.
- Billet Oxidation: The hot forging of gears in atmospheric air is susceptible to the formation of an oxide layer which results in reduced surface quality, wear and fatigue strength (Abdel-Rahman and Dean, 1981) of the gear. Furthermore, the development of an oxide layer inhibits the formation of a diffusion bond between metals. Hence the

use of an inert atmosphere during heating and forging may assist in the formation of a diffusion bond.

- Interface Bond Shear Tests: The coupling of three locking mechanisms, namely, macro-mechanical locking, micro-mechanical locking and diffusion bonding enhances the strength of a multi-metal gear by reducing the likelihood of material separation during operation. The performance of tensile (Holmquist *et al.*, 1999) or shear tests (Harvey *et al.*, 1985) on this interface may be used to evaluate the strength of a combined micro-mechanical and diffusion bond interface. This will determine the effectiveness of these locking mechanisms in enhancing the structural integrity of the gear.
- Mechanical Testing: Mechanical testing of multi-metal gears may be performed where a rig is constructed (Lewicki and Coy, 1987) allowing for a multi-metal gear produced from forging to be run alongside a solid steel gear to determine fatigue life as well as failure mechanisms of the multi-metal gear. Thus far, fatigue life has been estimated only through simulation.
- Alternative Material Combinations: Low density engineering alloys, such as magnesium alloys [two-thirds of aluminium (Cizek *et al.*, 2004)] already used in the automotive industry may be used for the core material to further reduce the overall mass of a multi-metal lightweight gear. However, limitations of such alloys, for example corrosion resistance and potential flammability when working at high temperatures may require further investigation as to their practicality and suitability.
- Alternative Gear Profiles: The focus of the current work has been on the forging of a spur gear profile. The production of other gear profiles, for example, helical or bevel gears may present additional challenges than those observed from spur gear forms.

References

Aalco Metals Ltd. (2013) *Aluminium Alloy 6082-T6~T651 Technical Information.* [Online] Available from: http://www.aalco.co.uk/datasheets/Aluminium-Alloy_6082-T6~T651_148.ashx [Accessed 5th June 2013].

Abdel-Rahman, A. R. O. & Dean, T. A. (1981) The quality of hot forged spur gear forms. Part I: Mechanical and metallurgical properties. *International Journal of Machine Tool Design and Research*, 21 (2), 109-127.

American Gear Manufacturers Association. (1966) AGMA Standard 220.02. *AGMA Standard for Rating the Strength of Spur Gear Teeth*. Alexandria, Virginia, American Gear Manufacturers Association AGMA.

Ajmi, M. & Velex, P. (2005) A model for simulating the quasi-static and dynamic behaviour of solid wide-faced spur and helical gears. *Mechanism and Machine Theory*, 40 (2), 173-190.

Altan, T., Ngaile, G. & Shen, G. (2005) *Cold and Hot Forging: Fundamentals and Applications*. Materials Park, OH, ASM International.

Alves, M. L., Rodrigues, J. M. C. & Martins, P. A. F. (2001) Cold forging of gears: Experimental and theoretical investigation. *Finite Elements in Analysis and Design*, 37 (6-7), 549-558.

Arikan, M. A. S. (1991) Dynamic load and contact stress analysis of spur gears. In: *Proceedings of the 17th Design Automation Conference*, *22-25 September 1991*. Miami, ASME Design Technical Conferences. pp. 85-91.

Avedesian, M. M. & Baker, H. (1999) *ASM Specialty Handbook: Magnesium and Magnesium Alloys*. Materials Park, OH, ASM International.

Bai, Q., Lin, J., Dean, T. A., Balint, D. S., Gao, T. & Zhang, Z. (2013) Modelling of dominant softening mechanisms for Ti-6Al-4V in steady state hot forming conditions. *Materials Science & Engineering A*, 559, 352-358.

Beghini, M., Presicce, F. & Santus, C. (2004) *A Method to Define Profile Modification of Spur Gear and Minimize the Transmission Error*. AGMA Technical Paper, Alexandria, Virginia, American Gear Manufacturers Association (AGMA).

Brooks, R. (2013) Amtek Auto Buys Neumayer Tekfor Group. *Forging Magazine*. [Online] Available from: http://forgingmagazine.com/forming/amtek-auto-buys-neumayer-tekfor-group [Accessed 5th December 2013].

BS ISO Standard. (2006a) *BS ISO 6336-1. Calculation of load capacity of spur and helical gears. Part 1: Basic principles, introduction and general influence factors*. London, UK, British Standards Institution.

BS ISO Standard. (2006b) *BS ISO 6336-2. Calculation of load capacity of spur and helical gears. Part 2: Calculation of surface durability (pitting)*. London, UK, British Standards Institution.

BS ISO Standard. (2006c) *BS ISO 6336-3. Calculation of load capacity of spur and helical gears. Part 3: Calculation of tooth bending strength*. London, UK, British Standards Institution.

Buckingham, E. (1949) *Analytical Mechanics of Gears*. London, McGraw-Hill.

Buckingham, E. (1935) *Manual of Gear Design Section Two - Spur and Internal Gears*. New York, American Gear Manufacturers Association, The Industrial Press.

Cáceres, C. H. & Selling, B. I. (1996) Casting defects and the tensile properties of an Al-Si-Mg alloy. *Materials Science and Engineering A*, 220 (1-2), 109-116.

Camacho, A. M., Vallellano, C., Garcia-Lomas, J. & Sebastian, M. A. (2009) Influence of friction, punch depth and shape factor on forces in localized-incremental forging operations. In: *Fifth I*PROMS Virtual Conference in Innovative Production Machines and Systems, IPROMS 2009, 6-17 July,* FP6 I*PROMS Network of Excellence. Whittles Publishing. pp. 369-374.

Car and Driver Magazine. (2013) *Automotive Gearbox*. [Online] Available from: http://media.caranddriver.com/images/09q4/318620/dual-clutch-automated-manual-transmissions-pdk-porsche-doppelkupplungsgetriebe-cutaway-photo-319161-s-1280x782.jpg [Accessed 18th August 2013].

Caron, E., Daun, K. J. & Wells, M. A. (2013) Experimental characterization of heat transfer coefficients during hot forming die quenching of boron steel. *Metallurgical and Materials Transactions B*, 44 (2), 332-343.

CES Edupack. (2010) *Aluminium - 6082 - Wrought - T6 Datasheet*. UK, Granta Design Limited.

Chacon, R. D., Andueza, L. J., Diaz, M. A. & Alvarado, J. A. (2010) Analysis of stress due to contact between spur gears. In: *Proceedings of the 9th WSEAS International Conference on Computational Intelligence, Man-Machine Systems and Cybernetics, Proceedings CIMMACS, 14-16 December 2010.* Venezuela, *WSEAS.* pp. 216-220.

Chandler, H. (1995) *Heat Treater's Guide: Practices and Procedures for Irons and Steels*, 2nd Edition. Materials Park, OH, ASM International.

Chen, J., Young, B. & Uy, B. (2006) Behaviour of high strength structural steel at elevated temperatures, *Journal of Structural Engineering,* 132 (12), 1948-1954.

Cheng, Y. Q., Zhang, H., Chen, Z. H. & Xian, K. F. (2008) Flow stress equation of AZ31 magnesium alloy sheet during warm tensile deformation. *Journal of Materials Processing Technology,* 208 (1-3), 29-34.

Childs, P. R. N. (2003) *Mechanical Design*, 2nd Edition. London, Elsevier Butterworth-Heinemann.

Chitkara, N. R. & Bhutta, M. A. (1996) Near-net shape forging of spur gear forms: An analysis and some experiments. *International Journal of Mechanical Sciences*, 38 (8-9), 891-916.

Choi, J., Cho, H. & Kwon, H. (1994) A new extrusion process for helical-gears: experimental study. *Journal of Material Process Technology,* 44 (1-2), 35-53.

Choi, J. C. & Choi, Y. (1999) Precision forging of spur gears with inside relief. *International Journal of Machine Tools and Manufacture*, 39 (10), 1575-1588.

Choi, J. C. & Choi, Y. (1998) A study on the forging of external spur gears: Upper-bound analyses and experiments. *International Journal of Machine Tools and Manufacture*, 38 (10-11), 1193-1208.

Choi, J. C., Choi, Y. & Tak, S. J. (1998a) The forging of helical gears (I): Experiments and upper-bound analysis. *International Journal of Mechanical Sciences*, 40 (4), 325-337.

Choi, J., Cho, H., Choi, J. & Jo, C. (1998b) A study on the forging of gear-like components. *KSME International Journal*, 12 (4), 615-623.

Cizek, L., Greger, M., Pawlica, L., Dobrzanski, L. A. & Tanski, T. (2004) Study of selected properties of Magnesium Alloy AZ91 after heat treatment and forming. *Journal of Materials Processing Technology*, 157-158, 466-471.

Cline, C. L. (1966) An analytical and experimental study of diffusion bonding. *Welding Journal*, 45, 481-489.

Commission of the European Communities. (2007) *Communication from the Commission to the Council and the European Parliament: Results of the Review of the Community Strategy to Reduce CO_2 emissions from Passenger cars and Light-Commercial Vehicles*, COM 2007, 7 February, Brussels. p.2. [Online] Available from: http://eur-lex.europa.eu/LexUriServ/LexUriServ.do?uri=COM:2007:0019:FIN:EN:PDF [Accessed 17th August 2013].

Conwell, J. C. & Johnson, G. E. (1996) Design, construction and instrumentation of a machine to measure tension and impact forces in roller chain drives. *Mechanism and Machine Theory*, 31 (4), 525-531.

Cowley, B. W. (2013) Micro skiving: Precision finishing of hardened small diameter fine module/pitch gears, splines, and serrations. *Gear Solutions*. [Online] 64-68. Available from: http://www.gearsolutions.com/article/detail/6343/micro-skiving-precision-finishing-of-hardened-small-diameter-fine-modulepitch-gears-splines-and-serrations- [Accessed 8th October 2013].

Curtis Wright Surface Technologies. (2010) *Shot Peening Success Stories for Metal Finishing*. *Metal Improvement Company*. [Online] Available from: http://www.metalimprovement.com/shotpeening_successstories_metal_finishing.php [Accessed 12th September 2013].

Daryani, P. H. (2002) *The Art of Gear Fabrication*, 1st Edition. New York, USA, Industrial Press Inc.

Dassault Systemes S. A. (2011) Simulia V6.11 Abaqus Analysis User's Manual, Section 27.1.4 - Three-dimensional solid element library, ABAQUS Inc., Vélizy-Villacoublay, France.

David Brown Engineering. (2013) *Girth Gears Overview*. [Online] Available from: http://www.davidbrown.com/business-units/mining-14/products/girth-gears-14 [Accessed 5th October 2013].

Davis, J. R. (1996) *Carbon and Alloy Steels (ASM Speciality Handbook).* Materials Park, OH, ASM International.

Davis, J. R. (2005) *Gear Materials, Properties and Manufacture*. Materials Park, OH, ASM International.

Dean, P. M. (1974) *Geometry and Theory of Gears, Gear Manufacture and Performance*. Materials Park, OH, The American Society of Metals.

Dean, T. A. (2000) The net-shape forming of gears. *Materials and Design,* 21 (4), 271-278.

Dieter, G. E., Kuhn, H. A. & Semiatin, S. L. (2003) *Handbook of Workability and Process Design*. Materials Park, OH, ASM International.

Dobrzanski, L. A., Tanski, T., Cizek, L. & Brytan, Z. (2007) Structure and properties of magnesium cast alloys. *Journal of Materials Processing Technology,* 192-193, 567-574.

Doege, E. & Nagele, H. (1994) FE simulation of the precision forging process of bevel gears. *CIRP Annals – Manufacturing Technology*, 43 (1), 241-244.

Dolan, T. J. & Broghamer, E. L. (1942) *A Photoelastic Study of Stresses in Gear Tooth Fillets*. *University of Illinois Bulletin*, XXXIX (31). IL, University of Illinois Urbana.

Domblesky, J., Kraft, F., Druecke, B. & Sims, B. (2006) Welded preforms for forging. *Journal of Materials Processing Technology*, 171 (1), 141-149.

Dugas, J. P. (1997) Gear shaving basics - Part I. *Gear Technology*. [Online] November/December Issue, 26-30. Available from: http://www.geartechnology.com/articles/1197/Gear_Shaving_Basics_-_Part_I [Accessed 12th October 2013].

DuPont. (2007) *Engineering Polymers for High Performance Gears*. [Online] Available from: http://plastics.dupont.com/plastics/pdflit/americas/markets/Gear_Brochure_10_2007.pdf [Accessed 10th October 2013].

Estrin, Y. (1998) Dislocation theory based constitutive modelling: foundations and applications. *Journal of Materials Processing Technology*, 80-81, 33-39.

Euler, L. (1754-55) De Aptissima figure rotarum dentibus tribuenda "On finding the best shape for gear teeth". *Academiae Scientiarum Imperiales Petropolitae,* Novi Commentarii, 299-316.

Everts, R. G. & Rickard, H. G. (1994) Laminated Gear and Method of Forming a Laminated Gear, Patent No. U.S. 5,337,626, August 16.

Farren, W. S. & Taylor, G. I. (1925) The heat developed during plastic extrusion of metals. *Proceedings of the Royal Society, Series A*, 107, 422-451.

Fein, A. (2009) New materials for efficient aircraft design. *Science, Technology and Innovations Projects*. [Online] Available from: http://www.projectsmagazine.eu.com/randd_projects/new_materials_for_efficient_aircraft_design [Accessed 17th August 2013].

Fields, D. S. & Backofen, W. A. (1957) Determination of strain-hardening characteristics by torsion testing. In: *Proceedings of the 60th Annual Meeting of the American Society for Testing and Materials*, 57, 1259-1272.

Forging Industry Association. (2007) *Forging Solutions: Design Engineering Information From FIA*. [Online] Available from: https://www.forging.org/system/files/field_document/ColdForgingArticles.pdf [Accessed 20th October 2013].

Foster, A., Mohamed, M., Lin, J. & Dean, T. (2008) An investigation of lubrication and heat transfer for a sheet aluminium heat, form-quench (HFQ) process. *Steel Research International*, 79 (11), VII, 133-140.

Foster, A. D. (2007) Modelling damage evolution during the hot deformation of free machining steels. Ph.D. Thesis, School of Engineering, University of Birmingham, UK.

Freedonia. (2010) *World Gears Industry*. [Online] Available from: http://www.reportlinker.com/p0188535/World-Gears-Industry.html [Accessed 12th August 2013].

Friction Welding Technologies Pvt. Ltd. (2013) *Bimetal Engine Valves*. [Online] Available from: http://www.frictionwelding.in/sub_contracting.htm [Accessed 20th October 2013].

Gronostajski, Z. (2000) The constitutive equations for FEM analysis. *Journal of Materials Processing Technology*, 106, 40-44.

Grzesik, W. (2008) *Advanced Machining Processes of Metallic Materials: Theory, Modelling and Applications*. Oxford, UK, Elsevier.

Guo, Q., Yan, H. G., Zhang, H., Chen, Z. H. & Wang, Z. F. (2005) Behaviour of AZ31 magnesium alloy during compression at elevated temperatures. *Materials Science and Technology*, 21 (11), 1349-1354.

Harvey, J., Partridge, P. G. & Snooke, C. L. (1985) Diffusion bonding and testing of Al-alloy lap shear test pieces. *Journal of Materials Science*, 20, 1009-1014.

Hatebur Umformmaschinen AG. (2013) *Hotmatic HM 35: The Reliable Hotformer for Maximum Output*. [Online] Available from: http://www.hatebur.com/hatebur-en/products/hotmatic/hm-35.php [Accessed 20th October 2013].

Hazelton, J. L. (2003) Gear grinding 2003. *Gear Technology: The Journal of Gear Manufacturing.* [Online] November/December Issue, 13-17. Available from: http://www.geartechnology.com/articles/1103/Gear_Grinding_2003 [Accessed 18th October 2013].

He, Y., Yang, K., Sha, W. & Cleland, D. J. (2004) Microstructure and mechanical properties of a 2000 MPa co-free maraging steel after aging at 753 K. *Metallurgical and Materials Transactions A*, 35 (9), 2747-2755.

Herring, D. H. & Lindell, G. D. (2007) Heat treating heavy duty gears. *Gear Solutions*. [Online] October Issue, 59-75. Available from: http://www.gearsolutions.com/media//uploads/assets/PDF/Articles/Herring1007.pdf . [Accessed 18th October 2013].

Hertz, H. (1881) Über die berührung fester elastischer Körper "about the contact of solid elastic bodies". *Journal Für Die Reine und Angewandte, Mathematik*, 92, 156-171.

Holmquist, M., Recina, V. & Pettersson, B. (1999) Tensile and creep properties of diffusion bonded titanium alloy IMI 834 to gamma titanium aluminide IHI Alloy 01A. *Acta Materialia,* 47 (6), 1791 - 1799.

Hsieh, C. M., Huston, R. L. & Oswald, F. B. (1992) Contact stresses in meshing spur gear teeth: Use of an incremental finite element procedure. *NASA Technical Memorandum 105388*. Technical report number: 90-C-029.

Hwang, S., Lee, J., Lee, D., Han, S. & Lee, K. (2013) Contact stress analysis for a pair of mating gears. *Mathematical and Computer Modelling*, 57 (1-2), 40-49.

Ibhadode, A. O. A. & Dean, T. A. (1988) The effect of billet location on completely closed cavity die forging, Proceedings of the Institution of Mechanical Engineers, Part B. *Journal of Engineering Manufacture*, 202, 227-235.

Imrek, H. (2009) Performance improvement method for Nylon 6 spur gears. *Tribology International*, 42 (3), 503-510.

Integy. (2013) *Type II Spur Gear for HPI Baja 5B, 5T & 5B2.0 BAJ008*. [Online] Available from: http://www.integy.com/st_prod.html?p_prodid=7138&p_catid=126#.UovOFcRmh8F [Accessed 16th October 2013].

Jiashan PVB Sliding Bearing Co. (2012a) *Bimetal Bearing*. [Online] Available from: http://www.oilesbearing.com/bimetal-bearing.html [Accessed 16th October 2013].

Jiashan PVB Sliding Bearing Co. (2012b) *Bimetal Bushing*. [Online] Available from: http://www.oilesbearing.com/bimetal-bushing.html [Accessed 16th October 2013].

Kahraman, A., Lim, J. & Ding, H. (2007) A Dynamic model of a spur gear pair with friction. In: *12th International Federation for the Promotion of Mechanism and Machine Science World Congress*, *18-21 June 2007*, Besançon, France.

Kahraman, A., Nevzat Ozguven, H. & Houser, D. R. (1990) Dynamic analysis of geared rotors by finite elements. *NASA Technical Memorandum 102349*. Technical memorandum number: 89-C-006.

Key to Metals AG. (2009) *Aluminium Alloy Development for the Airbus A380*. [Online] Available from:

http://www.keytometals.com/page.aspx?ID=CheckArticle&site=ktn&NM=227 [Accessed 20th April 2011].

Kim, Y. J. & Chitkara, N. R. (2001) Determination of preform shape to improve dimensional accuracy of the forged crown gear form in a closed – die forging process. *International Journal of Mechanical Sciences*, 43 (3), 853-870.

Klingelnberg GmbH. (2013) *Power Skiving*. [Online] Available from: http://www.klingelnberg.com/en/hot-topics/power-skiving.html [Accessed 15th October 2013].

Kobyskovsky, N. F., Shorochov, G. D. & Socrishin, J. P. (1967) Forging of spur gears on a high speed forge. *Kuznechno-shtamp. Proizv,* 8.

Kocks, U. F. (1976) Laws for work-hardening and low temperature creep. *Journal of Engineering Materials and Technology*, 98 (1), 76-85.

Kosal, D. (1998) Gear shaving basics - Part II. *Gear Technology*. [Online] January/February Issue, 45-48. Available from: http://www.geartechnology.com/articles/0198/%20Gear_Shaving_Basics,_Part_II [Accessed 18th November 2013.

Koyama, T. & Marshek, K. M. (1988) Toothed belt drives: past, present and future. *Mechanism and Machine Theory*, 23 (3), 227-241.

Krantz, T. L. (1993) *Mechanical Systems Technology Branch Research Summary, 1985-1992*. U.S Army Research Laboratory, Lewis Research Center, Cleveland, Ohio.

Ledbetter, H. M. (1982) Temperature behaviour of Young's moduli of forty engineering alloys. *Cryogenics*, 22 (12), 653-656.

Lewis, W. (1892) Investigation of the strength of gear teeth. In: Proceedings of Engineering Club, Philadelphia, PA, 16-23.

Lewicki, D. G. & Coy, J. J. (1987) Helicopter transmission testing. *NASA Lewis Research Center*. [Online] NASA Technical Memorandum 89912. Available from: http://ntrs.nasa.gov/archive/nasa/casi.ntrs.nasa.gov/19870013545_1987013545.pdf [Accessed 18th November 2013].

Li, Y., Liu, P., Wang, J. & Ma, H. (2008) XRD and SEM analysis near the diffusion bonding interface of Mg/Al dissimilar materials. *Vacuum*, 82 (1), 15-19.

Li, L., Zhou, J. & Duszczyk, J. (2006) Determination of a constitutive relationship for AZ31B magnesium alloy and validation through comparison between simulated and real extrusion. *Journal of Materials Processing Technology*, 172 (3), 372-380.

Li, B., Lin, J. & Yao, X. (2002) A novel evolutionary algorithm for determining unified creep damage constitutive equations. *International Journal of Mechanical Sciences*, 44 (5), 987-1002.

Lin, J. & Dean, T. A. (2005) Modelling of microstructure evolution in hot forming using unified constitutive equations. *Journal of Materials Processing Technology*, 167 (2-3), 354-362.

Lin, J., Liu, Y. & Dean, T. A. (2005) A review on damage mechanisms, models and calibration methods under various deformation conditions. *International Journal of Damage Mechanics*, 14 (4), 299-319.

Lin, J. & Liu, Y. (2003) A set of unified constitutive equations for modelling microstructure evolution in hot deformation. *Journal of Materials Processing Technology*, 143-144, 281-285.

Lin, J., Cheong, B. H. & Yao, X. (2002) Universal multi-objective function for optimising superplastic-damage constitutive equations. *Journal of Materials Processing Technology*, 125-126, 199-205.

Litvin, F. L. & Fuentes, A. (2004) *Gear Geometry and Applied Theory*, 2nd Edition. Cambridge, UK, Cambridge University Press.

Loh, N. L., Wu, Y. L. & Khor, K. A. (1993) Shear bond strength of nickel/alumina interfaces diffusion bonded by HIP. *Journal of Materials Processing Technology*, 37, 711-721.

Lucefin Group. (2011) *16MnCr5 Data Sheet*. [Online] Available from: http://www.lucefin.com/wp-content/files_mf/0916mncr597.pdf [Accessed 18th November 2013].

Manesh, H. D. & Taheri, A. K. (2005) An investigation of deformation behaviour and bonding strength of bimetal strip during rolling. *Mechanics of Materials*, 37 (5), 531-542.

Mathas, K. (2005) Forging ahead for gear applications. *Gear Solutions*. [Online] Available from: http://gearsolutions.com/article/detail/5550/title/forging-ahead-for-gear-applications [Accessed 12th August 2013].

Matweb. (2013a) *AISI Type H13 Hot Work Tool Steel Datasheet*. [Online] Available from: http://www.matweb.com/search/datasheet_print.aspx?matguid=e30d1d1038164808a85cf7ba6aa87ef7 [Accessed 28th September 2013].

Matweb. (2013b) *Overview of Materials for AISI 1000 Series Steel*. [Online] Available from: http://www.matweb.com/search/DataSheet.aspx?MatGUID=81a26031d1b44cbb911f70ab863281f5&ckck=1 [Accessed 28th September 2013].

McGuinn, J. (2011) The global gear industry: Insights, projections, facts and figures. *Gear Technology*. [Online] 33-38. Available from: http://www.geartechnology.com/issues/0511x/global.pdf [Accessed 5-6th June 2011].

McLellan, R. B. & Ishikawa, T. (1987) The elastic properties of aluminium at high temperatures. *Journal of Physics and Chemistry of Solids*, 48 (7), 603-606.

McQueen, H. J., Leo, P. & Cerri, E. (2009) Constitutive equations for mg alloy hot work modelling. *Materials Science Forum,* 604-605, 53-65.

McQueen, H. J. & Ryan, N. D. (2002) Constitutive analysis in hot working. *Materials Science and Engineering A*, 322, 43-63.

McQueen, H. J. (1993) Metal forming: Industrial, mechanical computational and microstructural. *Journal of Materials Processing Technology*, 37, 3-36.

Miller, R. C. (1967) Pneumatic-mechanical forging--state of the art. In: *The First International Conference of the Centre for High Energy Forming*, *19-23 June 1967, Estes Park,* Colorado, University of Denver.

Miller, W. H. (1974) Gear Blanks, Patent No. U.S. 3,847,557, November 12.

Mitchener, R. G. & Mabie, H. H. (1982) The determination of the Lewis form factor and the AGMA geometry factor J for external spur gear teeth. *ASME Journal of Mechanical Design*, 104 (1), 148-158.

Mohamed, M. S., Foster, A. D., Lin, J., Balint, D. S. & Dean, T. A. (2012) Investigation of deformation and failure features in hot stamping of AA6082: Experimentation and modelling. *International Journal of Machine Tools and Manufacture*, 53 (1), 27-38.

Moriguchi, I. (1992) Cold forging of gears and other complex shapes. *Journal of Materials Processing Technology*, 35 (3-4), 439-450.

Neugebauer, R., Hellfritzsch, U., Lahl, M., Milbrandt, M., Schiller, S. & Druwe, T. (2012) Gear rolling process. In: B. Denkena and F. Hollmann (eds.) *Process Machine Interactions: Prediction and Manipulation of Interactions between Manufacturing Processes and Machine Tool Structures (Lecture Notes in Production Engineering).* Berlin, Heidelberg, Springer-Verlag. pp. 475-490.

Nishan Group. (2010) *Bimetal Bushes*. [Online] Available from: http://www.nishangroup.com/products_bushes_bimetalbushes.html [Accessed 18th November 2013].

Ohrn, K. E. (2007) Aircraft energy use. *Encyclopaedia of Energy Engineering and Technology First Edition, CRC Press Taylor and Francis Group*, 1, 24-30.

Okubo, H., Hosono, K. & Sakaki, K. (1968) The stress concentration in keyways when torque is transmitted through keys. *Experimental Mechanics*, 8 (8), 375-380.

Orthwein, W. C. (1975) Keyway stresses when torsional loading is applied by the keys. *Experimental Mechanics*, 15 (6), 245-248.

Ostrovsky, I. & Henn, Y. (2007) Present state and future of magnesium applications in aerospace industry. In: *Proceedings of the International Conference 'New Challenges in Aeronautics', ASTEC 2007, 19-22 August 2007*, Moscow.

Pastore, G. (2010) Antikythera calculator advances modern science of 19 centuries. *Advances in Space Environment Research*, 46 (4), 552-556.

Pederson, N. L. (2010) Stress concentrations in keyways and optimisation of keyway design. *Journal of Strain Analysis for Engineering Design*, 45 (8), 593-604.

Penticton Foundry. (2007) *Bi-Metallic Wye and Lateral Hydrotransport Spool Update*. [Online] Available from: http://pentictonfoundry.com/new/wp-content/uploads/cross-section-wye.jpg [Accessed 18th November 2013].

Perez-Castellanos, J. L. & Rusinek, A. (2012) Temperature increase associated with plastic deformation under dynamic compression: Application to aluminium alloy Al 6082. *Journal of Theoretical and Applied Mechanics*, 50 (2), 377-398.

Precision Powdered Metal Parts Inc. (2013) *Precision Powdered & Sintered Metal Gears*. [Online] Available from: http://www.precisionpm.com/custom-precision-powdered.html [Accessed 18th November 2013].

Premier Machine & Gear Ltd. (2004) *Gear Machining*. [Online] Available from: http://www.premier-gears.com/ [Accessed 10th October 2013].

PXPrecimet S. A. (2012) *Mild Steel 1.0718 Data Sheet*. [Online] Available from: http://www.pxprecimet.ch/data/documents/fiches-techniques/EN/11SMnPb30.pdf [Accessed 28th September 2013].

Rakhit, A. K. (2000) *Heat Treatment of Gears: A Practical Guide for Engineers*. Materials Park, OH, ASM International.

Ramamurti, V. & Ananda Rao, M. (1988) Dynamic analysis of spur gear teeth. *Computers and Structures*, 29 (5), 831-843.

Rameshkumar, M., Venkatesan, G. & Sivakumar, P. (2010) *Finite element analysis of high contact ratio gear*. American Gear Manufacturing Association. Technical Paper number: 10FTM06.

Rathod, M. J. & Kutsuna, M. (2004) Joining of aluminium alloy 5052 and low-carbon steel by laser roll welding. *Welding Journal*, 83 (1), 6-S - 26-S.

Refaat, M. H. & Meguid, S. A. (1995) On the contact stress analysis of spur gears using variational inequalities. *Computers and Structures*, 57 (5), 871-882.

Reformatskaya, I. I., Zav'yalov, V. V., Rodionova, I. G., Podobaev, A. N. & Ashcheulova, I. I. (2000) Prospects for use of bimetal pipes in field oil and gas pipelines of West Siberia. *Protection of Metals*, 36 (1), 46-51.

Riegler, C. & Bichlmaier, C. (2007) The geared turbofan technology – Opportunities, challenges and readiness status. *MTU Aero Engines Gmbh, Dachauerstraße 665, 80995 München, Germany.* [Online] Available from:

http://www.mtu.de/en/technologies/engineering_news/others/Riegler_Geared_turbofan_technology.pdf [Accessed 21th April 2011].

Rieiro, I., Gutierrez, V., Castellanos, J., Carsi, M., Larrea, M. T. & Ruano, O. A. (2010) A new constitutive strain-dependent garafalo equation to describe the high-temperature processing of materials - Application to the AZ31 magnesium alloy, *Metallurgical and Materials Transactions A*, 41A, 2396 - 2407.

Rolls Royce Plc. (1996) *The Jet Engine*, 5th Edition. UK, The Technical Publications Department Rolls Royce Plc.

Saarstahl. (2004) *Material Specification Sheet Saarstahl 16MnCr5-16MnCrS5*. [Online] Available from: http://www.saarstahl.com/fileadmin/saarstahl_extranet/images/04_produkte/walzstahlsorten/english/7131_7139_16MnCr5_16MnCrS5.pdf [Accessed 14th March 2013].

Sadeghi, M. H. & Dean, T. A. (1994). Precision forging straight and helical spur gears. *Journal of Materials Processing Technology*, 45 (1-4), 25-30.

Sadeghi, M. H. & Dean, T. A. (1992) The ejection of precision-forged straight and helical spur-gear forms. *Journal of Materials Processing Technology*, 31, 147-160.

Samanta, S. K. (1976) Helical gear: A noble method of manufacturing it. In: *The Proceedings of the 4th North American Metalworking Research Conference, Society of Manufacturing Engineers,* 17–19 May 1976, Battele's Columbus Labs, OH, pp. 199-205.

Santi, J. D. (1998) Composite Gear and Method of Making Same, Patent No. U.S. 5,852,951, December 29.

Sato, H. (1998) Method and Apparatus for Forging Helical Ring Gear, Patent No. U.S. 5,815,922 A, October 6.

Sellars, C. M. (1990) Modelling microstructural development during hot rolling. *Journal of Materials Science and Technology*, 6 (11), 1072-1081.

Sfakiotakis, V. G., Vaitsis, J. P. & Anifantis, N. K. (2001) Numerical simulation of conjugate spur gear action. *Computers and Structures*, 79 (12), 1153-1160.

Shan, D. B., Xu, W. C. & Lu, Y. (2004) Study on precision forging technology for a complex shaped light alloy forging. *Journal of Materials Processing Technology*, 151 (1-3), 289-293.

Shigley, J. E. & Mischke, C. R. (2001) *Mechanical Engineering Design*, 6th Edition. New York, USA, Mc-Graw Hill International Edition.

Shi, Z., Doel, T. J. A., Lin, J., Bowen, P. & Bray, S. (2010) Modelling thermomechanical behaviour of Cr-Mo-V steel. Materials Science and Technology Conference and Exhibition (MS&T 2010), Mini track: *Welding Metallurgy and Arc Welding*, *17-21 October 2010*, Houston, Texas, USA, MA&T, 4, p. 2596.

Shturtz, G. T. (1998) Powder metallurgy gears. In: Eisen, W. B., Ferguson, B. L., German, R. M., Iacocca, R., Lee, P. W., Madan, D., Moyer, K., Sanderow, H. and Trudel, Y (eds.) *ASM Handbook Volume 07: Metal Technologies and Applications*, OH, ASM International.

Spittel, M. & Spittel, T. (2009) Steel symbol/number: 11SMn30/1.0715. *Metal Forming Data- Ferrous Alloys - Deformation Behaviour, Springer Materials - The Landolt-Börnstein Database, Springer-Verlag Berlin Heidelberg*, [Online] 2C1. Available from: http://www.springermaterials.com/docs/info/978-3-540-44760-3_38.html [Accessed 18th November 2013].

SteelSS. (2011) *Data Table for Carbon Steel 16MnCr5*. [Online] available from: http://www.steelss.com/Carbon-steel/16mncr5.html [Accessed 18th August 2013].

Streander, G. W. (1973) Laminated Gear Construction, Patent No. U.S. 3,719,103, March 6.

Suzuki Motorcycles. (2008) *Drive Chain of RM-Z250*. [Online] Available from: http://www.suzukimotorcycles.com.au/bikes/off-road/motocross/2008/rm-z250/gallery.html [Accessed 17th August 2013].

Tait, W. H. (1954) A Method of Making Bearings, Patent No. US 2,689,380, September 21.

Tondini, F., Bosetti, P. & Bruschi, S. (2011) Heat transfer in hot stamping of high-strength steel sheets. Proceedings of the Institution of Mechanical Engineers, Part B. *Journal of Engineering Manufacture*, 225, 1813-1824.

Townsend, D. P. (1992) *Gears Made by Dies, Dudley's Gear Handbook: The Design, Manufacture and Application of Gears,* 2nd Edition. New York, McGraw Hill Book Company, p. 17.1-17.21.

Tuncer, C. & Dean, T. A. (1988) Precision forging hollow parts in novel dies. *Journal of Mechanical Working Technology*, 16 (1), 39-50.

Tuncer, C. & Dean, T. A. (1987) Die design alternatives for precision forging hollow parts. *International Journal of Machine Tools and Manufacture*, 27 (1), 65-76.

Tuncer, C. & Dean, T. A. (1985) Die design alternatives for precision forging in completely closed die cavities. In: *The Proceedings of the 25th International MTDR Conference, April 1985, Birmingham*, University of Birmingham, pp. 479-483.

Uherek, F. C. (2012) Gear material selection and construction for large gears. *AGMA Technical Paper*. [Online] Available from: http://www.agma.org/assets/uploads/publications/12FTM13_Uherek.pdf [Accessed 18th November 2013].

UN Chronicle. (2009) To Protect Succeeding Generations. *Special Climate Change Issue*. *Vol. XLVI, No. 3&4*. [Online] Available from: http://viewer.zmags.com/publication/9c49a2b8#/9c49a2b8/1 [Accessed 3rd October 2013].

Valberg, H. S. (2010) *Applied Metal Forming Including FEM Analysis*. Cambridge, UK, Cambridge University Press.

Van Dyck, S. (2011) The case for cold rolling. *Gear Solutions Magazine*. [Online] 46-52 Available from: http://www.gearsolutions.com/media/uploads/assets/PDF/Articles/May_11/0511_Grob.pdf [Accessed 18th November 2013].

Vijayarangan, S. & Ganesan, N. (1994) Static contact stress analysis of a spur gear tooth using the finite element method, including frictional effects. *Computers and Structures,* 51 (6), 765-770.

Vijayarangan, S. & Ganesan, N. (1993) A study of dynamic stresses in a spur gear under a moving line load and impact load conditions by a three-dimensional finite element method. *Journal of Sound and Vibration*, 162 (1), 185-189.

Wadleigh, A. S. (1993) Multi-metal Composite Gear/Shaft, Patent No. U.S. 5,271,287, December 21.

Wallace, D. B. & Seireg, A. (1973) Computer simulation of dynamic stress, deformation and fracture of gear teeth. *Journal of Engineering for Industry, Transactions of the ASME*, 95 (4), 1108-1114.

Wang, L. K. & Cheng, H. S. (1981) A numerical solution to the dynamic load, film thickness, and surface temperatures in spur gears, Part I Analysis. *Journal of Mechanical Design, Transactions of the ASME*, 103 (1), 177-187.

Wang, K. L. & Cheng, H. S. (1980) *Thermal Elastohydrodynamic Lubrication of Spur Gears.* NASA Contractor. Report number: 3241.

Whittaker, D. (1991) Powder metallurgy for gear production: Current status and potential future trends. *Materials and Design*, 12 (2), 97-100.

Wired. (2008) *Belt Drive*. [Online] Available from: http://www.wired.com/images_blogs/photos/uncategorized/2008/09/25/spot2.jpg [Accessed 17th August 2013].

Wolfe, R. F. & Trebnik, A. (1971) Method for Manufacturing an Improved Composite Gear, Patent No. U.S. 3,557,423, January 26.

Wright, N. W. & Schriefer, H. (1997) Basic honing and advanced free-form honing. *Gear Technology*. [Online] July/August Issue, 26-33. Available from: http://www.geartechnology.com/articles/0797/Basic_Honing_~_Advanced_Free-Form_Honing [Accessed 18th November 2013].

Yiasemides, G. P. (1987) Diffusion bonding using hot isostatic pressing. In: R. Pearce (ed.) *Diffusion Bonding.* Bedfordshire, UK, Cranfield Institute of Technology. pp. 259-269.

Zener, C. & Hollomon, J. H. (1944) Effect of strain rate upon plastic flow of steel. *Journal of Applied Physics*, 15 (1), 22-32.

Zhao, Z., Hu, C. & Ruan, X. (2010) Chinese national report on cold forging. *43rd ICFG Plenary Meeting.* [Online] *12-15 September, Darmstadt,* Germany. Available from: http://www.lft.uni-erlangen.de/SEITEN/ICFG/China10.pdf [Accessed 18th November 2013].

Appendix A Tool-Set Engineering Drawings

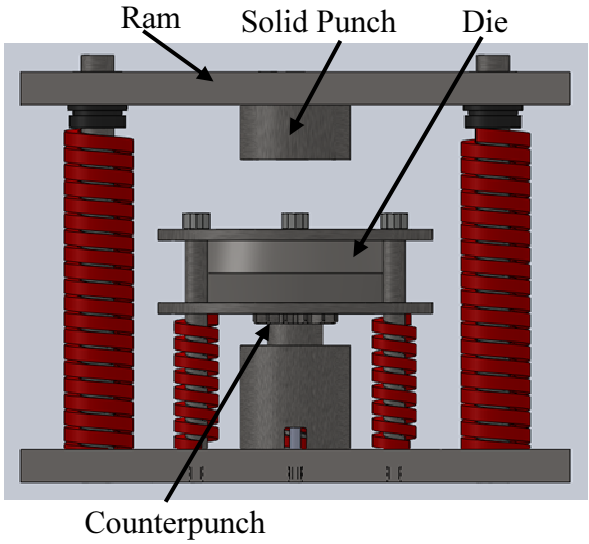


Figure A1: Toolset fully open

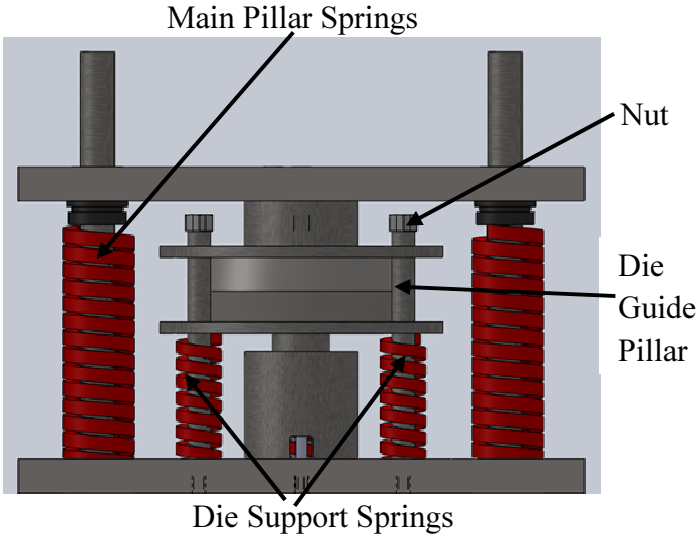


Figure A2: Toolset fully closed

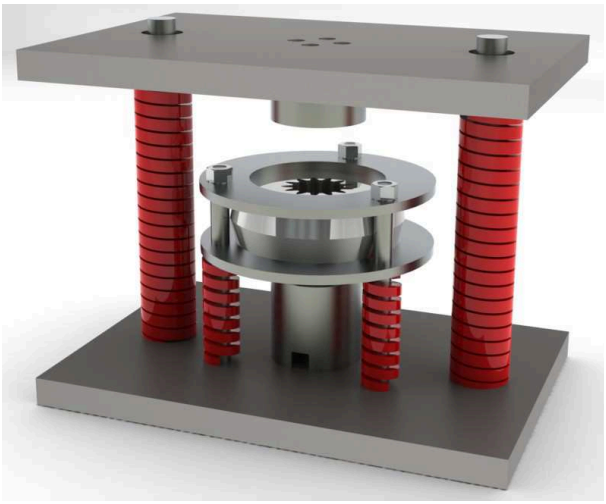
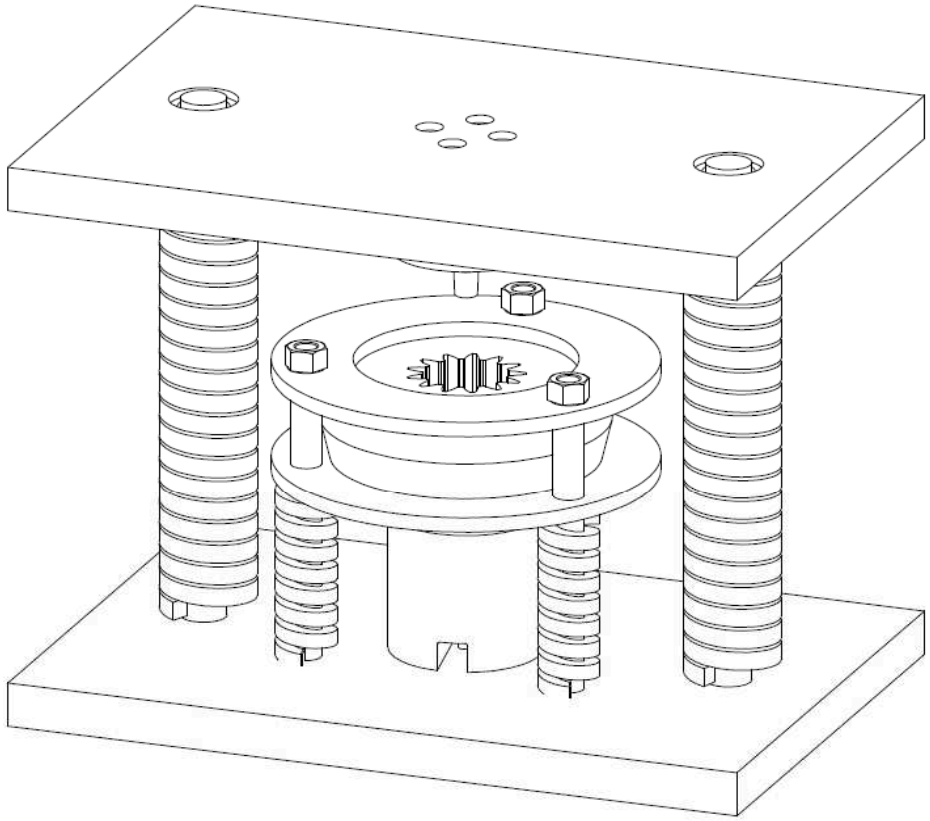
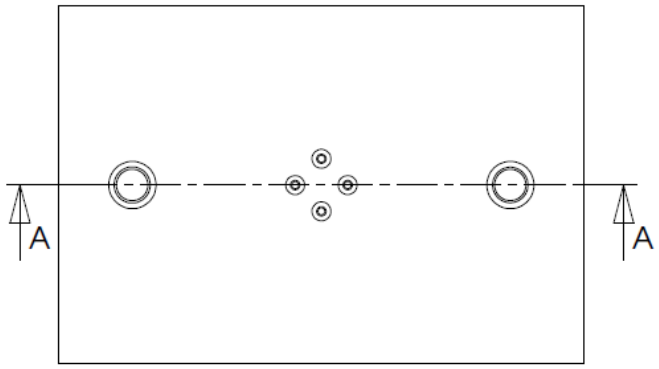


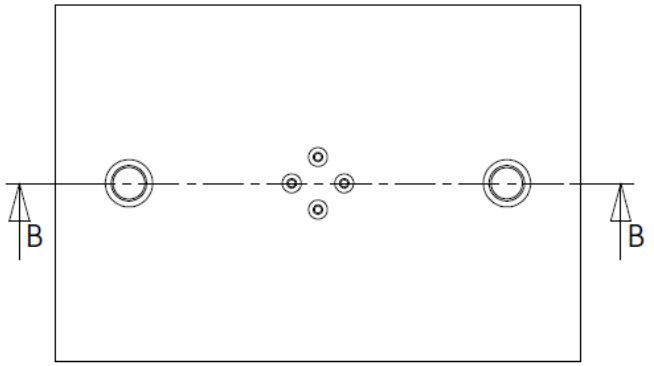
Figure A3: Toolset rendering

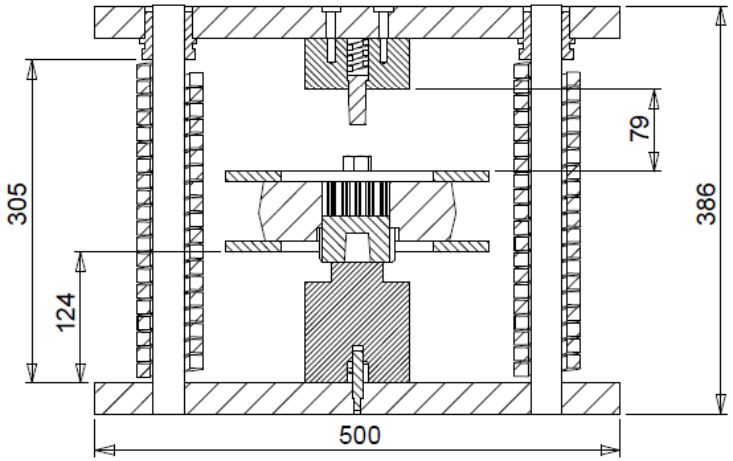


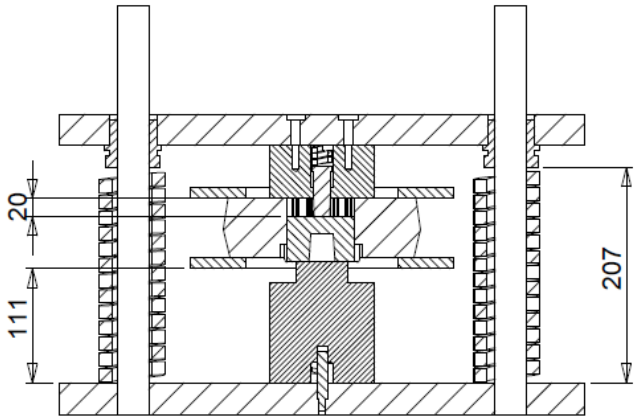
TOLERANCES		THIRD ANGLE PROJECTION	MATERIAL:	TITLE:	Imperial College London
X =± 0.5 X.X =± 0.1 X.XX =± 0.02	ANGULAR ±1° SURFACE FINISH MACHINED FACES Ra 6.3			TOOL ASSEMBLY	Department of Mechanical Engineering
	NAME	DATE	ALL DIMENSIONS ARE IN MILLIMETRES		
DRAWN	DENIS POLITIS	12/12/10	DO NOT SCALE DRAWING	DWG No.	
CHECKED			A4 SCALE 1:4	A1	SHEET 1 OF 1 REVISION
APPROVED					

SolidWorks Student License
Academic Use Only



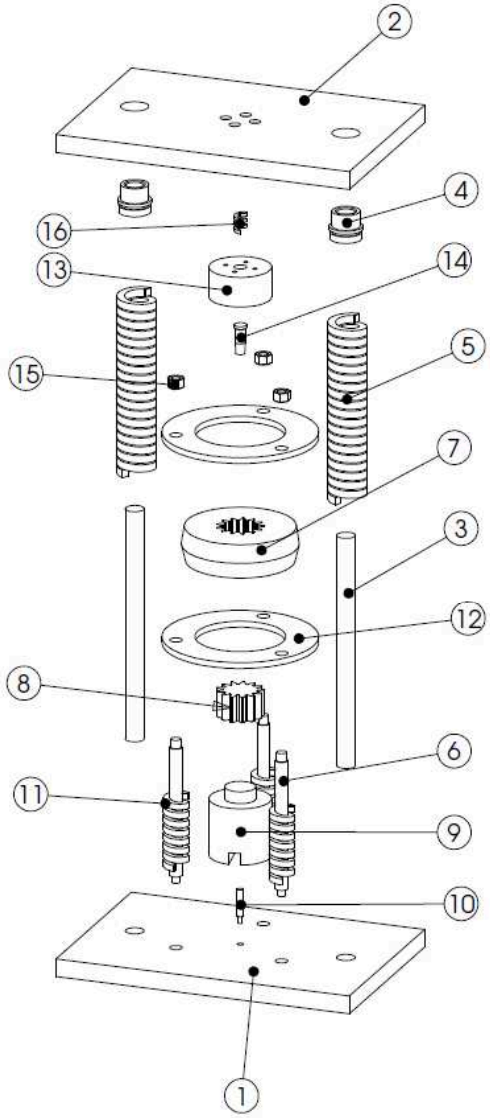






TOLERANCES		THIRD ANGLE PROJECTION	MATERIAL:	TITLE:	Imperial College London
X =± 0.5 X.X =± 0.1 X.XX =± 0.02	ANGULAR ±1° SURFACE FINISH MACHINED FACES Ra 6.3			CROSS SECTION VIEW	Department of Mechanical Engineering
	NAME	DATE	ALL DIMENSIONS ARE IN MILLIMETRES		
DRAWN	DENIS POLITIS	12/12/10	DO NOT SCALE DRAWING	DWG No.	
CHECKED			A4 SCALE 1:6	C1	SHEET 1 OF 1 REVISION
APPROVED					

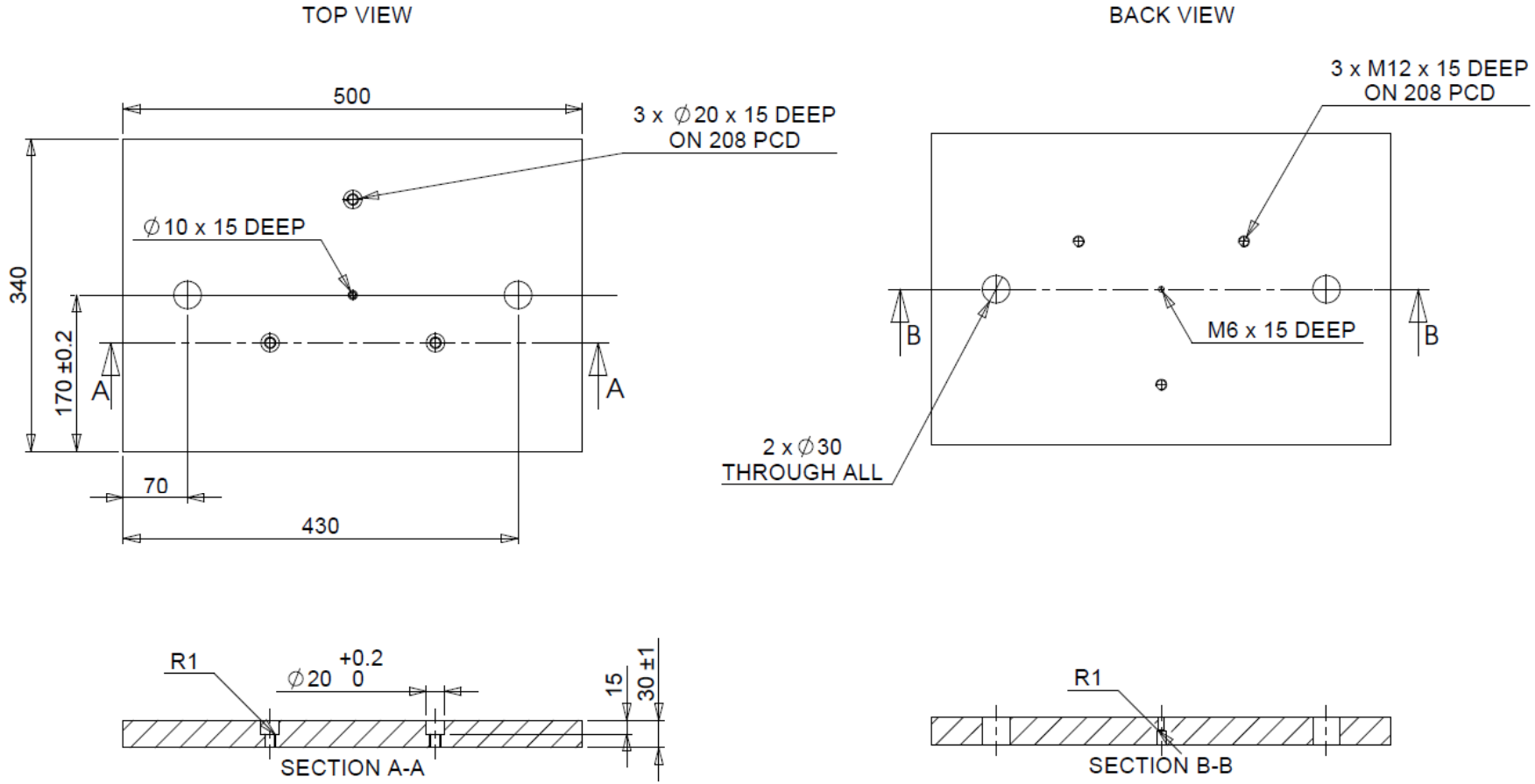
SolidWorks Student License
Academic Use Only



ITEM NO.	PART NUMBER	QTY.
1	BASE PLATE	1
2	RAM	1
3	MAIN PILLAR	2
4	BEARING BUSH CATALOGUE NO. 6-3045-33	2
5	MAIN PILLAR SPRING CATALOGUE NO. 9-4048-110	2
6	DIE GUIDE PILLAR	3
7	DIE	1
8	COUNTERPUNCH	1
9	EJECTOR	1
10	EJECTOR SUPPORT GUIDE	1
11	DIE SUPPORT SPRING CATALOGUE NO. 9-2420-110	3
12	DIE CLAMPING RING	2
13	MANDREL PUNCH	1
14	MANDREL	1
15	M16 NUT	3
16	MANDREL SPRING CATALOGUE NO. 9-1207-110	1

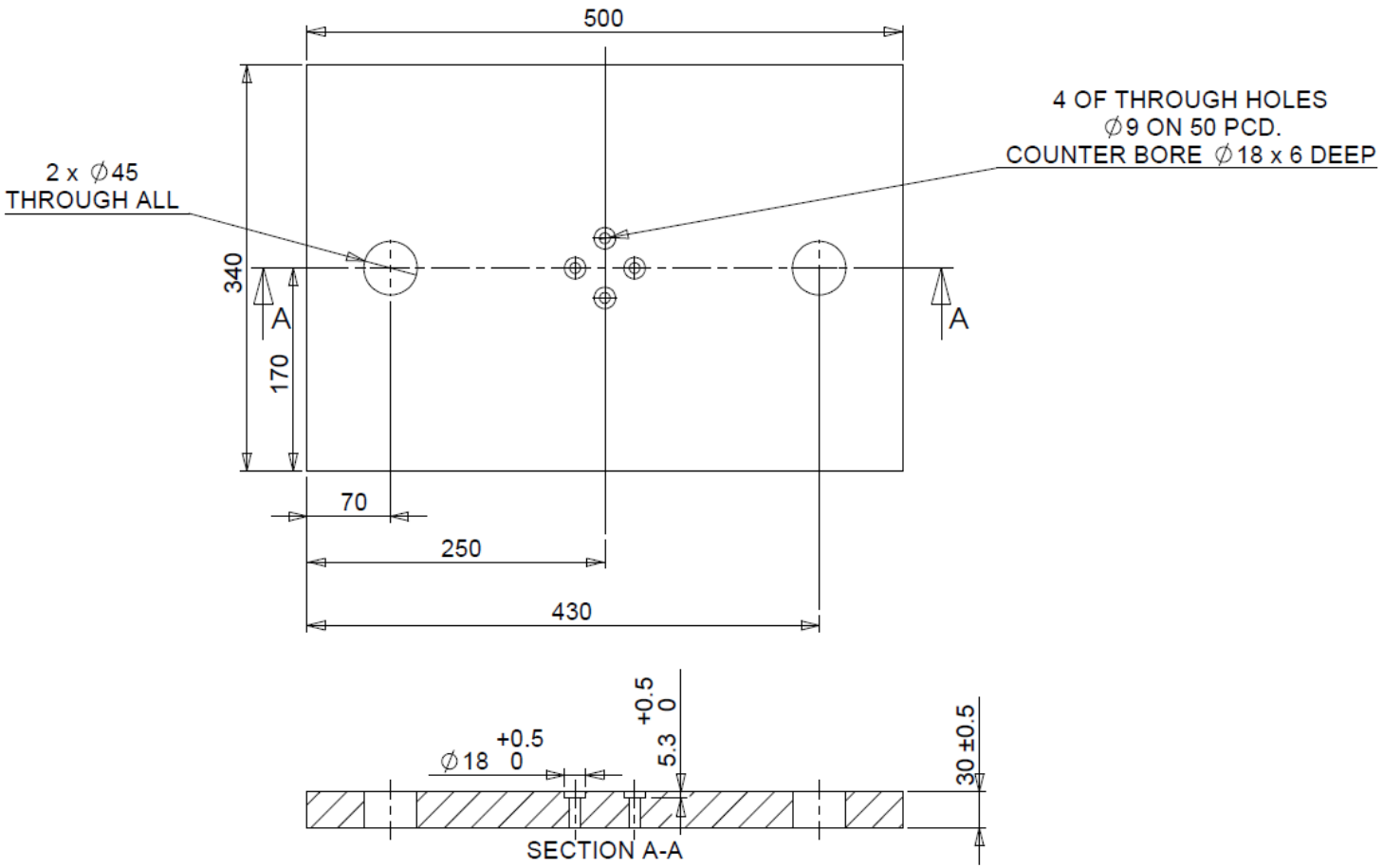
SolidWorks Student License
Academic Use Only

TOLERANCES		THIRD ANGLE PROJECTION	MATERIAL:	TITLE:	Imperial College London
X =± 0.5 X.X =± 0.1 X.XX =± 0.02	ANGULAR ±1° SURFACE FINISH MACHINED FACES Ra 6.3		ALL DIMENSIONS ARE IN MILLIMETRES	EXPLODED VIEW	Department of Mechanical Engineering
	NAME	DATE			
DRAWN	DENIS POLITIS	28/8/11	DO NOT SCALE DRAWING	DWG No. E1	
CHECKED			A4 SCALE 1:10		SHEET 1 OF 1 REVISION
APPROVED					



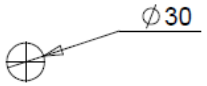
TOLERANCES		THIRD ANGLE PROJECTION	MATERIAL:	TITLE:	Imperial College London
X =± 0.5 X.X =± 0.1 X.XX =± 0.02	ANGULAR ±1° SURFACE FINISH MACHINED FACES Ra 6.3		PLAIN CARBON STEEL ALL DIMENSIONS ARE IN MILLIMETRES	BASE PLATE x1	Department of Mechanical Engineering
	NAME	DATE			
DRAWN	DENIS POLITIS	12/12/10	DO NOT SCALE DRAWING	DWG No. 1	
CHECKED			A4 SCALE 1:6		SHEET 1 OF 1 REVISION
APPROVED					

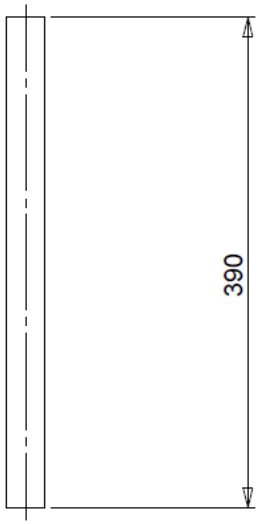
SolidWorks Student License
Academic Use Only



TOLERANCES		THIRD ANGLE PROJECTION	MATERIAL:	TITLE:	Imperial College London
X =± 0.5 X.X =± 0.1 X.XX =± 0.02	ANGULAR ±1° SURFACE FINISH MACHINED FACES Ra 6.3		PLAIN CARBON STEEL ALL DIMENSIONS ARE IN MILLIMETRES	RAM x1	Department of Mechanical Engineering
	NAME	DATE			
DRAWN	DENIS POLITIS	12/12/10	DO NOT SCALE DRAWING	DWG No. 2	
CHECKED			A4 SCALE 1:5		SHEET 1 OF 1 REVISION
APPROVED					

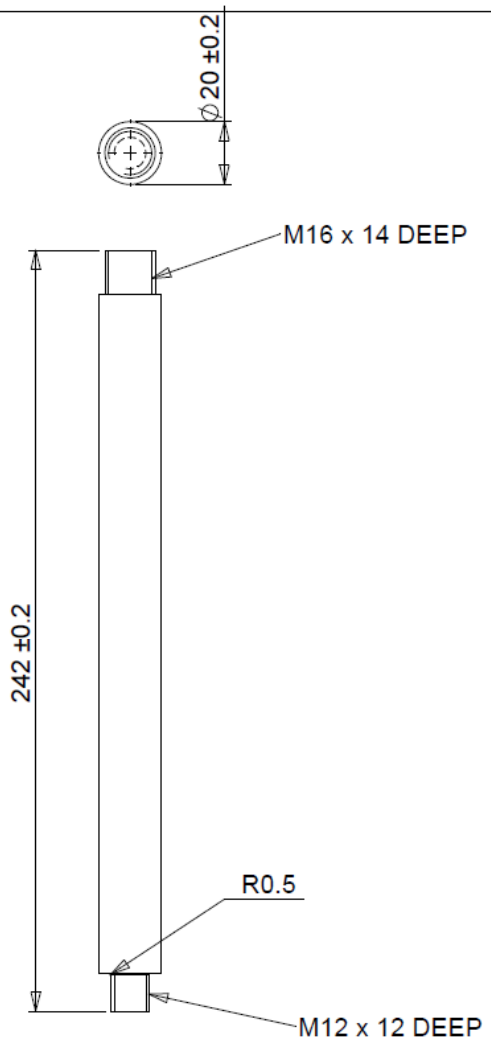
SolidWorks Student License
Academic Use Only





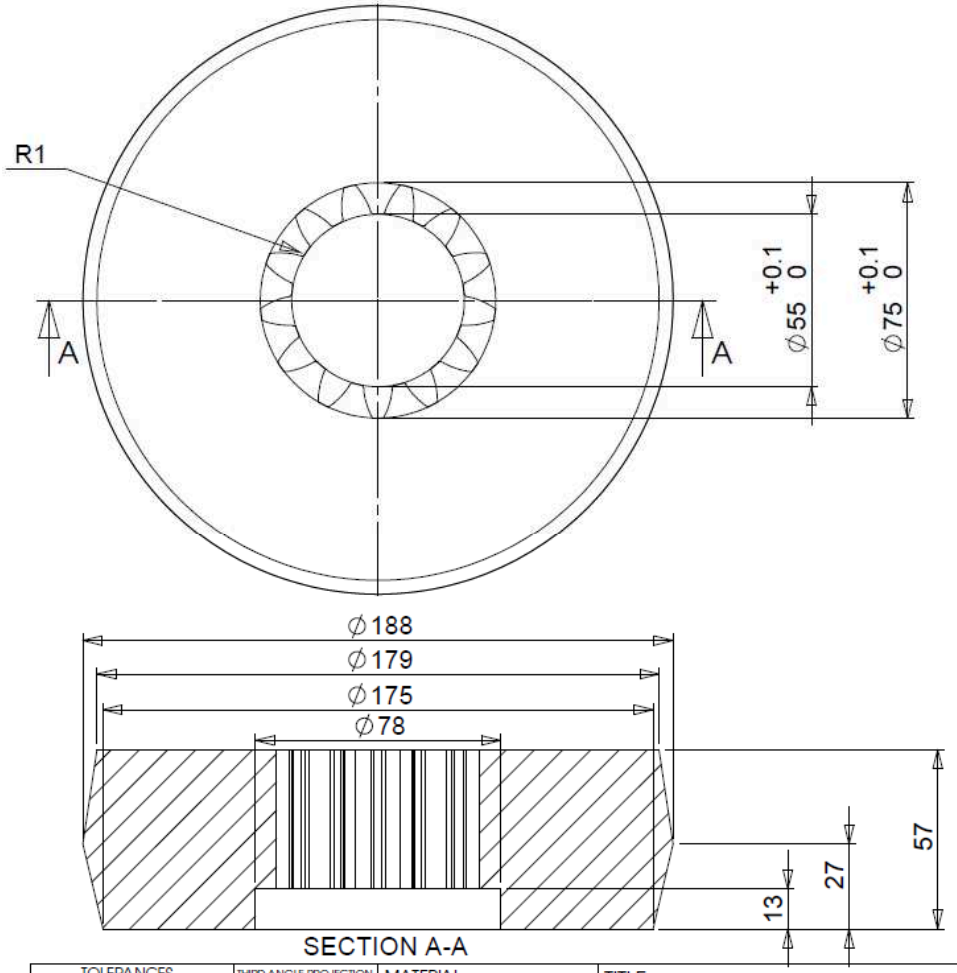
TOLERANCES X =± 0.5 X.X =± 0.1 X.XX =± 0.02 ANGULAR ±1° SURFACE FINISH MACHINED FACES Ra 6.3		THIRD ANGLE PROJECTION	MATERIAL: Plain Carbon Steel ALL DIMENSIONS ARE IN MILLIMETRES DO NOT SCALE DRAWING	TITLE: Main Pillar x 2	Imperial College London Department of Mechanical Engineering
	NAME	DATE			
DRAWN	DENIS POLITIS	12/12/10			
CHECKED					
APPROVED			A4 SCALE 1:5	DWG No. 3	SHEET 1 OF 1 REVISION

SolidWorks Student License
Academic Use Only



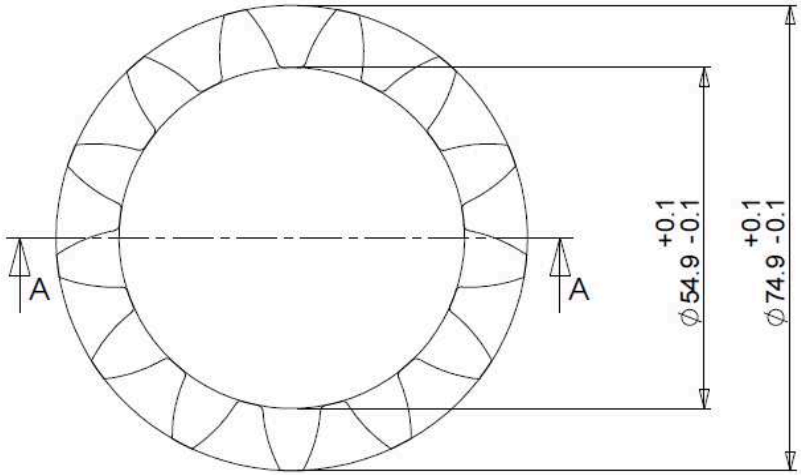
TOLERANCES		THIRD ANGLE PROJECTION	MATERIAL:	TITLE:	Imperial College London
X =± 0.5 X.X =± 0.1 X.XX =± 0.02	ANGULAR ±1° SURFACE FINISH MACHINED FACES Ra 6.3		PLAIN CARBON STEEL	DIE GUIDE PILLAR x3	Department of Mechanical Engineering
	NAME	DATE	ALL DIMENSIONS ARE IN MILLIMETRES		
DRAWN	DENIS POLITIS	12/12/10	DO NOT SCALE DRAWING	DWG No. 4	
CHECKED			A4 SCALE 1:2		SHEET 1 OF 1 REVISION
APPROVED					

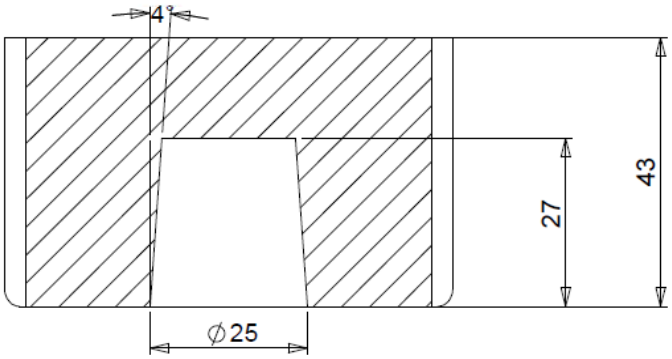
SolidWorks Student License
Academic Use Only



TOLERANCES		THIRD ANGLE PROJECTION	MATERIAL:	TITLE:	Imperial College London
X =± 0.5 X.X =± 0.1 X.XX =± 0.02	ANGULAR ±1° SURFACE FINISH MACHINED FACES Ra 6.3		H13 Tool Steel	Die x1	Department of Mechanical Engineering
	NAME	DATE	ALL DIMENSIONS ARE IN MILLIMETRES		
DRAWN	DENIS POLITIS	12/12/10	DO NOT SCALE DRAWING	DWG No. 5	
CHECKED			A4 SCALE 1:3		SHEET 1 OF 1 REVISION
APPROVED					

SolidWorks Student License
Academic Use Only





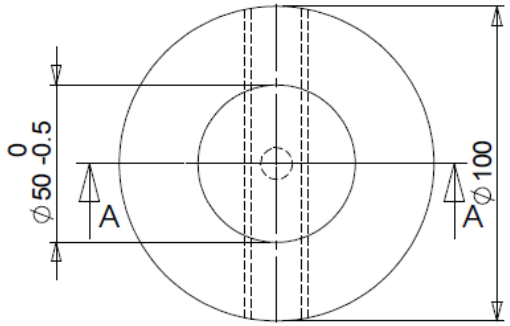
SECTION A-A

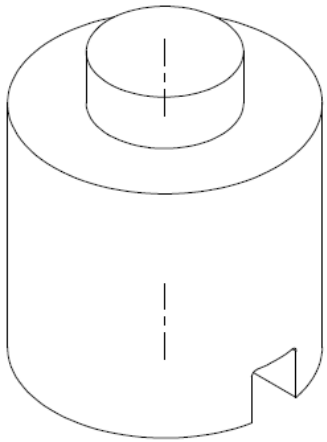
TOLERANCES		THIRD ANGLE PROJECTION	MATERIAL:	TITLE:
X =± 0.5 X.X =± 0.1 X.XX =± 0.02	ANGULAR ±1° SURFACE FINISH MACHINED FACES Ra 6.3		H13 Tool Steel	Counterpunch x 1
			ALL DIMENSIONS ARE IN MILLIMETRES	
	NAME	DATE	DO NOT SCALE DRAWING	DWG No. 6
DRAWN	DENIS POLITIS	12/12/10		
CHECKED			A4 SCALE 1:1	
APPROVED				

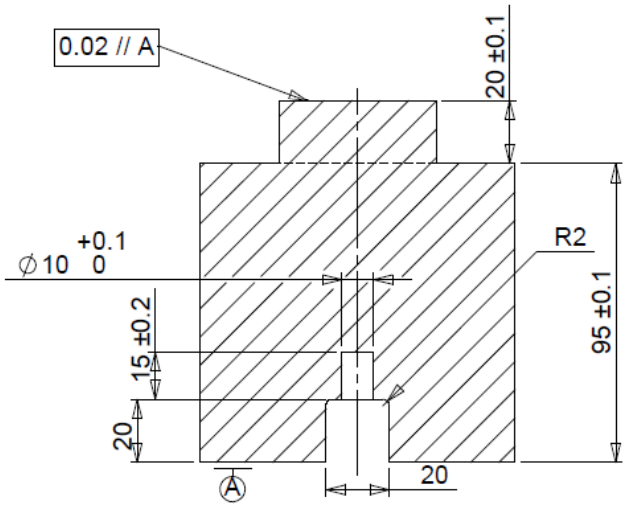
Imperial College London
Department of Mechanical Engineering

SHEET 1 OF 1 | REVISION

SolidWorks Student License
Academic Use Only



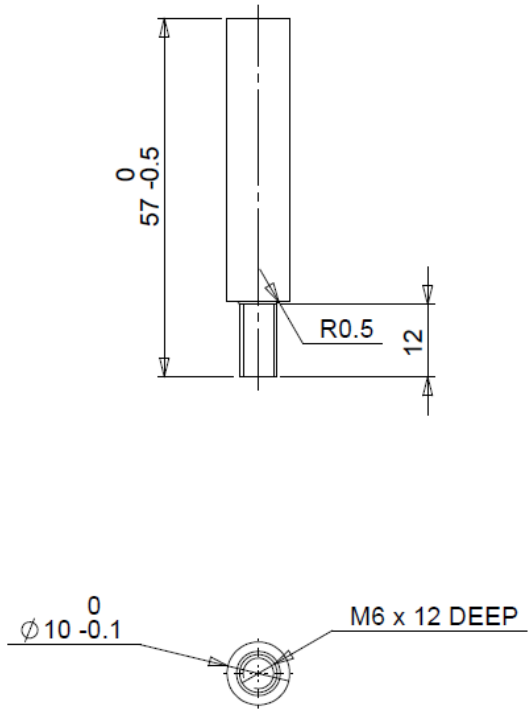




SECTION A-A

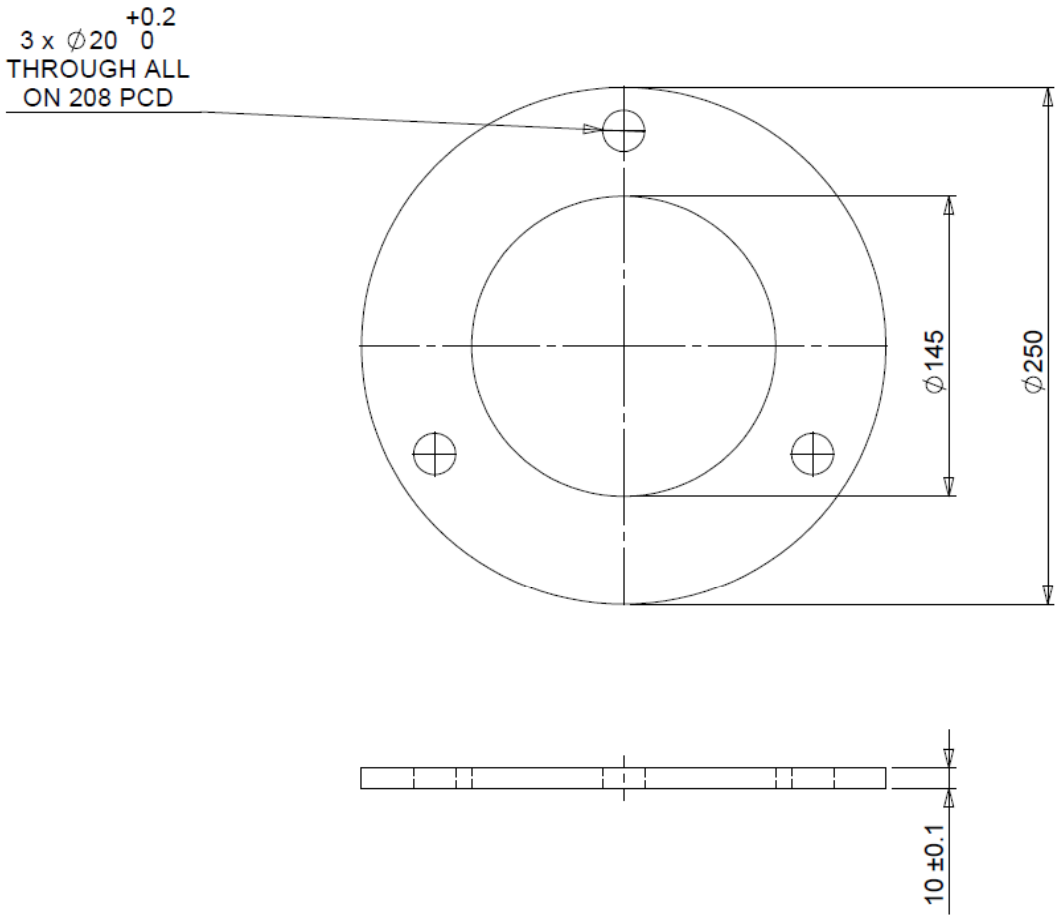
TOLERANCES		THIRD ANGLE PROJECTION	MATERIAL:	TITLE:	Imperial College London
X =± 0.5 X.X =± 0.1 X.XX =± 0.02	ANGULAR ±1° SURFACE FINISH MACHINED FACES Ra 6.3		H13 TOOL STEEL	EJECTOR X1	Department of Mechanical Engineering
	NAME	DATE	ALL DIMENSIONS ARE IN MILLIMETRES		
DRAWN	DENIS POLITIS	12/12/10	DO NOT SCALE DRAWING	DWG No. 7	
CHECKED			A4 SCALE 1:2		SHEET 1 OF 1 REVISION
APPROVED					

SolidWorks Student License
Academic Use Only



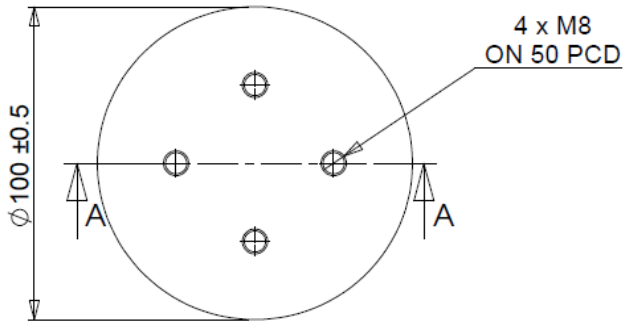
TOLERANCES		THIRD ANGLE PROJECTION	MATERIAL:	TITLE:	Imperial College London
X =± 0.5 X.X =± 0.1 X.XX =± 0.02	ANGULAR ±1° SURFACE FINISH MACHINED FACES Ra 6.3		PLAIN CARBON STEEL ALL DIMENSIONS ARE IN MILLIMETRES	EJECTOR SUPPORT GUIDE X1	Department of Mechanical Engineering
	NAME	DATE			
DRAWN	DENIS POLITIS	12/12/10	DO NOT SCALE DRAWING	DWG No. 8	
CHECKED					
APPROVED			A4 SCALE 1:1		SHEET 1 OF 1 REVISION

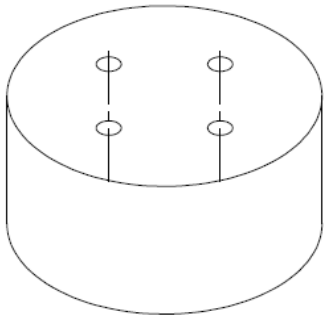
SolidWorks Student License
Academic Use Only

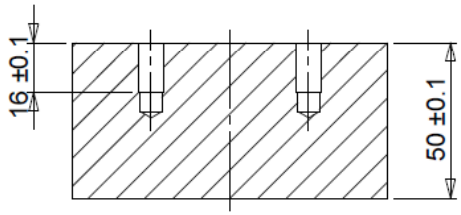


TOLERANCES: X =± 0.5, X.X =± 0.1, X.XX =± 0.02; ANGULAR ±1°; SURFACE FINISH MACHINED FACES Ra 6.3	THIRD ANGLE PROJECTION	MATERIAL: PLAIN CARBON STEEL	TITLE: DIE CLAMPING RING x2	Imperial College London Department of Mechanical Engineering	
	NAME: DENIS POLITIS	DATE: 12/12/10	ALL DIMENSIONS ARE IN MILLIMETRES		
DRAWN			DO NOT SCALE DRAWING	DWG No. 9	
CHECKED			A4	SCALE 1:3	SHEET 1 OF 1
APPROVED					REVISION

SolidWorks Student License
Academic Use Only



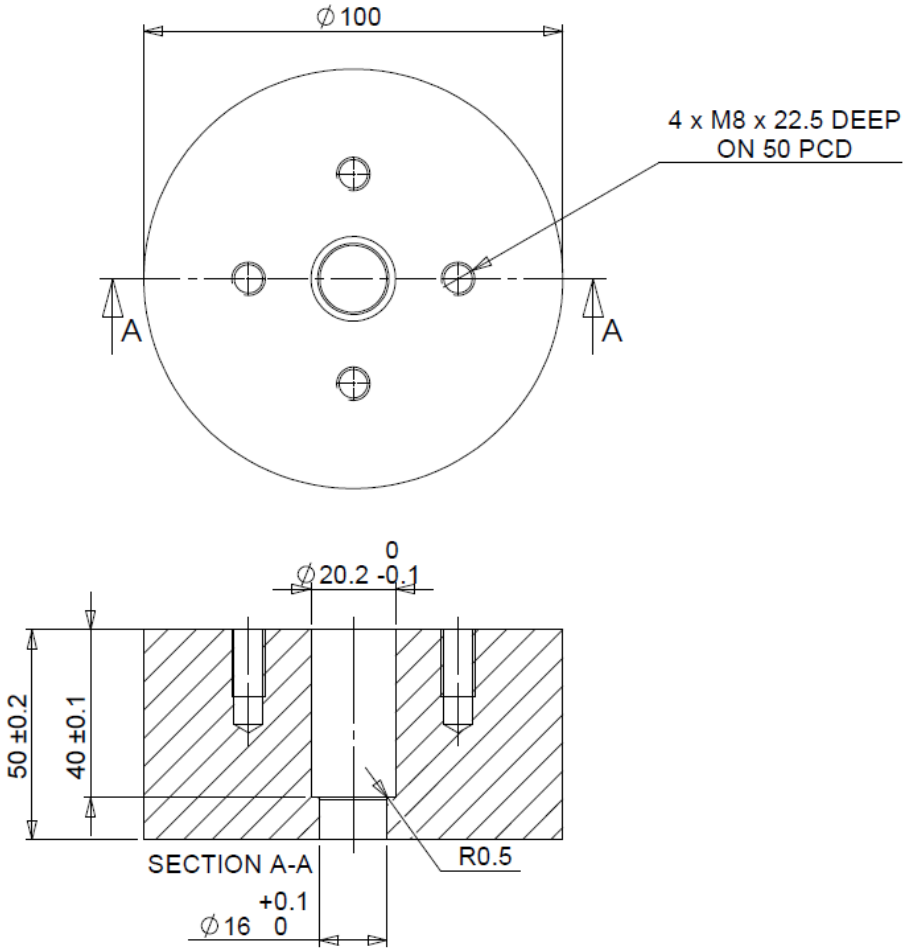




SECTION A-A

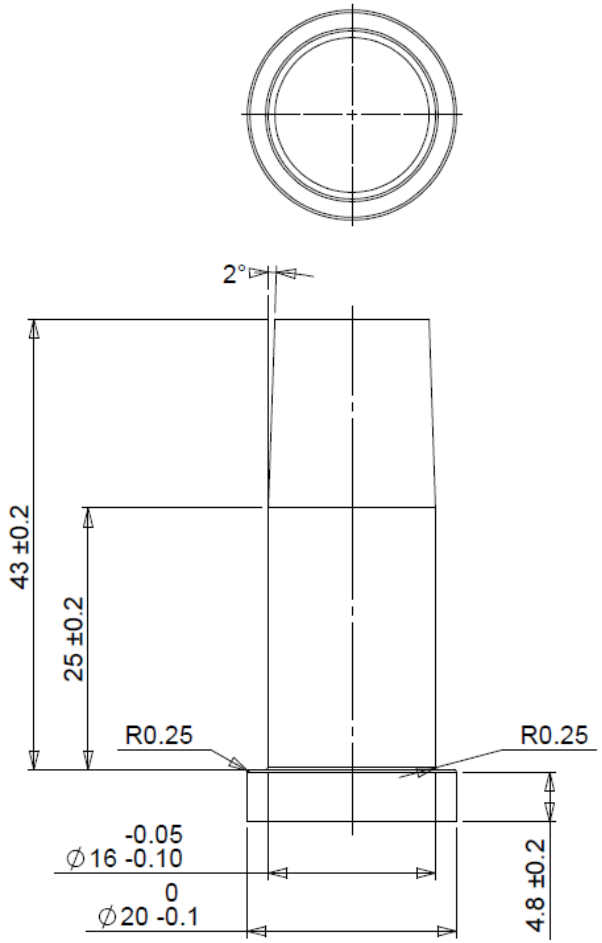
TOLERANCES: X = ± 0.5, X.X = ± 0.1, X.XX = ± 0.02; ANGULAR ±1°; SURFACE FINISH MACHINED FACES Ra 6.3		THIRD ANGLE PROJECTION	MATERIAL: H13 TOOL STEEL	TITLE: SOLID PUNCH X1	Imperial College London Department of Mechanical Engineering
	NAME	DATE	ALL DIMENSIONS ARE IN MILLIMETRES		
DRAWN	DENIS POLITIS	12/12/10	DO NOT SCALE DRAWING	DWG No. 10	SHEET 1 OF 1 REVISION
CHECKED			A4 SCALE 1:2		
APPROVED					

SolidWorks Student License
Academic Use Only



TOLERANCES		THIRD ANGLE PROJECTION	MATERIAL:	TITLE:	Imperial College London
X =± 0.5 X.X =± 0.1 X.XX =± 0.02	ANGULAR ±1° SURFACE FINISH MACHINED FACES Ra 6.3		H13 TOOL STEEL	MANDREL PUNCH x1	Department of Mechanical Engineering
	NAME	DATE	ALL DIMENSIONS ARE IN MILLIMETRES		
DRAWN	DENIS POLITIS	28/8/11	DO NOT SCALE DRAWING	DWG No. 11	
CHECKED			A4 SCALE 1:1.5		SHEET 1 OF 1 REVISION
APPROVED					

SolidWorks Student License
Academic Use Only



TOLERANCES		THIRD ANGLE PROJECTION	MATERIAL:	TITLE:	Imperial College London
X =± 0.5 X.X =± 0.1 X.XX =± 0.02	ANGULAR ±1° SURFACE FINISH MACHINED FACES Ra 6.3		H13 TOOL STEEL	MANDREL x1	Department of Mechanical Engineering
			ALL DIMENSIONS ARE IN MILLIMETRES		
	NAME	DATE	DO NOT SCALE DRAWING	DWG No.	
DRAWN	DENIS POLITIS	24/8/11			
CHECKED			A4 SCALE 1:0.6	12	SHEET 1 OF 1 REVISION
APPROVED					

SolidWorks Student License
Academic Use Only

Appendix B Analytical/Empirical Stress Calculations

B.1 AGMA Tooth Contact Stress

The AGMA tooth contact stress can be calculated from equation B1 below.

$$\sigma_c = Z_e \left(W_t K_{OF} K_v^{'} K_s \frac{K_H}{Fd} \frac{Z_R}{Z_I} \right)^{0.5} \qquad Eqn\ B1$$

In this equation, the elastic coefficient factor (Z_e) accounts for the material properties of the pinion and gear and is calculated from equation B2 below:

$$Z_e = \sqrt{\frac{1}{\pi \left(\frac{1 - v_P^2}{E_P} + \frac{1 - v_G^2}{E_G} \right)}} \qquad Eqn\ B2$$

Where: ν_P and ν_G are the Poisson's ratios for pinion and gear, and E_P and E_G are the elastic modulus of the pinion and gear respectively. As both gears for this analysis are steel, ν = 0.3 and E = 210 GPa, hence $Z_e = 191.64567\sqrt{MPa}$. Moreover, the transmitted load W_t can be calculated by $W_t = \frac{P}{V} = \frac{T\omega}{r\omega} = \frac{T}{r} = \frac{150}{\frac{0.065}{2}} = 4{,}615.38N$. The overload factor K_{OF} accounts for externally applied loads in excess of the transmitted load and is set as $K_{OF} = 1$ for smooth operation (Childs, 2003). The dynamic factor K_V' can be calculated from equation B3 below:

$$K_v^{'} = \left(\frac{A + \sqrt{200V}}{A} \right)^B \qquad Eqn\ B3$$

Where: the constants B and A are calculated using equations $B = \frac{(12 - Q_V)^{\frac{2}{3}}}{4}$ and $A = 50 + 56(1 - B)$ respectively. According to the standards, Q_V is the AGMA quality of the gear, which assuming is in the upper band of commercial quality gears for machinery, has a value of 6. As a quasi-static analysis has been performed, the resulting dynamic factor $K_v^{'}$ = 1. Furthermore, the size factor (K_s) which accounts for non-uniformity in material of large dimensions is $K_s = 1$. Moreover, the surface condition factor Z_R which accounts for surface finish is set as $Z_R = 1$. The load distribution factor K_H which accounts for non-uniform distribution of load across the line of contact is calculated using equation B4 below.

$$K_H = 1 + C_{mc}\left(C_{pf} C_{pm} + C_{ma} C_e \right) \qquad Eqn\ B4$$

Where: C_{mc} is the factor accounting for crowned teeth of the gear, C_{pf} is the pinion proportion factor, C_{pm} defines position of the gear on the shaft, C_{ma} is the mesh alignment factor and C_e is related to the position at assembly. According to the literature (Childs, 2003), for the geometry of the gears under consideration, $C_{mc} = 1$, $C_e = 1$ and $C_{pm} = 1$. Moreover, the face width (F) of 20mm for the forged gear, is below the threshold of 25.4mm, thus resulting in the use of equation B5 below (Childs, 2003):

$$C_{pf} = \frac{F}{10d} - 0.025 \qquad Eqn\ B5$$

However, as the face width F = 20mm, the value of $\frac{F}{10d} < 0.05$, and thus, according to the literature, is automatically set to $\frac{F}{10d} = 0.05$ in the above equation, hence resulting in a value $C_{pf} = 0.025$. The mesh alignment factor C_{ma} can be calculated from $C_{ma} = A + BF + CF^2$, whereby for commercial enclosed gears, the constants used in the equations are as follows: A = 0.127, B = 0.622 and C = - 0.0144 (Childs, 2003). For F = 20mm, $C_{ma} = 0.139$. Through the use of these factors, it can be calculated that $K_H = 1.16443$. Finally, the surface geometry factor for external gears (Z_I) is calculated from the equation B6 below:

$$Z_I = \frac{\cos\varphi_t \sin\varphi_t}{2m_N} \cdot \frac{m_G}{m_G + 1} \qquad Eqn\ B6$$

In this case, m_n, the load sharing ratio for spur gears m_n = 1. The transverse pressure angle (φ_t) applies for helical gears and is replaced with φ for spur gears. The speed ratio (m_G) can be calculated from the number of teeth of the gear and the pinion as $m_G = \frac{N_G}{N_P}$. As both pinion and gear are modeled as the same 13 toothed gear, m_G = 1. Hence, $Z_I = 0.08034845$. Thus, from the AGMA equation for contact stress, the value has been calculated as:

$$\sigma_c = 191.64567\sqrt{4{,}615.38 \cdot 1 \cdot 1 \cdot 1 \cdot \frac{1.16443}{0.065 \cdot 0.02} \cdot \frac{1}{0.08034845}} = 1{,}374{,}672.44kPa$$

B.2 British Standard Tooth Contact Stress

The British Standard tooth contact stress ($\sigma_{H1,2}$) can be found from equation B7 and B8 below, where σ_{HO} defined as 'the nominal contact stress at the pitch point' BS ISO Standard (2006b) must first be calculated before calculating the 'contact stress at the inner point of single pair tooth contact' (BS ISO Standard, 2006b) ($\sigma_{H1,2}$).

$$\sigma_{HO} = Z_H Z_E Z_\varepsilon Z_\beta \sqrt{\frac{F_t}{d_1 b} \cdot \frac{u+1}{u}} \qquad Eqn\ B7$$

$$\sigma_{H1,2} = Z_B \sigma_{HO} \sqrt{K_A K_v K_{H\beta} K_{H\alpha}} \qquad Eqn\ B8$$

According to the literature (BS ISO Standard, 2006b), the zone factor (Z_H) is calculated by equation B9 below.

$$Z_H = \sqrt{\frac{2\cos\beta_b \cos\alpha_{wt}}{(\cos\alpha_t)^2 \sin\alpha_{wt}}} \qquad Eqn\ B9$$

Where: β_b = base helix angle, α_{wt} = normal pressure angle, α_t = transverse pressure angle. In the case of the spur gear geometry, the normal pressure angle = 20^o, the helix angle $\theta = 0^o$, the transverse pressure angle α_t is calculated as $\tan^{-1}\left(\frac{\tan\alpha_{wt}}{\cos\theta}\right)$ and the base helix angle is calculated from $\sin^{-1}(\cos\alpha_{wt}\sin\theta)$. This results in $\alpha_t = 20^o$ and $\beta_b = 0^o$, resulting in $Z_H = 2.49$. The elasticity factor (Z_E) is calculated as in the AGMA standard resulting in $Z_E = 191{,}645.67\sqrt{N/m^2}$. Furthermore, the contact ratio factor for spur gears is set to $Z_\varepsilon = 1$ (BS ISO Standard, 2006b). The helix factor (Z_β) exists for a helical gear, and thus for a spur gear with helix angle = 0^o, $Z_\beta = 1$. The gear ratio (u) as in the AGMA standard is calculated from the number of teeth on each gear and hence u = 1. The tangential force is calculated by $F_t = \frac{2000T}{d}$ (BS ISO Standard, 2006a). For a torque of 150Nm, this gives a value of F_t = 4615.38N as calculated in section B.1 above. Substituting with the gear dimensions in equation B7 gives $\sigma_{HO} = 1{,}273.92\ MPa$. From equation B8, as smooth operation is assumed, variations in torque and load distribution can be ignored and hence $\sigma_{H1,2} = Z_B \sigma_{HO}$. The contact ratio ($Z_B$) requires several other parameters to be calculated which are summarised below. Further explanations of these factors can be found in the literature (BS ISO Standard, 2006b).

$$\varepsilon_\alpha = \frac{2\tan 20^o}{\frac{2\pi}{13}} = 1.506$$

and:

$$M = \frac{\tan 20^o}{\sqrt{\left(\sqrt{\frac{0.075^2}{0.06108^2} - 1} - \frac{2\pi}{13}\right) \cdot \left(\sqrt{\frac{0.075^2}{0.06108^2} - 1} - (1.506 - 1)\frac{2\pi}{13}\right)}}$$

So, M=1.111. as M>1, then Zb=M

$$Z_B = 1.111$$

Hence:

$$\sigma_{H1,2} = 1.111 \cdot 1{,}273.92$$

$$\sigma_{H1,2} = 1.111 \cdot 1{,}273.92 = 1{,}415.33 MPa$$

which has a difference with the AGMA estimated value of approximately 3%.

B.3 Lewis Bending Stress

The Lewis bending stress equation can be written as in equation B10.

$$\sigma_L = \frac{F_t}{byp} \qquad Eqn\ B10$$

Where: F_t= transmitted load (N), b = face width (mm), y = Lewis form factor/π and p = pitch diameter (mm). As module m = p / N_t, the equation can be rewritten as $\sigma_L = \frac{F_t}{bmY}$ where: m = module (mm), and Y = Lewis form factor. The Lewis form factor for the current gear with 13 teeth can be found from the literature (Mitchener and Mabie, 1982). A section of the table presented in (Mitchener and Mabie, 1982) is shown in Table B1 below.

Table B1: Determination of Lewis Form Factor (Mitchener and Mabie, 1982)

N_t, No. of teeth	Y (φ=20°, a=0.8mod, b=mod)	Y (φ=20°, a=mod, b=1.25mod)
13	0.34827	0.24317

In Table B1 above, Y = Lewis form factor, φ = pressure angle, a = addendum, b = dedendum. As for the current gear, the outer diameter = 75mm, pitch diameter = 65mm and base diameter = 52.5mm, the form factor used is found as Y = 0.24317. For a tangential force calculated as F_t = 4615.38N, and a face width b = 20mm.

$$\sigma = \frac{4615.38}{20 * 5 * 0.24317} = 189.8\ MPa$$

B.4 AGMA Bending Stress

The AGMA equation (Eqn B11) for bending stress is given as:

$$\sigma = W_t K_{OF} K_V' K_s \frac{1}{Fm} \frac{K_H K_B}{Y_J} \qquad Eqn\ B11$$

Previous calculations have shown that some of the constants in the equations have been determined as: W_t = 4615.38N, K_{OF} = 1, K_V' = 1, K_s = 1, F = 20mm, m = 5, and K_H = 1.16443. Furthermore, according to the literature (Childs, 2003), the rim thickness factor (K_B) is used to account for insufficient support for bearings. In this case, it is assumed that there is full support and hence K_B = 1. Finally, the AGMA geometry factor (Y_J), can be obtained graphically (Childs, 2003) as Y_J = 0.215. Hence the bending strength is calculated as:

$$\sigma = 4615.38 \cdot 1 \cdot 1 \cdot 1 \cdot \frac{1}{0.02 \cdot 5} \cdot \frac{1.16443 \cdot 1}{0.215} = 250000KPa = 250MPa$$

Appendix C FE Model Convergence Test

C.1 Node Convergence Test per Tooth

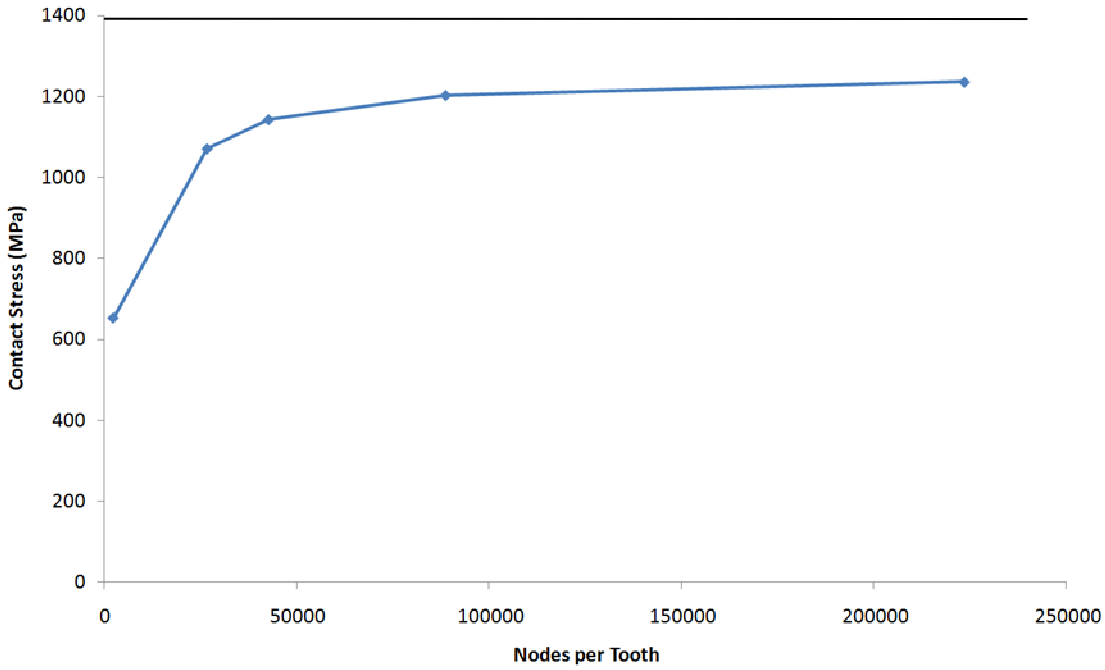


Figure C1: Convergence test showing contact stress vs no. nodes per tooth